The Development and Application of Real-Time Protein Interaction Technology

Thesis submitted in accordance with the requirements of the University of Liverpool for the degree of Doctor in Philosophy by

Nicholas Aled Jones

September 2012

Acknowledgements

Thanks go to both Dr. Daimark Bennett and Prof. Mike White for all their help and encouragement over the course of this PhD.

Thank you to everyone in the Bennett Lab for all the help, to Anita, Nick, Louise, Neville, Lauren, Vincent, Peter, and especially to Eleanor for all those *Drosophila* skills I put to such good use and keeping me company in the fly lab at ridiculous hours of the night. Thanks must of course also go to Chris L for generally keeping me sane and sharing in the joy of constant failure. Thanks to Jean for letting me annex so much lab space in lab G and not making too much of my messy desk!

Thanks to everyone in the White lab, especially to Sheila. Thank you for everything. There is too much to even begin mentioning, but thanks for very patiently teaching me everything I know about lab work, helping me out with data in those crucial last few weeks and with cloning when I just couldn't get it to work! Thanks must go to Dave S. for teaching me everything I know about microscopy and helping pull this thing together in the Nick of time! Connie and Louise A, thanks for all the cell culture you did for me in Manchester, I would have been quite screwed without you! Thanks to Marco for the FRET discussions, wouldn't have been much of a thesis without it! John, Baggers, and Simon, thanks so much for reading through this monstrosity and for the positive feedback that kept me going when I would have much rather slept. Thanks goes to Antony (and John) for all the hugs and general abuse, and scientific assistance over the years, and of course thanks to James Boyd for being my thesis write up buddy. Thanks also to everyone else Pawel, Carol, Violen Kate S., Rachel, Denise, Claire, David T, Raheela, Anne, Karen, Kate G., Steph and everyone (special mention to the lunch time collective) for making it such a fun place to expend the last few years of my life.

Declaration

This thesis is the result of my own work unless otherwise stated, and is based upon results from experimental and theoretical work performed as a PhD student between Opctober 2008 and September 2012 in the department of biological sciences within the University of Liverpool and in the University of Manchester.

Neither this thesis nor any part of it has been submitted in support of an application for another degree of qualification at this or any other University of other institute of learning.

Nicholas Jones

September 2012

Abstract

Protein interactions are a fundamental part of cellular processes, and represent a key target in the understanding of cell behaviour, communication and function. These interactions are dynamic in nature, and change over time. Furthermore, interactions can be dependent on co-localisation in cellular compartments. Both of these characteristics can be obscured through observation by bulk molecular cell assays such as co-immunoprecipitation (co-IP) and can obscure the intricacies of single cell dynamics.

The development of tools and new methodologies to observe single cell protein interaction dynamics are key to understanding the underlying mechanisms that direct cell fate. Systems biology aims to incorporate into predictive models of the whole system. In this way, the development of quantitative experimental tools is a key component of systems biology. Förster Resonance Energy Transfer is a widely used technique in the field of protein-protein interaction studies. Dependent on the non-radiative transfer of energy from a fluorescent molecule of higher excitation energy to a fluorescent molecule of lower excitation energy with sufficiently overlapping spectra, the process occurs across a 1-10nm (100Å) range. As a result, FRET interactions between fluorophores attached to biologically functional proteins are a strong indication of protein interaction.

The photoswitchable protein Dronpa offers a unique opportunity to develop a real-time live cell variant of this technique. Through the modulation of Dronpa fluorescence, repeated donor quenching can be observed, allowing quantification of FRET interactions between fluorophores without spillover. This is achieved sequentially through the optimisation of Dronpa imaging parameters for live cell imaging, followed by the identification and testing of candidate FRET partners using an optimised imaging protocol. Direct fusions were used to qualify potential FRET responses between tested pairs of fluorophores. FRET responses using positive control constructs were rigorously tested and quantified to ensure repeatable and consistent reporting of FRET. The spectral properties of Dronpa and chosen FRET partners were also rigorously tested to ensure FRET could be accurately measured through sensitised emission.

Following the confirmation of a reliable FRET response using positive control constructs, the assay was applied to the NF-κB protein p105, and other interacting family members to measure any changes in protein dynamics. The system was applied both on a single switch basis to make comparisons between different combinations of co-expressed fusion proteins and, in time series experiments, to measure potential changes in dynamics over time. p105 showed interesting behaviour not reported in the literature, specifically the detection of full length p105 in the nucleus before stimulation and the strong intramolecular interaction of N and C terminal regions which become perturbed by co-expression of p65. p65 displayed a stronger interaction with the c-terminal region of p105, indicating preferential binding of p65 with ankyrin repeat region rather than the Rel homology domain of p105. Fluorescence Cross Correlation Spectroscopy (FCCS) was used as a complimentary technique to confirm findings in the FRET assay. Considered together, these data suggest Dronpa is a viable component for the accurate detection of FRET in real time, free from complication by spillover. The use of this technique could help to elucidate dynamic protein interactions key to the development and improvement of existing models in systems biology approaches.

Contents

List of Figures and Tables

Figures

Tables

Commonly Used Abbreviations

aa	Amino Acid
β-ME	2-Mercaptoethanol
AFP	*Aequorea* Derived Fluorescent Protein
AOTF	Acousto-optical tuneable filter
APD	Avalanche Photo Diode
ATP	Adenosine triphosphate
AU	Arbitrary Units
att	Attachment Site
BSA	Bovine Serum Albumin
CCD	Charged Coupled Device
cDNA	Complementary DNA
CMV	Cytomegalovirus
Co-IP	Co-Immuno Precipitation
CSS	Charcoal-Stripped Serum
Cyto	Cytoplasm
DD	Death Domain
DMEM	Dulbecco's Modified Eagle's Medium
DNA	Deoxyribonucleic Acid
dNTP	Deoxynucleotide Triphosphate
dsRed	Red Fluorescent Protein (from *Discosoma*)
dsRed-XP	dsRed-Express
ECFP	Enhanced Cyan Fluorescent Protein
EGFP	Enhanced Green Fluorescent Protein
EYFP	Enhanced Yellow Fluorescent Protein
F_C	Sensitised emission
FCS	Foetal Calf Serum
FCS	Fluorescence Correlation Spectroscopy
FCCS	Fluorescence Cross-Correlation Spectroscopy
FRET	Fluorescence Resonance Energy Transfer
galvo	Scanning Galvanometer Mirror
GFP	Green Fluorescent Protein

GRR	Glycine-Rich Region
IKK	IκB Kinase
IL	Interleukin
It.	Iteration
IκB	Inhibitor-κB
LN_2	Liquid Nitrogen
LPS	Lipopolysaccharide
LSM	Laser Scanning Microscope
MCS	Multiple Cloning Site
mRNA	Messenger RNA
mRaspberry	Monomeric Raspberry Fluorescent Protein
mRFP	Monomeric Red Fluorescent Protein
mStrawberry	Monomeric Strawberry Fluorescent Protein
mTFP	Monomeric Teal Fluorescent Protein
NA	Numerical Aperture
NEMO	NF-κB Essential Modulator
NES	Nuclear Export Signal
NF-κB	Nuclear Factor-κB
NIK	NF-κB-Inducing Kinase
NLS	Nuclear Localization Signal
Nuc	Nucleus
PBS	Phosphate-Buffered Saline
PCR	Polymerase Chain Reaction
PEST	Proline, Glutamic Acid, Serine, Threonine Rich Region
PMT	Photo Multiplier Tube
PR	Progesterone Receptor
RHD	Rel-Homology Domain
RIP	Receptor Interacting Protein
RNA	Ribonucleic Acid
ROI	Region of Interest
RTKs	Receptor Tyrosine Kinases
SD	Standard Deviation
SDS	sodium dodecyl sulphate
SEM	Standard Error of the Mean

TAD	Transactivation Domain
TAE	Tris-Acetate/EDTA Electrophoresis Buffer
TBS	Tris-Buffered Saline
TBS-T	TBS with Tween-20)
TEMED	N,N,N′,N′-Tetramethylethylenediamine
TNFR	TNF Receptor
TNFα	Tumour Necrosis Factor
TRADD	TNF Receptor-Associated Death Domain Protein
TRAF	TNF Receptor Associated Protein
Tris	Tris(hydroxymethyl)methylamine
UV	Ultra violet light
wtGFP	Wild Type GFP

Chapter 1: Introduction

1.1- Introduction I – The Importance of Protein Interactions

1.1.1 The Protein

Proteins are functional products of genes encoded in genetic DNA, the fundamental building blocks of life, and key to cell communication, function and survival. In collaboration, proteins have the power to direct cell fate through apoptosis and proliferation and migration or can function benignly as structural sub units such as collagen.

Proteins control cell processes and behaviour at almost every level, from the endocrine and paracrine inter-communication of cells through excretion of proteins into the inter cellular matrix to the control of early and late gene expression through time-dependent or conditional nuclear translocation of transcription factors (Nelson, Ihekwaba *et al.* 2004; Bancos, Natt *et al.* 2012). Some processes like the transduction of intercellular signals following treatment with Tumour Necrosis Factor α (TNFα) result in a signalling cascade involving the phosphorylation and degradation of many transient protein interactions or the movement of cells through the formation of actin rich protrusions known as lamellapodia facilitating cell migration, proliferation and growth. Such processes are key to cell survival and multicellular interaction (Tartaglia and Goeddel 1992; Lyulcheva, Taylor *et al.* 2008).

For the most part, changes in the activity of proteins have been shown to be controlled through covalent modifications that change the 3D structure, usually via phosphorylation or dephosphorylation of serine, threonine, and tyrosine residues of specific amino acids (Johnson and Barford 1993; Pawley). Covalent modification affects the orientation and activity of domains within the protein (Bowie, Luthy *et al.* 1991), which, in turn, affects their ability to interact with other molecules. This is key to protein function as the majority of fundamental cellular processes, such as transcription, translation, and intracellular signal transduction, have been shown to be regulated by protein complexes containing up to ten or more proteins (Kornberg 1999; Gavin, Bosche *et al.* 2002; Lyulcheva, Taylor *et al.* 2008).

Protein interactions are often dynamic and can mediate changes in protein activity or subcellular localisation (such as the shuttling of proteins to and from the nucleus (Hayden and Ghosh 2004)). These interactions can be transient (Nooren and Thornton 2003) or long lived (Heessen, Masucci *et al.* 2005) depending on the nature of the response. Understanding where and when protein interactions occur is of critical importance to understanding the role and regulation of these proteins in cellular processes.

Heterogeneity between individual cells is a well known feature of dynamic cellular processes. This heterogeneity has been suggested to confer a significant advantage in maintaining robustness in overall coordination and stability of cell population responses (Paszek, Ryan *et al.* 2010).

This gives single cell data particular significance. Molecular methods for observing protein levels and binding partners not only require the denaturing of proteins, the lysing of cells and destruction of intracellular compartmentalisation; they also rely on large populations of cells, giving an indiscriminate global picture of cell response to stimuli. Non-invasive methods of measuring cellular processes in the same cell over time are necessary to gain a deeper understanding of what protein behaviours occur in cell populations. With the capability of measuring protein-protein interactions, protein movement and transcriptional output from single living cells (Rutter, White *et al.* 1995; Stirland, Seymour *et al.* 2003; Nelson, Ihekwaba *et al.* 2004; See, Rajala *et al.* 2004).

1.1.2 Observing Protein Interactions

There are many methods of observing protein interactions, all with their own advantages and disadvantages. Methods can broadly be separated into two categories; Biochemical assays and biophysical methods.

Many biochemical assays, such as co-immunoprecipitations (IPs), are designed to examine interactions from cellular extracts. By selecting an antibody that targets a known protein within a complex of proteins, it is possible to purify the entire protein complex from the rest of the cell lysate and subsequently identify unknown members of the complex (Salim, Fenton *et al.* 2002). An under-reported issue with this method

of observing protein interactions is that the interactions could be occurring in the cell lysate following disruption of the cell structures, so it may not be a true representation of the interactions occurring within an intact cellular compartment. Conversely, intracellular compartmentalisation can affect any number of cellular processes and the ability of a protein to form a complex and its subsequent behaviour.

The contextual information relating to the localisation of the proteins is also lost by testing these interactions outside the cell as the cell lysate contains components from many subcellular compartments that would not ordinarily mix with each other under physiological conditions. This feature of protein interaction can also be a contributing factor to detection of false positives in methods such as the yeast two-hybrid method, involving over-expression of proteins without the appropriate spatial context of protein localisation (Wang, Rapp *et al.* 1996; Van Criekinge and Beyaert 1999).

1.2 Introduction II- The Imaging Toolbox

1.2.1 Microscopy and Confocal Microscopy

Light Microscopy has been in general use in biology for over 300 years. In fact the term cell originates from Robert Hooke and his comparison of cork cells to that of monks' cells while using a compound microscope (Fara 2009). Over that time, light microscopy has become more refined and complex to the extent that the main limiting factor for obtaining higher resolution through traditional means are the physical properties of light and diffraction in relation to refractive index.

$$d = \frac{\lambda}{2(n \sin \theta)}$$

Figure 1-1 Abbe's Equation estimating diffraction limit of a microscope.
d is the resolvable distance, λ is the wavelength of light, n is the refractive index of the medium being imaged in, and θ is half the angle of the cone of light from specimen plane accepted by the objective.

In his paper of 1873, Abbe reported that the smallest resolvable distance between two points using a conventional microscope cannot be smaller than half the wavelength of the imaging light (Abbe 1873). Abbe concluded that the resolution was limited by diffraction to half the wavelength modified by the refractive index of the medium and the angle of the cone of focused light (Figure 1-1). Based on this equation, it is possible to improve spatial resolution either by increasing the numerical aperture, which is limited by the refractive index the image is observed though, or by using light with a shorter wavelength (e.g. ultraviolet). This, however, risks damage to biological samples through oxidative stress or DNA damage (depending on the wavelength), and is undesirable due to increased light scattering within a tissue. Conversely, longer wavelengths improve tissue penetration at the expense of resolution (Wang, Konig *et al.* 2010).

The use of shorter wavelengths to enhance resolution through autofluoresence was implemented through epifluoresence microscopy (Heimstädt 1911). The staining of samples with antibodies bound to fluorescent chemicals combined with

epifluoresence microscopy meant for the first time labelling of cellular structures and proteins could be used to study more subtle elements of cell structure and function (Coons, Creech *et al.* 1941). However, resolution of samples remained an issue.

The solution was conceived through the design and implementation of the confocal microscope (Egger and Petran 1967). Traditional widefield epifluoresence is hindered by out of focus light from the sample and ambient sources. By including a confocal aperture before a detector, out of focus light is removed from the sample (Sheppard and Wilson 1981; White, Amos *et al.* 1987). The inclusion of the aperture means samples must be raster scanned and build up digitally via photon to electron conversion using Photo Multiplier Tubes (PMT) or various other types of photon detector. This is achieved through movement of the point of illumination by X and Y galvo mirrors (White, Amos *et al.* 1987). Modern confocal microscopes make use of laser excitation, which is monochromatic, polarised and coherent and has the advantage of converging *via* the objective, at a single point of excitation in the focal plane of the sample eliminating the need for a pinhole at the light source (van Meer, Stelzer *et al.* 1987). The combination of confocal microscopy with the discovery of fluorescent proteins and their application as fusion partners in proteins complexes, has become invaluable to studies of single cell and protein behaviour (Chalfie, Tu *et al.* 1994; Shaner, Patterson *et al.* 2007).

1.2.2 Fluorescent Proteins

The development of fluorescent proteins (FPs) alongside confocal microscopy has had a major impact in the understanding of the dynamics and movement of proteins within cells. Wild Type Green Fluorescent Protein (wtGFP), was first purified alongside the bioluminescent molecule *aequorin*, (Shimomura, Johnson *et al.* 1962), but only became a viable tool once it had been cloned as cDNA by Douglas Prasher (Prasher, Eckenrode *et al.* 1992). Initially, wild type GFP (wtGFP) had several disadvantages as a viable tool, including poor folding at 37ºC, dual peak emission spectra and poor photostability (Inouye and Tsuji 1994). A brief period of optimisation by the scientific community through point mutation of wtGFP cDNA lead to the optimised form known as Enhanced Green Fluorescent Protein (EGFP) (Heim, Cubitt *et al.* 1995; McRae, Brown *et al.* 2005). Since the adoption of EGFP as a tool for labelling and probing protein behaviour, the range of available

fluorophores has grown exponentially (Shaner, Steinbach *et al.* 2005; Shaner, Patterson *et al.* 2007). There is now a wide variety of colours, improved maturation time (Mikkelsen, Sarrocco *et al.* 2003), improved quantum yield and stability (Shaner, Patterson *et al.* 2007) and novel behaviours such as photoactivation and photoconvertibility (Chudakov, Verkhusha *et al.* 2004; Henderson and Remington 2006; Bourgeois and Adam 2012).

Fluorescent proteins have become widely used as labels in fusion proteins. Fusion proteins allow the observation of protein localisation, movement and dynamics of cells *in vivo* without the need for cofactors to facilitate fluorescence (Chalfie, Tu *et al.* 1994; Nelson, Ihekwaba *et al.* 2004). These fusion proteins are made through cloning FP CDS at either N or C terminal ends of the protein of interest with a linker sequence (Spector and Goldman 2006).

Table 1-1 Sample list of Fluorescent Protein properties

obtained from Shaner et. al. (Shaner, Campbell et al. 2004)[1](Shaner, Patterson et al. 2007)[2] (Padilla-Parra, Auduge et al. 2009)[3] *weakly dimerised in high concentrations.

Name	Structure	Excitation Max (nm)	Emission Max (nm)	Relative Quantum Yield	Excitation Coefficient ($M^{-1}cm^{-1}$)	Brightness
Red						
mRaspberry[1]	Monomer	598	625	0.15	86,000	12,900
mCherry[1]	Monomer	587	610	0.22	72,000	15,840
mStrawberry[1]	Monomer	574	596	0.29	90,000	26,100
mRFP[1]	Monomer	558	583	0.25	50,000	12,500
DsRedEx	Tetramer	563	579	0.90	19,000	17,100
Orange						
tdTomato[1]	Tandem Dimmer	554	581	0.69	69,000	47,610
Yellow						
EYFP[2]	Monomer*	514	527	0.85	64,000	54,400
Green						
EGFP[2]	Monomer*	484	510	0.70	23,000	16,100
Dronpa[4]	Monomer	503	518	0.62	57,000	35,340
Cyan						
mTFP[3]	Monomer	462	492	0.85	64,000	54,400
AmCyan[2]	Tetramer	458	489	0.85	44,000	37,400
ECFP[2]	Monomer*	439	476	0.40	32,500	13,000

Historically, fluorescent imaging has been conducted through Immunocyto Chemistry (ICC). This method, however, requires the fixation of cells, perforation of cell membranes and cross-linking of proteins before fluorescently conjugated antibodies bind fluorophores to protein domains (HASSELL and HAND 1974; Haugland 2001). Artefacts from fixation and staining process also presented a problem. Friedman *et .al.* showed that paraformaldehyde fixation altered the localisation of wheat-germ agglutinin in cells (Friedman, Dewar *et al.* 1986). This showed that controls must be carried out to show localisation of proteins is not effected through ICC.

The expression of fusion proteins in live cells, it might be argued, is comparatively less invasive than fixation. Through introducing cDNA for transient expression or permanent integration into cell chromosomes, protein structure and function is usually maintained (Felgner, Gadek *et al.* 1987). This allows images of the same live cells to be collected over time, and it becomes possible to observe many different cell processes and responses in an individual cell such as responses to specific stimuli, in real time. An example of this can be seen in the NF-κB pathway and with TNFα treatment and the resulting oscillations in p65 nuclear cytoplasmic localisation (Nelson, Ihekwaba *et al.* 2004).

Two possible artefacts that are important for consideration when expressing fusion protein constructs are over-expression and interference with wild type behaviour. Simply by introducing fusion constructs into cell lines without first inhibiting or removing endogenous protein expression could be considered as over-expression of a protein. Over-expression is more often than not considered the point at which protein level saturates the cell's machinery. It may be more accurate to describe expression of a fluorescent protein fusion from a viral (eg. CMV) promoter as "out of context" as the protein might be expressed constitutively and not regulated at the transcriptional level by the protein's own promoter.

Achieving a more physiological level of expression is no mean feat. Transient transfection offers no control of over-expression other than selecting cells with the appropriate level (Spector and Goldman 2006). Short of using molecular counting techniques like fluorescence correlation spectroscopy (FCS) or calibration of intensity with known standards, quantification of protein level is difficult.

Lentivirus and BAC (bacterial artificial chromosomes) approaches offer a more permanent alternative to transient transfection which can allow cell expression to be selected and made into a homogenous population of expressers (Spector and Goldman 2006). However, both of these techniques could be argued to be nonphysiological, with lentiviral and BAC expression being effected by copy number and integrating into a random part of the genome with the potential for expression to be effected by local chromatin structure. This is probably not as important in BAC

constructs as the long flanking sequences can act to insulate the gene of interest from site of integration effects (de Wet, Wood *et al.* 1987).

It is also important to ensure that the label being fused to the target protein has had no effect on wild type protein function or behaviour. Linker sequences or even fluorophore size and termini position might affect protein behaviour. Controls such as Ires vectors (separately expressing protein and FP from a single transcription event by ribosomal skipping of the linking sequence) can be used to ensure cell behaviour remains consistent.

Important qualities of fluorescent proteins include brightness, photostability, oligomerisation, environmental sensitivity and spectral excitation and emission profiles (Shaner, Steinbach *et al.* 2005). Brightness is a rather arbitrary determinate of an FP's aptitude, it is determined by its maturation speed and efficiency, extinction coefficient, and quantum yield and effected by filter set efficiency on the system in use for any given spectra. Brightness is best considered alongside photostability, as fluorophores that are overexcited will begin to bleach. In experimental situations, where expression level is of significance this can affect results (Shaner, Steinbach *et al.* 2005; Shaner, Patterson *et al.* 2007). The best way of establishing the usefulness of a particular FP under a given set of experimental parameters is to image the freely-expressed fluorophore in the correct live cell context.

Oligomerisation of fluorescent proteins could potentially cause fusion proteins to form complexes through fluorophore interactions. This is of particular importance for molecular counting techniques such as FCS which can use relative molecular brightness as a measure of protein oligomerisation (Chen, Wei *et al.* 2003). Environmental sensitivity can affect fluorophore folding, either through pH sensitivity, oxygen requirement or temperature-dependent folding. An example of the importance of oxygen sensitive folding is the difference between *Aequorea*-derived fluorescent proteins and red shifted coral fluorophores. These red fluorophores generate twice the number of H_20_2 molecules than that of AFPs indicating that twice the amount of molecular oxygen is required for fluorophore maturation. This is of vital consideration for fusion constructs used to study cells in hypoxic conditions

(Tsien 1998; Gross, Baird *et al.* 2000). Folding temperature should also be considered when selecting FPs, for example the fluorophore CyPet folds poorly at 37ºC limiting its use for *in vivo* expression in mammalian model systems (Shaner, Patterson *et al.* 2007).

Spectral emission and excitation profiles are most important when imaging multiple fluorophores in the same system. While linear unmixing provides the ability to separate emission from overlapping spectra, a more straightforward approach is to choose fluorophores with appropriate spectral separation. ECFP (Figure 1-2) for example has a wide emission spectra, this means it is a poor choice for spectrally separate imaging with other FPs such as EGFP (Patterson, Day *et al.* 2001).

1.2.3 Exotic Fluorescent Proteins

Recent study into the photophysical properties of FP variants have led to the generation of FPs that can either activate fluorescence from a quiescent state (photoactivation) or can be optically converted from one emission bandwidth to another (photoconversion). These new FP variants offer new approaches to the study of protein dynamics in live cells. (Lukyanov, Chudakov *et al.* 2005; Shaner, Patterson *et al.* 2007). Three separate groups of these FPs have been classified; photoconvertable, photoswitchable and photoactivatable FPs. Photoconvertable proteins are FPs which can be optically converted from one emission bandwidth to another, from a smaller wavelength to a longer wavelength (Chudakov, Verkhusha *et al.* 2004; Stark and Kulesa 2007). Photoactivatable proteins are activated by intense illumination, using a separate activation spectra than that of the fluorophores excitation. Following this activation they behave as standard fluorophores with defined quantum yield and photostability (Henderson and Remington 2006; Stark and Kulesa 2007). Similar to Photoactivatable FPs, Photoswitchable fluorophores are activated by illumination at a specific wavelength. Unlike photoactivatable FPs, photoswitchable fluorophores may be activated and deactivated many times without the fluorophore suffering any damage. A number of photoswitchable GFP variants were developed, but many lacked durable and prompt photoswitching characteristics (Habuchi, Ando *et al.* 2005; Zhang, Chang *et al.* 2012).

Table 1-2 Example Optical Highlighter fluorescent proteins.

Photoconvertable, photoswitchable, and photoactivatable fluorescent proteins (Habuchi, Ando *et al.* 2005)[1](Chudakov, Belousov *et al.* 2003)[2](Patterson and Lippincott-Schwartz 2002)[3.] (Gurskaya, Verkhusha et al. 2006)[4]

Name	Classification	Excitation Max(nm)	Emission Max(nm)	Activation wavelength	Quantum Yield	Extinction Coefficient ($M^{-1}cm^{-1}$)
Dronpa[1]	Photoswitchable	503nm	518nm	405nm	0.79	17,400
Kindling[1]	Photoswitchable	580nm	600nm	457nm(quench)	0.07	59,000
Pa-GFP[2&3]	Photoactivateable	504nm	517nm	405nm	0.79	17,400
Dendra (g)[3&4]	Photoconvertable	457nm	507nm	405nm	0.72	21,000
Dendra (r)[3&4]	Photoconvertable	553nm	573nm	n/a	0.70	20,000

Photoswitchable fluorophores have the unique possibility of being used as FRET partners which can be modulated. This gives a huge advantage in the ability to repeatedly quantify FRET *in-vivo* using the principle of acceptor photobleaching (see 1.2.4). Dronpa and Kindling show clear superiority in their ability to be switched repeatedly, and also have the added advantage of being spectrally separate (Table 1-2) suggesting that both could be used simultaneously *in vivo*.

1.2.3.1 **Dronpa**

First developed by Ryoko Ando, Hideaki Mizuno, and Atsushi Miyawaki in 2004 (Ando, Mizuno *et al.* 2004), Dronpa is a robust photoswitchable fluorescent protein which has been demonstrated to be switchable more than 100 times on the single molecule level (Habuchi, Ando *et al.* 2005). The absorption maximum of Dronpa is at 503nm, and emission spectra peaks at 518nm. While illumination with 488nm causes the fluorophore to fluoresce , it simultaneously converts the fluorophore into a dim state. In this dim state, Dronpa has a different absorption peak of 390nm. Minimal UV excitation at 405nm is required to convert Dronpa back to its bright state, (Ando, Mizuno *et al.* 2004; Habuchi, Ando *et al.* 2005).

The ‘dark’ and ‘light’ states of Dronpa are referred to as deprotonated (on state) and protonated (off state). The switching ability of Dronpa has recently been elucidated by x-ray crystallography and is related to a light-activated *cis/trans* isomerization of the chromophore moiety, accompanied by complex structural rearrangements of four nearby amino acid residues facilitating the changed protonation state (Habuchi, Ando *et al.* 2005; Andresen, Stiel *et al.* 2007).

The on state is thought to be maintained via hydrogen bonding. This is of importance as the initial ratio of protonated and deprotonated forms is determined by pH of the surrounding environment. Furthermore, acid induced protonated forms cannot be interconverted to deprotonated photoswitching forms. This implies that a reservoir population of unswitchable Dronpa will be present in samples depending on substrate pH. Dronpa switching is still shown to occur at pH as low as pH 5.0. Intracellular pH can be pH 7 in the cytosol, and as low as pH 4.5 in lysosomes, therefore it is important to take this behaviour of Dronpa into consideration when visualising fusion protein behaviour (Waddell and Bates 1969; Habuchi, Ando *et al.* 2005).

1.2.4 Fluorescence Resonance Energy Transfer

As mentioned previously, objects under approximately 200nm in size cannot be resolved, super-resolution techniques are methods which allow the inference of molecular interaction through the use of photophysical principles and mathematics to deconvolve these interactions.

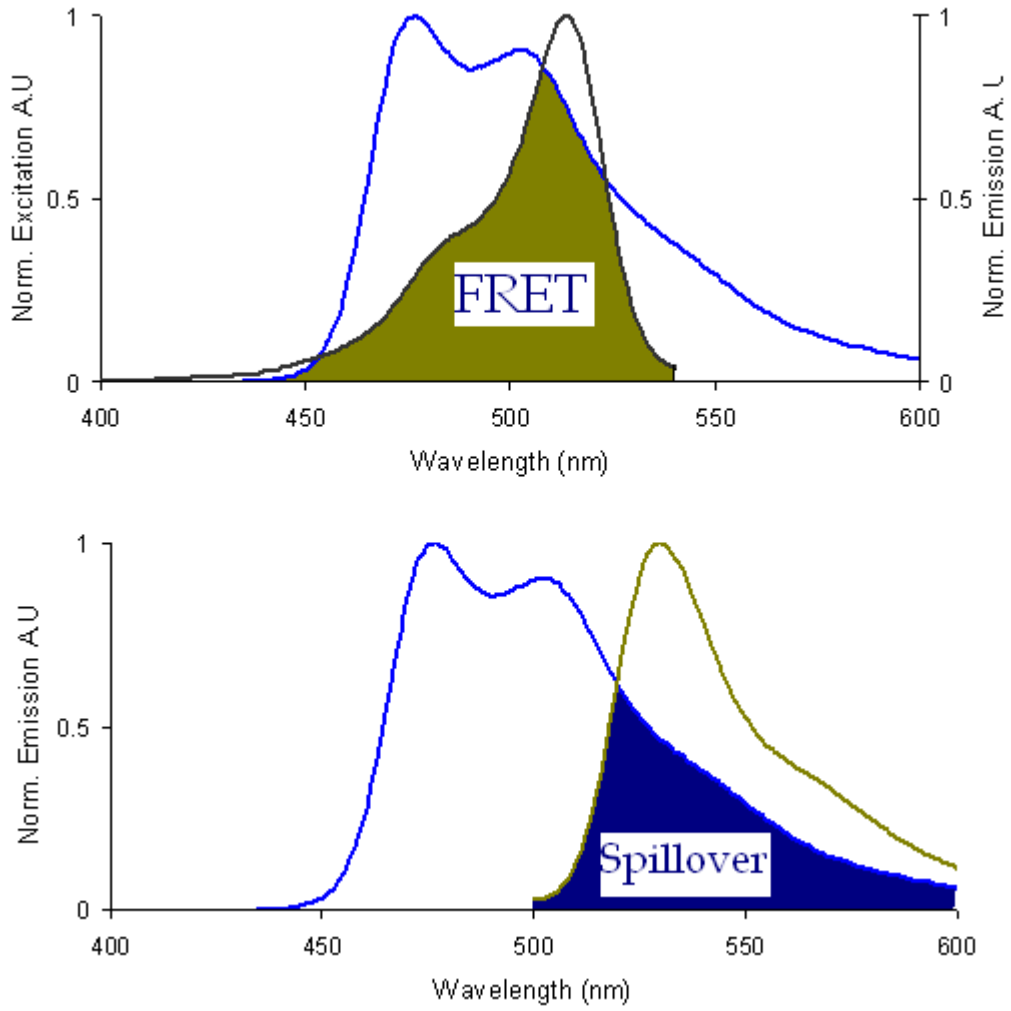

Figure 1-2 . Spectral overlap of ECFP and EYFP.

Spectra normalised against maximum emission and excitation. Top Graph: Emission spectra of ECFP (blue) and Excitation spectra of EYFP (black) showing efficient overlap facilitating FRET. Bottom Graph: Excitation spectra of ECFP (blue) and EYFP (yellow) showing significant spillover. Spectra taken from (Wood 1994).

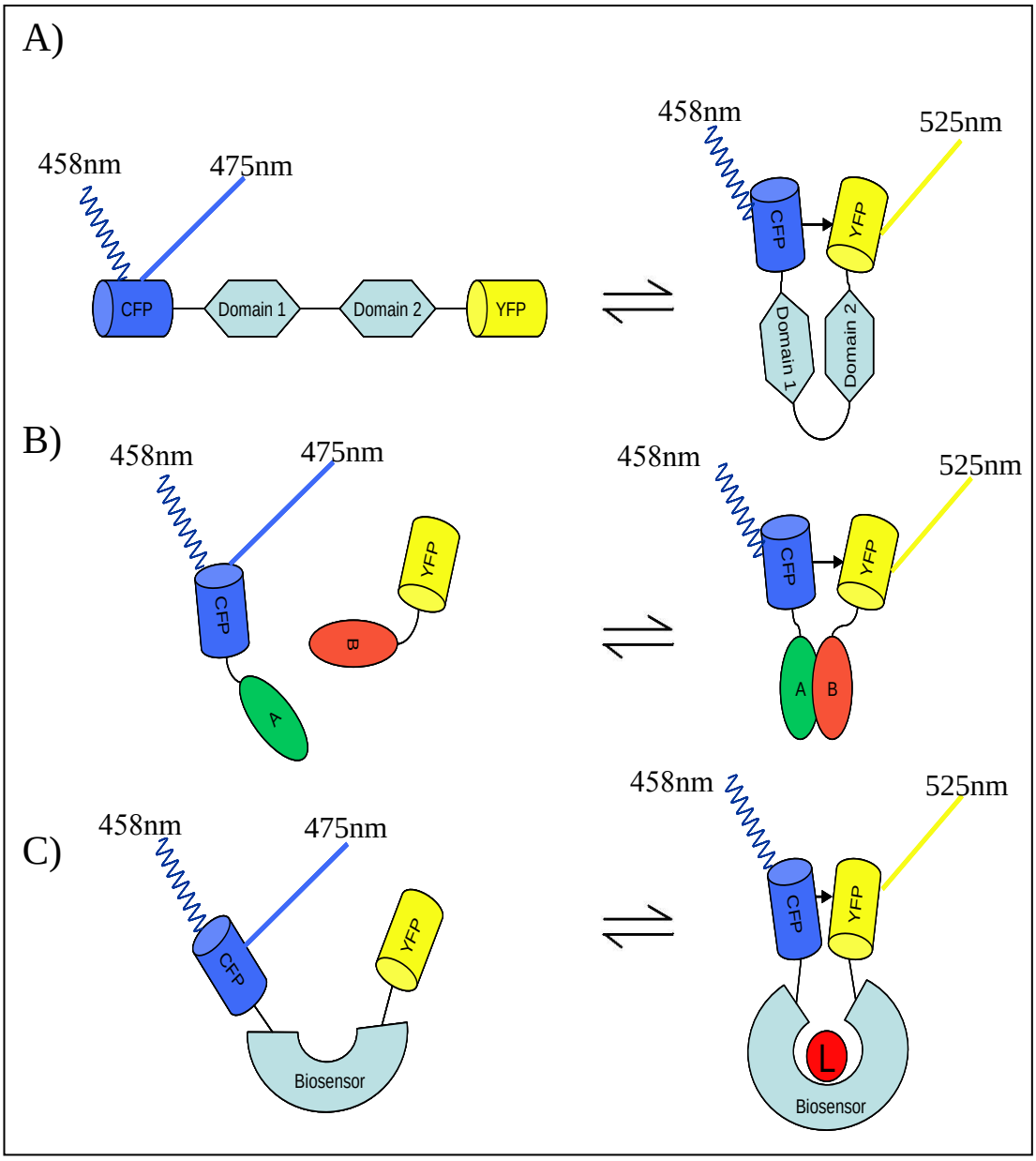

Figure 1-3 Diagram demonstrating the basic principle of FRET.

A), B) and C) represent three major uses for FRET. A) Intramolecular interaction, FRET of single protein. B) Intermolecular interactions, FRET between proteins and C) A molecular biosensor changing conformation in the presence of a binding ligand. Non interacting proteins are too far away for fluorophores to interact and therefore no FRET occurs (left column), where as interacting proteins might be close enough and FRET does occur (right column)

One of the most commonly used of these methods is Förster (or Fluorescence) Resonant Energy Transfer (FRET). Named after the German scientist Theodor Förster (Förster 1948; Wallrabe, Chen *et al.* 2006), FRET is the non-radiative transfer of energy from a higher energy fluorophore to a lower energy acceptor of appropriate spectral absorbance in close proximity (1-10nm). For a FRET pair to

efficiently transfer energy, a donor and acceptor must be selected with sufficient spectral overlap. Figure 1-2 shows the spectral overlap for the classic pair ECFP and EYFP. The donor emission spectrum (CFP) sufficiently overlaps with the acceptor absorption spectrum (EYFP).

When FRET occurs, quenching of the donor fluorescence results in energy being transferred non-radiatively between the excited electrons of the donor and electrons in the acceptor (Figure 1-3). The excited electrons in the acceptor then decay to their ground state releasing a photon at the characteristic acceptor emission wavelength. It is also possible to use a non-fluorescent acceptor to quench donor fluorescence. This has been shown through use of a 'dark' YFP acceptor protein by Ganesan *et.al* (Ganesan, Ameer-Beg *et al.* 2006). In theory, this interaction can only occur when donor and acceptor molecules are between 1-10nm (10-100Å) from one another. (Gordon, Berry *et al.* 1998; Zal and Gascoigne 2004). Successful transfer of energy is used as inference that proteins are interacting. If the energy transfer were to be 100% efficient the donor excited acceptor FP emission (sensitised emission) would be the only signal emitted, however, this is shown to be theoretically impossible (Förster 1948; Karpova, Baumann *et al.* 2003).

Förster proposed that energy transfer is inversely proportional to the sixth power of distance between the donor and acceptor molecules; however, efficiency is limited through the steric properties of interacting fluorophore radii and spectral overlap of the excitation and emission spectra of acceptor and donor fluorophores respectively. The Förster radius, commonly termed R_0, defines where the distance at which energy exchange is at 50% efficiency between fluorophores. Coined by Förster, equation [I] demonstrates how energy exchange between flurophores is inversely proportional to the sixth power of distance, and calculates energy transfer (E) (Förster 1948; Valeur 2001; Gurskaya, Verkhusha et al. 2006).

$$E = \frac{R_0^6}{R_0^6 + r^6} \qquad [I]$$

It should be noted that Ro is not only dependant on a steric and spectral proporties of the fluorophores, but factors such as fluorescence quantum yield of the donor, the refractive index of the solution and the dipole angular orientation of each fluorophore.

The interacting dipoles of fluorophores must also be aligned to transfer energy non-radiatively. Termed $\mathbf{k_2}$ this interaction is determined by the alignment of dipoles in three dimensional space. It can be seen as existing between 0 (no interaction) and 4 (continuous uninterrupted dipole interaction). Dipoles must not only be aligned in parallel, but must also be collinear, and extreme $\mathbf{k_2}$ values such as these are the result of complete donor and acceptor fluoresence polarisation which is unusual (Domanov and Gorbenko 2002).

Although there have been many attempts within the literature to develop methods to experimentally determine the orientation factor between fluorescent pairs, determinations remain difficult at best, and can often be impossible to confirm conclusively. As a way of circumnavigating this, interacting dipoles of fluorophores can be assumed to freely rotate at a rate that is faster than the fluorescent decay rate of the donor (isotropic dynamic averaging). In this instance the average value of $\mathbf{k_2}$ is 2/3 (0.67). If $\mathbf{k_2}$ is shown to be effected through methods such as x-ray diffraction, anisotropy or FRET spectroscopy this parameter can be altered appropriately (Dale, Eisinger et al. 1979; Valeur 2001; Domanov and Gorbenko 2002).

As a result of this inefficient energy transfer sensitised emission signal is masked by spillover from the donor, or spurious excitation of the acceptor by wavelengths intended to excite only the donor (Karpova, Baumann *et al.* 2003; Wallrabe, Chen *et al.* 2006). This crosstalk between channels becomes significantly problematic when FPs levels are inconsistent between samples.

1.2.4.1 Crosstalk Correction and Sensitised Emission

As previously mentioned, Sensitised Emission (F_C) is the donor excited acceptor emission. Due to the physical limitations on energy transfer efficiency, this interaction requires the subtraction of spill-over from both donor and acceptor fluorophores to observe the true F_C (Gordon, Berry *et al.* 1998; Wouters, Verveer *et al.* 2001). This method of observing FRET is often termed the three filter-cube approach, due to its dependence on three separate filter sets (or cubes) to measure donor, acceptor and sensitised emission (Chen, Puhl *et al.* 2006). This is achieved through linear regression using the spillover of single reference donor or acceptor FP. The relative spillover of fluorophores remains linear as long as microscope settings are not altered. Table 1-3 shows the nomenclature adopted for referring to these reference spectra and FRET samples.

Table 1-3 A list of abbreviations for FRET filter combinations.
Combinations of samples and filters used to establish spillover and true sensitised emission in samples

Code	Fluorophore	Excitation	Filter set	Meaning
I_{DD}	Donor, Acceptor	Donor	Donor	Donor-acceptor specimen using the donor excitation and donor filter set
I_{DA}	Donor, Acceptor	Donor	Acceptor	Donor-acceptor specimen using donor excitation acceptor filter set (raw FRET)
I_{AA}	Donor, Acceptor	Acceptor	Acceptor	Donor-acceptor specimen using acceptor excitation and acceptor filter set
D_{DD}	Donor	Donor	Donor	Donor only specimen using the donor excitation and donor filter set
D_{DA}	Donor	Donor	Acceptor	Donor only specimen using the donor excitation and acceptor filter set
D_{AA}	Donor	Acceptor	Acceptor	Donor only specimen using acceptor excitation and acceptor filter set
A_{DD}	Acceptor	Donor	Donor	Acceptor only specimen using donor excitation and donor filter set
A_{DA}	Acceptor	Donor	Acceptor	Acceptor only specimen using donor excitation and acceptor filter set
A_{AA}	Acceptor	Acceptor	Acceptor	Acceptor only specimen using acceptor excitation and acceptor filter set
F_c	Donor, Acceptor	Donor	Acceptor	Spillover corrected sensitised emission in samples containing both donor and acceptor

Once control samples have been used to gauge spillover, spillover can be subtracted as demonstrated below [II] (equation derived from Youvan *et al.* and *Gordon et al.* (Youvan, Silva et al. 1997; Gordon, Berry et al. 1998).

$$F_C = I_{DA} - (I_{AA}(A_{DA} / A_{AA})) - (I_{DD}(D_{DA} / D_{DD})) \qquad [II]$$

Once spillover has been accounted for, corrected F_C should theoretically represent energy transfer.

1.2.4.2 Acceptor photobleaching

A commonly used technique for determining FRET efficiency is acceptor photobleaching. This involves bleaching the acceptor fluorophore and monitoring donor recovery from quenching illustrated in Figure 1-4 (Wouters, Verveer *et al.* 2001; Pietraszewska-Bogiel and Gadella 2011). Acceptor photobleaching works on the principle that donor recovery is free from spill-over of the acceptor due to the physical properties of FP excitation. This means that donor recovery is directly related to energy transfer and number donor fluorophores in the FRET complex.

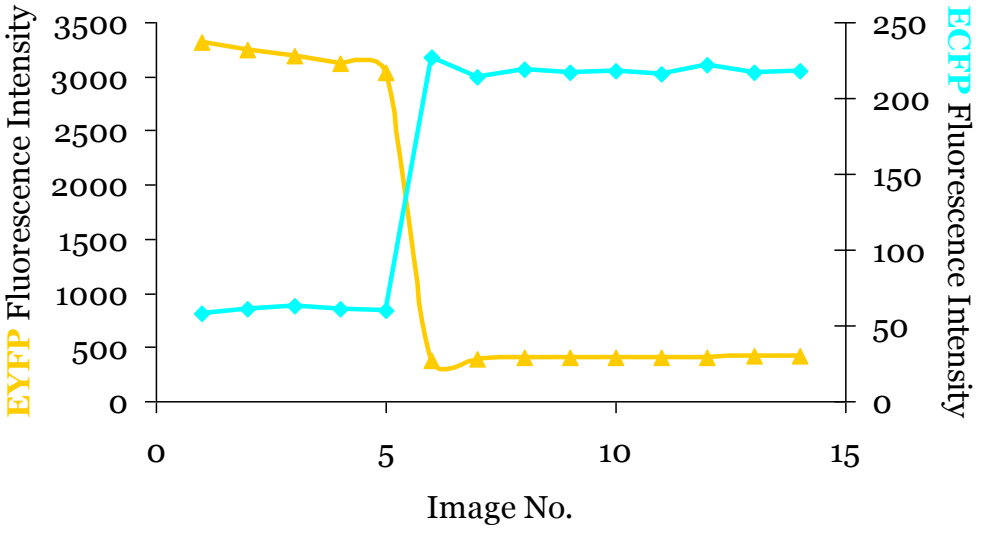

Figure 1-4. Data illustrating acceptor photobleaching.

Graphs shows spectrally deconvolved data using Zeiss linear unmixing algorithm. Acceptor photobleaching in HeLa cell expressing ECFP-mGR and EYFP-p65 together. Acceptor EYFP is bleached after scan 5 resulting in strong recovery of ECFP. Data provided by James Johnson.

By using equation [III] FRET can be quickly inferred from samples, where I_{DD} is pre-bleached donor fluorescence in a sample and I_{DD}' represents a sample post acceptor photobleaching in the same sample.

$$E = 1 - \frac{I_{DD}}{I_{DD}'} \quad \text{[III]}$$

This reliance on acceptor photobleaching means that protein interactions can only be observed once in any one cell by conventional fluorophore pairs.

1.2.4.3 **Artefacts and Issues**

While not an issue for intramolecular biosensors and chimeric proteins such as the chameleon family of calcium sensors, fluorophore ratio can be problematic when quantifying FRET efficiency. This is manifested through intra fluorophore competition. An excess of either fluorophore can lead to nonlinear changes in efficiency. For example, if acceptor concentration exceeds that of donor concentration, competition between acceptor molecules becomes a determining factor in observed energy exchange between donor and acceptor FPs. Once acceptor molecules saturate a system, a sub-population of non-interacting acceptor molecules will be present. This means that past the point of saturation the linear relationship between sensitised emission and change in acceptor fluorescence breaks down. Although quenching will still be present, its relative change will not be proportional to changes in acceptor fluorescence. Conversely, if donor concentration exceeds acceptor concentration, sensitised emission will not correlate with acceptor fluorescence (Wouters, Verveer *et al.* 2001; Pietraszewska-Bogiel and Gadella 2011).

Another factor that must be taken into consideration when probing FRET results is the heterogeneity of FRET complexes in live cells. Not only can heterogeneity occur between cells, but can occur within cells. In this way it becomes important to group and visualise cell responses to FRET. For these reasons, FRET only provides a good indication of protein interaction, lack of a FRET signal does not rule out interactions as the proteins may bind to each other in a conformation where the fluorophores are

too far apart for FRET to occur. FCCS might be a strongly complementary method for FRET, and should be used in conjunction with FRET where protein interactions remain in question following FRET experiments.

1.2.5 Fluorescence Correlation Spectroscopy

Fluorescence Correlation Spectroscopy provides a different way of circumventing the conventional limit of resolution of standard microscopy. FCS works by 'parking' a stationary laser using X and Y galvo mirrors resulting in a small diffraction limited confocal volume placed within cell. This means that data is not raster scanned and requires the use of sensitive detectors such as avalanche photodiodes (APDs) as opposed to PMTs. The localisation and dynamics of fluorescently labelled protein can be observed by measuring the fluctuations of low numbers of fluorescent molecules as they pass through this small diffraction limited confocal volume of known size. As fluctuations in signal are detected over time, these measurements can be statistically analysed through autocorrelation analysis. Autocorrolation is defined to be (Bacia and Schwille 2007);

$$G(\tau) = \frac{\langle F(t+\tau) \cdot F(t) \rangle}{\langle F(t) \rangle^2}, \qquad \tau \geq 0. \qquad \text{[i]}$$

Where τ represents the lag time, and $\langle \cdot \rangle$ denotes averaging over time. For freely diffusing fluorophores, the following equation can be fit to describe the autocorrelation curve,

$$G(\tau) = 1 + \frac{1}{N(1-T)} \cdot \left[1 - T \cdot \left(1 - e^{\frac{-\tau}{\tau_T}}\right)\right] \cdot \sum_i \left[a_i \cdot \left(1 + \frac{\tau}{\tau_{D_i}}\right)^{-1} \cdot \left(1 + \frac{\tau}{\tau_{D_i} \cdot S^2}\right)^{-\frac{1}{2}}\right]. \qquad \text{[ii]}$$

Here, the average number of fluorescent molecules in the confocal volume is represented by the term N, T represents the nonfluorescent component due to transitions of the fluorescent molecules through the triplet state, i is the index for the diffusing species i.e. species diffusing at rate D_i, a_i is the relative fraction of each species, and S represents the structural parameter i.e. the ratio of the axial (Z_0) to

lateral (W_0) radius. The characteristic diffusion time τ_D is related to the diffusion coefficient D by,

$$D = \frac{w_0^2}{4 \cdot \tau_D}. \qquad \text{[iii]}$$

It can be seen from Eq. [ii] that the autocorrelation is inversely proportional to molecular number as there is a $1/N$ term. With lower molecule numbers, the relative change in fluorescence as molecules pass through the confocal volume is more pronounced. If molecule number is too high (>1000 molecules) an unreliable autocorrelation curve is generated. Lag time corresponds to time spent in the confocal volume, and by taking into account the lateral width of the confocal volume, Eq [iii] can be used to calculate molecular diffusion rates . Visually, slower diffusing molecules will have a longer decay profile in the associated autocorrelation curve shifting the curve to the right. If a molecule diffuses at two different rates, then two decay profiles will be seen in the autocorrelation curve, and Eq. [ii] can be used to establish the percentage of the different diffusion fractions. Note also, by comparing the diffusion rate of a molecule to that of a molecular of known molecular mass, for example free GFP, diffusion rates can be used to estimate molecular mass (Dross, Spriet et al. 2009). In this way, from autocorrelation curves information such as the diffusion rates, estimated molecular weight and different diffusing fractions of fluorophores may be established (Figure 1-5) (Kim, Heinze *et al.* 2007; Spiller, Wood *et al.* 2010).

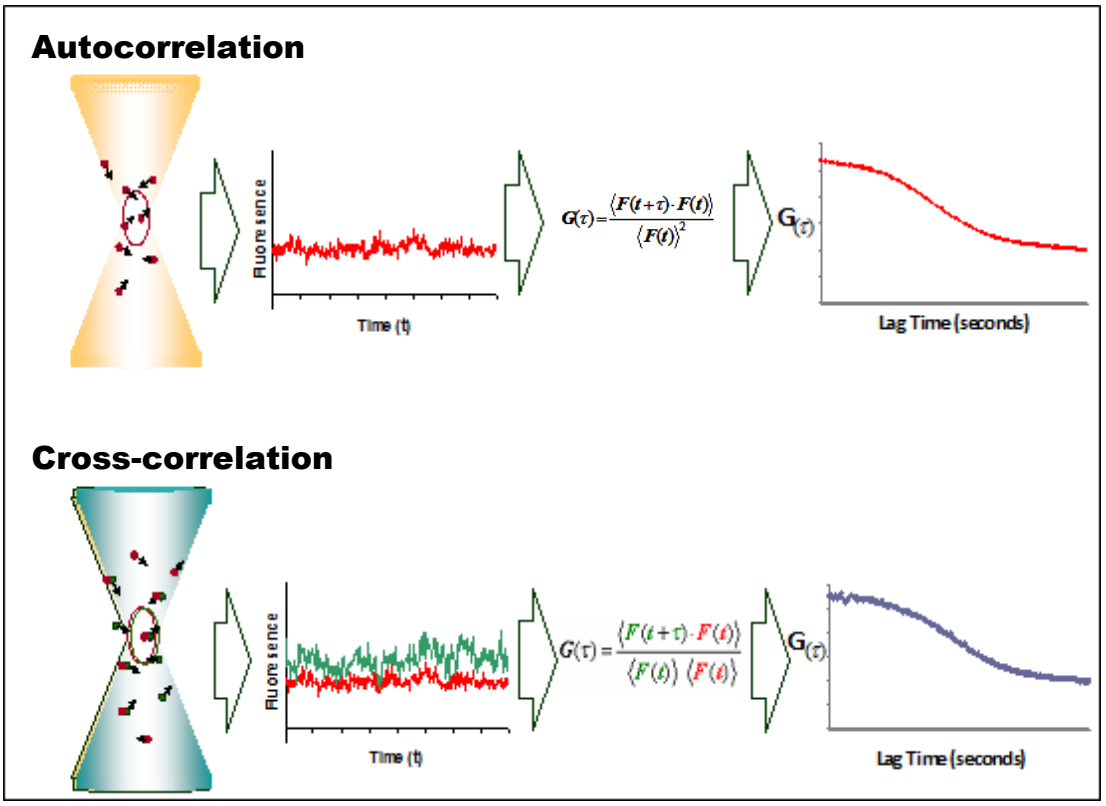

Figure 1-5 Diagrammatic representation of FCS and FCCS.

The process of forming autocorrelation (single colour) and cross-correlation (two colour) curves from fluorescence fluctuation readings measured from individual fluorophores passing through the confocal volume in a sample. Figure derived from Bacia *et al.*(Bacia, Kim *et al.* 2006)

Fluorescence Cross Correlation Spectroscopy (FCCS) allows the simultaneous correlation analysis of two spectrally separate fluorophores (such as DsRedExpress and EGFP). The cross-correlation curve is analogues to the autocorrelation curve but is calculated through correlating the fluorescence fluctuation profiles of the two colours (Figure 1-5), and so the cross-correlation amplitude corresponds to the degree of molecular interaction. In conjunction with the autocorrelation amplitudes, FCCS provides information on molecular binding as well as dynamic co-localisation. (Bacia, Kim *et al.* 2006; Kim, Heinze *et al.* 2007). In contrast to FRET, FCCS does not depend on the very close proximity of the interacting fluorescent labels and as a result does not require the optimisation of fluorophore orientation and linker length optimisation. However, due to imaging of a single spot, issues with regard to photobleaching makes its use to measure interactions over time limited. This makes it a good complementary method to use with FRET.

1.3 Introduction III - The NF-κB Signalling Pathway

1.3.1 NF-κB Overview

NF-κB was first discovered as a transcription factor in immune B cells and required for the transcription and translation of immunoglobulin kappa light chain gene (Sen and Baltimore 1986). NF-κB family proteins were quickly found to be a critical part of cell response to inflammation (Shakhov, Kuprash *et al.* 1990) apoptosis (Schauvliege, Vanrobaeys *et al.* 2002) and even functions not related with immune response such as neuronal embryonic development as shown in mouse embryos mediated though TRAF6 (Dickson, Bhakar *et al.* 2004). In fact, NF-κB dimers are shown to promote transcription of over 150 target genes (Pahl 1999). As a key transcription factor involved in so many processes, NF-κB when unchecked can lead to rheumatoid arthritis, cancer and even septic shock. The NF-κB family has garnered significant attention from the scientific community. This has resulted in significant study of how these transcription factors are controlled (Makarov 2001; Karin, Cao *et al.* 2002; Liu and Malik 2006).

1.3.2 NF-κB Family Members

NF-κB family members can be broadly separated into three categories (Figure 1-6). Rel proteins, Inhibitor kappa B proteins (IκB) and I*kappa*B Kinase (IKK). Rel Proteins are the functioning transcription factors, binding to kappaB consensus sites. Mature Rel proteins consist of p65/RelA, p50/ NF-KB1, p52/ NF-KB2, RelB and c-Rel. It should be noted that p50 and p52 are formed from full length p105 and p100 respectively (Verma, Stevenson *et al.* 1995; Hayden, West *et al.* 2006).

NF-κB functions as a dimer of two Rel subunits and bind discrete κB transcription sites depending on the dimer. Most members form homo and heterodimers in vitro except for RelB, which only forms dimers with p52 and p50 (Ryseck, Bull *et al.* 1992; Dobrzanski, Ryseck *et al.* 1993; Verma, Stevenson *et al.* 1995). The p65-p50 heterodimer is considered to be one of the most abundant signalling dimers in the NF-κB pathway. However both p65 and p50 can form homodimers, causing these proteins to behave differently. Dimers will translocate to the nucleus following

activation, where as p65 homodimers will bind to separate transcription sites and p50 homodimers will actually inhibit transcription (Ganchi, Sun *et al.* 1993)

IκB Proteins are somewhat more difficult to define. The IκB proteins IκBα, IκBβ, IκBε are discrete mature proteins functioning of their own volition, where as IκBγ is a part of p105 and while it behaves as an inhibitor to other Rel proteins, preventing translocation into the nucleus, it can also be freely expressed in the cytoplasm of certain cells via an intronic promoter sequence. A well-characterised example in mice is expressed as a 70kDa protein (Inoue, Kerr *et al.* 1992), furthermore recent study has shown both IκBγ and p105 to be elevated in human cases of Alzheimer 's disease (Huang, Liu *et al.* 2005). p100 also possesses inhibitory behaviour for REL B (Solan, Miyoshi *et al.* 2002). IκBζ and BCL-3 are also considered to be IκB proteins due to their series of ankarin repeats consistent with IκB structure, but these proteins localise to the nucleus and appear to assist p50 and p52 DNA binding (Bours, Franzoso *et al.* 1993; Haruta, Kato *et al.* 2001), though it should be noted that p50 is thought to be transcriptionally repressive. For this reason it is possible to view IκB as modifiers of steady state rather than explicitly as inhibitors of nuclear translocation.

IKK exists as two separate complexes; a high molecular weight complex responsible for the canonical response and low molecular weight complex responsible for the non-canonical response. Both complexes consist of functional kinases IKK1 and IKK2 but use two separate regulatory sub units. The canonical complex contains the regulatory subunit NEMO which allows interaction with TNFR following TNFα stimulation (Figure 1-5) (Hayden and Ghosh 2004). The non canonical pathway is mediated through NIK, causing the activation of IKK1 dimers and providing a docking site for p100 (Sun 2012).

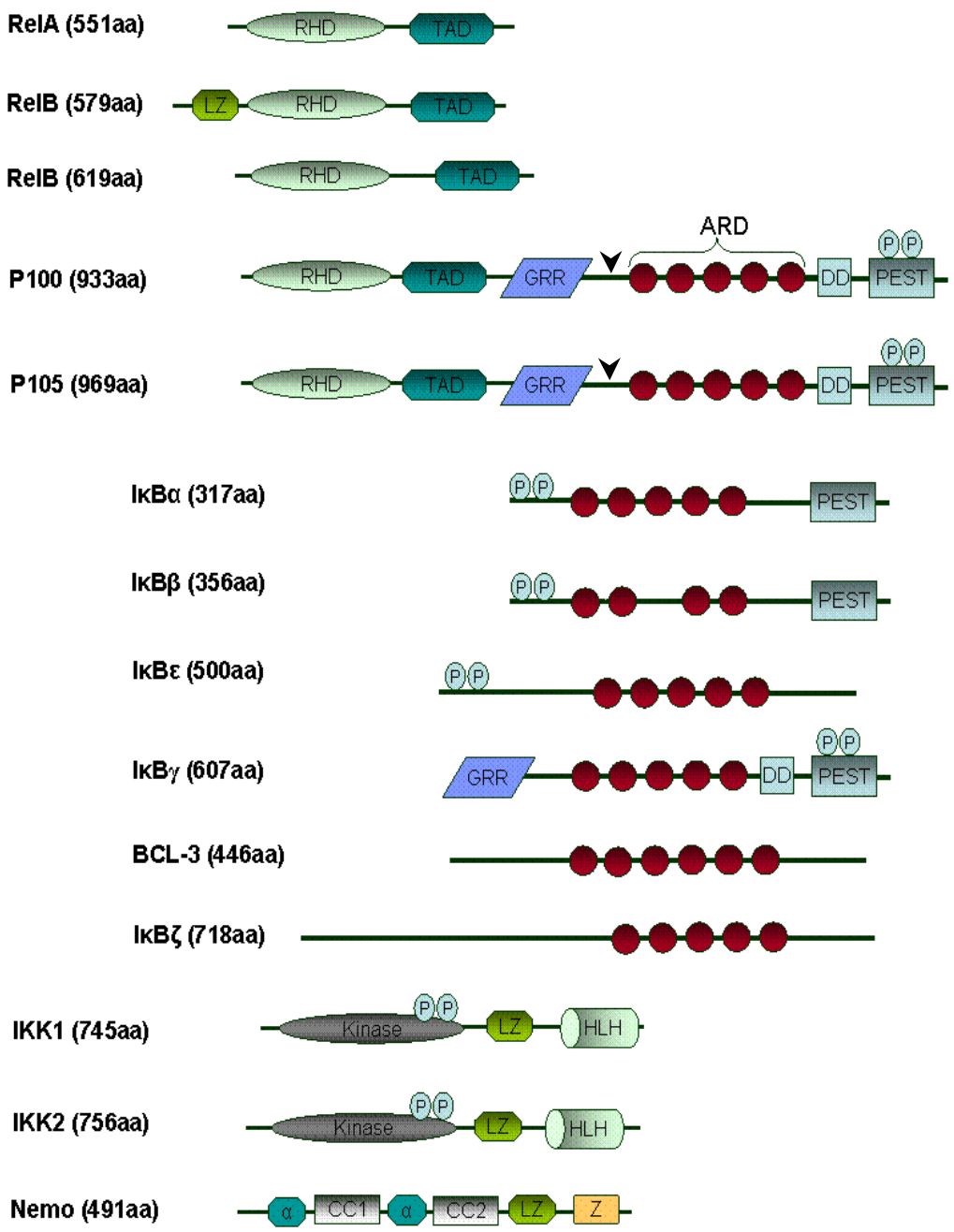

Figure 1-6. Diagram depicting NF-κB proteins

Structural domains are indicated for each family member. Rel proteins are characterised by an N-terminal Rel Homology Domain (RHD) and a C-terminal Transactivation Domain (TAD). RelB differs structurally from p65 and c-Rel due to the presence of its Leucine Zipper (LZ) domain. IκB proteins are defined by the presence of Ankyrin Repeat Domains (ARDs), these bind RHDs of Rel proteins and prevent nuclear localisation. The immature proteins p100 and p105 are processed to p52 and p50 respectively through the degradation of their IκB-like Ankyrin repeat domains indicated by the arrows. Phosphorylation sites (p) shown on IκB proteins are those which target them for degradation, phosphorylation sites shown for IKK1 and 2 are those located on the activation loop. Figure derived from (Hayden and Ghosh 2012).

Unstimulated, NF-κB is sequestered in the cytoplasm in its inactive form by IκB proteins (Figure 1-6). Stimuli such as TNFα or LPS activates the upstream IκB kinase (IKK) complex. This complex of kinase phosphorylates the IκB proteins, which are then targeted by the ubiquitin ligase machinery and degraded via the 26S proteasome. The NF-κB dimers are then free to translocate into the nucleus and bind to specific promoters where NF-κB is involved in the expression of over 150 target genes (Pahl 1999).

This general model for nuclear transduction of NF-κB uses the archetypical Rel complex p65-p50, and IκBα (Nelson, Ihekwaba *et al.* 2004). NF-κB oscillations between cytoplasmic and nuclear compartments have been shown to be directly out of phase with the levels of IκBα (Hoffmann, Levchenko *et al.* 2002; Nelson, Ihekwaba *et al.* 2004). Through the degradation and subsequent re-synthesis of IκB, NF-κB oscillations are observed. Western blotting only measures average responses of a population, making it difficult to see asynchronous oscillations within a population of cells. For this type of study, live cell fluorescence microscopy is essential as dynamics can be tracked in the same single cell over time. This has been used to great effect in observation of oscillations in p65 localisation in live cells, as these oscillations are shown to be essential transcription of late genes such as Rantes (Nelson, Ihekwaba *et al.* 2004; Paszek, Lipniacki *et al.* 2005).

The product of the NF-KB1 gene p105, is shown to adhere to the principles of this model but functionally differs in key aspects. As previously mentioned, p105 is the pre-processed form of p50 containing both p50 linked by a glycine-rich region between the p50 and a C-terminal portion as described by Li Lin and Sankar Ghosh as identical to IκBγ (Lin 1996). When unprocessed, p105 remains in the cytoplasm and also complexes with p65 keeping p65 localised in the cytoplasm (Palombella, Rando *et al.* 1994).

There is some disagreement within the literature as to how p105 is processed by cells. While it is universally accepted that IKK1 and IKK2, are activated through the TNFα pathway and directly phosphorylate p105 at serine 927 and 932 which results in the proteolytic degradation of c-terminal p105. There is disagreement whether

proteolytic processing is by endoproteolytic cleavage followed by c-terminal degradation, or proteolysis starting at the c-terminus of p105 and terminating at the GRR sequence. It is notable that deletion of the GRR domain allowed complete proteolysis of p105 indicating its importance (Yinon and Steven 2006) (Heissmeyer, Krappmann *et al.* 1999; Salmeron, Janzen *et al.* 2001). The classic model for co-translational processing suggested by lin *et.al* indicates that random ribosomal pausing during translation allows the c-terminal region of p105 to undergo proteolysis via the 26s proteosome. When the ribosome does not pause, p105 cannot be processed (Lin, DeMartino *et al.* 1998). Other models suggests that phosphorylation of p105 by IKK leads to the ubiquitin dependent partial proteolysis of the p105 molecule leaving the p50 subunit intact thanks to the GRR region of the molecule acting as a stop signal to the proteasome. (Orian, Schwartz *et al.* 1999). Another possibility is the cleavage of p105 before proteolysis of the C-terminal end shown to occur at the flexible region of the GRR region between residues 430 and 465. This would imply that p50 is produced prior to degradation of the C-terminal region of p105. This has been shown by both placement of cleavage site between two stable proteins and *in vitro* through use of purified proteins (Lin 1996; Moorthy, Savinova *et al.* 2006).

Similar cleavage behaviour can be seen in the *Drosophila* homologue Relish. It has been shown that *Drosophila* IκB Kinase complex (DmIKKβ and DmIKKγ) is required for the signal-dependent proteolytic cleavage of Relish. The N terminus of Relish then translocates to the nucleus and activates the transcription of antibacterial immune response genes (Silverman, Zhou *et al.* 2000).

Interestingly, free C-terminal p105 has yet to be detected in vivo, possibly due to its rapid degradation, and it is currently unknown whether indiscriminate endoproteolytic cleavage of p105 occurs. Although both IκBγ and p105 appear to be elevated in human cases of Alzheimer's disease (Huang, Liu *et al.* 2005), it remains to be seen if this is due to an intron-specific promoter sequence as seen in mice or the generation of IκBγ through p105 cleavage.

There are also some discrepancies in the literature as to what role the 20S proteasome plays in p105 degradation. Degradation through this pathway appears to be ubiquitin independent and translation-independent (Moorthy, Savinova *et al.* 2006). It may be that this pathway is used for constitutive processing of p105, generating p50 without need for stimulation of cells and ubiquitination and processing of p105 through the 26S proteosome, rather than ribosomal pausing.

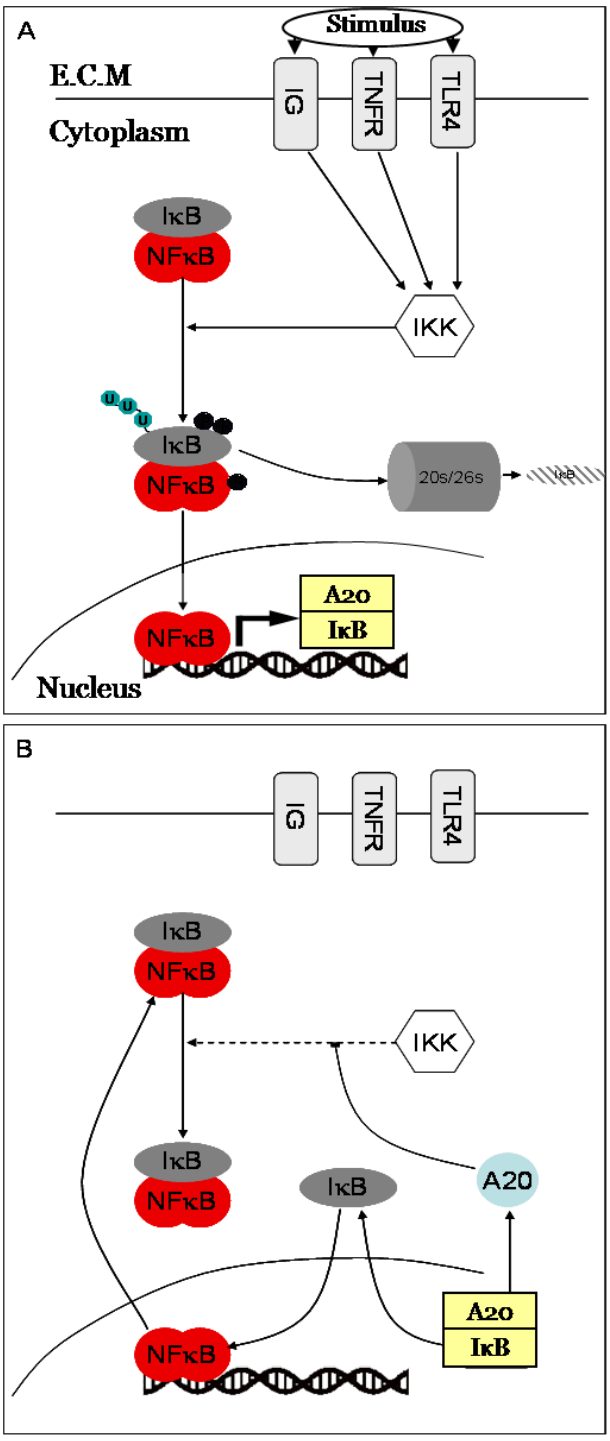

Figure 1-7 Schematic of NF-κB signalling.

NF-κB dimers translocate into the nucleus in response to an external stimulus (such as tumor necrosis factor alpha, lipopolysaccharide or an antigen). Phosphorylation and labeling for ubiquitination of IkB by IKK and IκB's subsequent ubiquitin-targeted degradation allows the p50-p65 heterodimer to translocate freely into the nucleus enabling expression of target genes. Transcription of IκB causes the heterodimer to be re-sequestered into the cytoplasm.

1.3.3 Multicellular Model Systems

Drosophila melanogaster has been used for nearly a century as a biological model system (St Johnston 2002). *Drosophila* have a short generation time and are well characterised genetically. They are relatively simple with only 4 chromosomes and many of the *Drosophila* genes have been found to have homologues in humans (St Johnston 2002). These characteristics make them ideal for use as a multicellular model system in which to investigate the role of protein-protein interactions and cell signalling dynamics *in vivo*.

1.4 Project Aims

The main aim of this project was to develop and apply the photoswitchable fluorescent protein Dronpa to pre-existing super resolution techniques; specifically the technique FRET. This technique is renowned for the complications introduced by spectral overlap and stoichiometric inconsistencies. Traditional fluorescent proteins do not allow the repeated probing of FRET through acceptor photobleaching due to its destructive effect on the fluorophore. By using the photoswitching properties of Dronpa, it was hoped that FRET efficiency can be repeatedly interrogated using the measure of both sensitised emission and donor quenching to help elucidate relevant and important dynamic biological functions within individual live cells over time.

It was also an aim to investigate if Dronpa could be used as a FRET partner in both mammalian and *Drosophila* systems, to demonstrate the flexibility of Dronpa in multiple systems. Due to the notable difference between homeostatic environments provided by the two systems this would demonstrate the utility of the technique for multiple applications. *Drosophila* also provide a unique system to study multicellular interactions with comparatively quick generation times compared to that of mammalian systems.

The first step was to find optimal pairs of donor and accepter FPs so that energy transfer between fluorophores was optimised to provide the most resolution in biological systems. It is also necessary to ensure the individual properties of potential FRET partners did not conflict with Dronpa (i.e. are not too bright, or dim, or unstable). Furthermore due to the mechanism employed by Dronpa to modulate its fluorescence, it was necessary to characterise fluorophores individually, to ensure that any unforeseen abnormalities in behaviour could be characterised and taken into consideration when quantifying protein FRET. The next step was to generate these pairs as artificial direct fusion constructs. These direct fusions could then be used to test FRET response in a system unaffected by biological variation introduced by functional cellular processes. This step was necessary to establish that the characteristics of Dronpa did not present any unexpected FRET effects from its conformational change.

Finally, the objective was to use Dronpa in known signalling systems. Initially, it was planned to apply Dronpa-modulated FRET to the NF-κB pathway. This was well characterised in mammalian cells and are readily amenable to the use of fluorescent proteins and confocal microscopy. The NF-κB pathway presents many opportunities for testing protein interactions due to the dimeric nature of transcription factors and tight regulation through IkB binding and masking of transcription factor nuclear localisation sequences (NLS). It should then be possible to elucidate live cell protein interaction dynamics in single cells that occur in this pathway which have previously been shown through co-localisation of fluorophores and bulk molecular assays such as co-IPs. As a complimentary microscopy method, FCCS was also used to validate any results observed through FRET.

The development of photoswitchable fluorescent proteins offers an exciting opportunity to develop a more quantitative approach for FRET analysis of protein interactions. In particular this offers the potential for real-time analysis of the dynamics of protein interactions. This is a major challenge in cell biology and a key aim is to develop new approaches that can be complementary to other imaging and biochemical techniques and which can identify and exclude the artefacts (often false positives) that have previously affected FRET measurements.

Chapter 2: Materials and Methods

2.1 Materials

2.1.1 Reagents

Tissue culture medium and non essential amino acids were purchased from Gibco Life Technologies (UK) and Foetal Bovine Serum (FCS) from Harlan Seralab (UK). Human TNFα was supplied by Calbiochem (UK). Oligodeoxynucleotides were purchased from Invitrogen (UK). Schneiders S2 tissue culture media and Penicillin-Streptomycin was purchased from Gibco (UK). All other chemicals were supplied by Sigma-Aldrich (UK).

2.1.2 Expression Vectors

Expression of all mammalian fluorescent fusion protein was controlled by a cytomegalovirus (CMV) immediate-early promoter unless otherwise stated. The orientation of FP and protein of interest is always written left to right as the proteins are expressed N- to C-terminally. The expression vectors containing pp65 CDS (Clontech, UK) have been described elsewhere ((Nelson, Ihekwaba *et al.* 2004)) Other cDNAs used to create Gateway™ expression vectors were obtained and cloned as indicated in the appropriate following sections of this thesis. All FP fusion vectors used to create Gateway™ destination vectors were obtained from Clontech. The reading frame cassettes, employed to create destination vectors, were purchased from Invitrogen.

2.2 Molecular Biology

2.2.1 Transformation of Chemically Competent E. coli Cells

Cells were thawed on ice for 30 min with the addition of 1-10ng of circularised DNA or 2µl ligation mixture (2.2.9). Heat shock was carried out at 42°C for 45 s. Cells were then placed on ice for 2 min, 250µl of room temperature S.O.C Medium was added, and cells placed into a 37°C shaker at 230 RPM for 1 h. Cells were then centrifuged at 11,500g for one min, re-suspended into 100µl of S.O.C. medium and plated onto agar plates plate (1% (w/v) bacto-tryptone; 0.5% (w/v) yeast extract; 1% (w/v) NaCl, pH 7.0; 1.5% (w/v) agar) with appropriate selection antibiotic (100µg/ml ampicillin or kanamycin, or 34µg/ml chloramphenicol as appropriate). Plates were then incubated for 16 h at 37°C. Suitable colonies were selected, and grown overnight in 5ml LB-Broth with appropriate antibiotic selection. These cultures were then DNA extracted using a Qiagen miniprep kit (described in following section).

2.2.2 DNA Purification

2.2.2.1 Small Scale DNA Extraction (Mini-prep)

E.coli cells containing plasmid DNA were cultured overnight in 5ml LB broth containing an appropriate selection agent at 37°C at 230rpm. The following morning, 2ml of the stationary culture was transferred to a 2ml micro-centrifuge tube and centrifuged at 12,000g for 1min. The remaining culture was stored at 4°C for future use. The supernatant was poured off and the DNA extracted from the bacterial pellet using the Qiagen Plasmid Mini Purification Kit (Qiagen, Germany) or the GenElute Plasmid Miniprep Kit (Sigma) according to the manufacturer's instructions. Both methods use an alkaline SDS cell lysis buffer and an acid precipitation buffer step to remove contaminating genomic DNA, and unwanted cell components. Precipitated DNA was centrifuged at 17,200xg, for 1min and the supernatant was passed through a column which adsorbed DNA onto an anion-exchange resin in the presence of high salt. After washing, the plasmid DNA was eluted in 50µl Elution Buffer (10mM Tris-HCl (pH 8.0), 1mM EDTA). Final DNA concentration was construct copy number dependent. DNA quality and identity was confirmed using an appropriate diagnostic restriction endonuclease digest followed by agarose gel electrophoresis (2.2.4).

2.2.2.2 Large Scale DNA Extraction (Maxi-prep)

E.coli cells containing plasmid DNA were cultured in a starter culture of 5 ml containing an appropriate selection for 8 h. 2ml of this culture was then used to inoculate 250ml LB broth containing an appropriate selection agent and incubated at 37°C with shaking at 230rpm for 16 h. The culture was then harvested through centrifugation at 15,000g in a bucket centrifuge for 15min at 4°C. The QIAfilter Plasmid Maxi Kit (Qiagen) or the GenElute Plasmid Maxiprep Kit (Sigma) was used in accordance with the manufacture's guidelines. DNA eluted from the anion-exchange columns was relatively dilute and was concentrated by isopropanol precipitation. The eluted DNA solution was combined with 0.7 volumes of room-temperature isopropanol and centrifuged using a Thermoscientific CL40 SS-34 rotor at 15,000g for 30min at 4°C. The supernatant was discarded and the DNA pellets were washed by centrifugation at 15,000xg for 15min in 70% $_{(V/V)}$ ethanol at room temperature to remove salt and isopropanol from the DNA. The pellets were air-dried for 5-10min and dissolved in 350µl TE. The concentration of the plasmid DNA was determined by NanoDrop (2.2.3), adjusted to 1µg/µl with TE and stored at -20°C.

2.2.3 DNA Quantification

DNA concentration was quantified through use the Thermo Scientific NanoDrop™ 1000 Spectrophotometer. The NanoDrop uses a 1-2µl sample held in place by surface tension of the liquid. The NanoDrop measures absorbance of the sample over a 220nm-750nm spectrum reporting DNA concentration and relative purity of the sample with 230/260 and 260/280 ratio measurements. The NanoDrop was able to measure samples up to 3700µg/µl and so removed the need for serial dilution of DNA samples to ensure accurate measurment.

DNA was also semi-quantified through restriction analysis and the subsequent intensity of visualised bands compared to reference ladder concentration to confirm results of NanoDrop.

2.2.4 Restriction Endonuclease Digests

Restriction enzymes (New England Biolabs) were used to cut cDNA. Standard digestion protocol for complete digestion in a 20µl reaction volume consisted of 500ng DNA, 0.5µl restriction enzyme (RE), 1x reaction buffer (supplied) and remaining volume was made up to 20µl using MilliQ dH_20. Double digest used 0.5 µl per RE. RE concentration was kept below 5% to minimize possible STAR activity of endonucleases. Digests were incubated for a minimum of 3 hr to ensure efficient digestion. Digestions were also conducted overnight if endonuclease showed low non-specific activity. In instances where buffer incompatibility meant double digests would not be feasible, products were purified using Qiagen PCR cleanup kit, as per manufacturer's instructions, and eluted into 35µl volumes. 5µl of this was used between digest steps to run on an agarose gel to check digest efficiency. Previously described in house mammalian Gateway expression vectors were used as the basis for customised expression vectors (Nelson, Paraoan *et al.* 2002).

2.2.5 Gel Electrophoresis

DNA fragments were separated by agarose gel electrophoresis using 1x TAE buffer (Tris-acetate-EDTA: For 50x solution – 242g Tris base, 57.1ml glacial acetic acid, 100ml 0.5M EDTA (pH 8.0)). Agarose gels were made at varying concentrations depending on the size of fragment for visualisation with TAE. Gels were heated to below boiling point of TAE to dissolve agarose without reducing volume (Table 2-1). CyberSafe/EtBr was added to a final concentration of 0.5µg/ml. The loading buffer Orange G was then added to the DNA samples as a 1:5 dilution. Samples were

run with DNA ladder HL1 (10,000-100bp) (NEB) for vectors, backbones and large PCR products. HL4 (1000-100bp) (NEB) was used for most PCR products. Gels were suspended in TAE and run at 100volts for 30 min for visualising products and 2 h at 80volts for gel extractions.

Table 2-1 Agarose Gel Percentages for DNA Fragment Separation

Agarose in gel% w/v	Best range of separation (kb)
0.3	5.0-50
0.5	1.0-25
0.8	0.7-8.0
1.0	0.5-7.0
1.2	0.4-6.0
1.5	0.2-3.0
2.0	0.1-2.0

Gels were visualised under 302nm (UV) light using a trans-illuminator and imaged using GeneFlash with PULNiX TM-300 CCD (Syngene). Desired DNA fragments were cut from the gel by scalpel blade and purified using the QIAquick Gel Extraction Kit (Qiagen). In this protocol, agarose is dissolved to release the DNA, which is then bound to an anion-exchange membrane as used in plasmid preparation kits. Purified DNA fragment is then eluted in 30µl TE.

2.2.6 PCR and introducing Cut Sites

Polymerase Chain Reaction (PCR) and subsequent visualisation of fragments was used to confirm successful ligation of backbone and insert cDNA and success of Gateway recombination. For these diagnostic procedures, NEB Taq (1.25U/50ml) supplied with standard 10xTaq buffer was used (catalogue no. #M0273) along with 10mM NEB dNTPs (N0447L) (final concentration 100µM) and 10µM forward & reverse primer (final concentration 100nM per primer). A PCR Thermocycler px2 (ThermoScientific) using standard thermocycling conditions (as per manufactures instructions) was used for amplification. The lowest primer annealing temperature was used to determine annealing step temperature. A maximum of 30 cycles was used to amplify DNA.

A standard thermocycling program used as a template for standard PCR reactions as follows.

Denaturation	98°C	15sec	1 cycle
Denaturation	98°C	30sec	30 cycles
Annealing	50-70°C	30sec	
Primer Extension	72°C	15-30sec/kb	
Final Extension	72°C	10min	1 cycle

Loading buffer was then added and PCR products were run on agarose gel for analysis.

For cDNA requiring insertion into circularised DNA, new flanking complimentary restriction sites could be introduced by PCR using primers with a new restriction site sequence synthesised before or after the region homologous to the sample DNA. In this way, inserts could be amplified with small regions of additional sequence. The high fidelity DNA polymerase KOD Hot Start (Novagen® product no. 71086-3) was used for amplifying inserts with new cut sites.

2.2.7 Site Directed Mutagenesis

This was carried out to mutate a STOP codon sequence to truncate transcribed CDS sequence where needed. The QuikChange Lightning Site-Directed Mutagenesis Kit (Alient Technologies Catalogue no. 210518) was used for mutagenesis of circularised plasmid DNA. The kit uses overlapping sense and antisense primers with flanking homology to the desired site of mutation, with altered bases at the mutation site to generate the desired sequence. Using PCR, template DNA was amplified by PCR, using 10-100ng template DNA and 125ng of both 5’ to 3’ and 3’ to 5’ primers for 1h at 37°C.

The PCR conditions were as follows:

Denaturation	94°C	2min	1 cycle
Denaturation	94°C	20sec	20 cycles
Annealing	60°C	10sec	
Extension	68°C	30sec/cDNA kb	
Final Extension	68°C	10min	1 cycle

The restriction endonuclease *Dpn* I was added to PCR products. *Dpn* I digests parent methylated and hemimethylated circularised DNA, while leaving unmethylated DNA generated through PCR. 2µl of the PCR reaction was then transformed into 50µl MAX Efficiency XL10 Gold® chemically competent cells as described using the method in Section2.2.1. DNA mutation and fidelity was confirmed through sequencing.

2.2.8 5'-Phosphate removal

To prevent self-ligation of backbone cDNA, incubation with 1U/µg DNA with Shrimp Alkaline Phosphotase (SAP) was employed to remove 5'-phosphates from RE-digested vector backbones. Products were purified using Qiagen PCR cleanup kit, as per manufacturers instructions, and eluted into 30µl volumes.

2.2.9 Ligation and Transformations

Digested products were run on an appropriate percentage agarose gel and fragments extracted using Qiagen gel extraction kit as per manufacturer's instructions. Complementary linear DNA fragments formed from digestion and extraction as previously described were ligated into circular plasmids using T4DNA ligase (Roche). For ligation, two fragments totalling approximately a 3:1 molar ratio of insert:vector was used as per manufacturer's instructions. The following equation was used to calculate appropriate amounts of DNA to use for a 3:1 molecular ratio:

$$\frac{\text{ng of vector} \times \text{kb size of insert}}{\text{kb size of vector}} \times \text{insert : vector molar ratio} = \text{ng of insert}$$

Molecular ratios could be altered as needed depending on success of ligation. 1U of T4 DNA ligase was incubated with a total of 100ng of DNA using a final concentration of 1x reaction buffer. Reaction volumes were kept at 20µl as per manufacturers guidelines. Reaction mixtures were incubated at 16°C for 20h. 2-4µl of the ligation reaction was then transformed into competent DH5α *E.coli*. Ligations were screened by PCR using primers on the backbone and insert, the ligated plasmid was transformed into chemically competent *E.coli*.

2.2.10 Directional TOPO® Cloning

Drosophila Gateway entry vectors were created using the pENTR Directional TOPO® Cloning kit from Invitrogen. PCR primers were designed to amplify the DNA sequence of specific genes of interest from Drosophila wild type cDNA. The forward primers for both proteins contained an additional CACC sequence at the 5'end to ensure that the PCR product was cloned into the entry vector in the correct orientation.

The PCR products were purified using the Qiagen PCR cleanup kit and DNA concentration was quantified by NanoDrop. 5-20ng of the PCR product was mixed with the entry vector, pENTR/D-TOPO, in a 2:1 molar ratio, along with 1µl proprietary salt solution and sterile water, to a final volume of 5ul, and incubated at room temperature for 30 min. One Shot® Top10 competent cells were thawed on ice for 10 min, 2µl of the TOPO cloning reaction was then added to 50µl of the thawed cells and incubated on ice for 30 min. Cells were then treated as transformants in section 2.2.9.

2.2.11 Generating mRNA and cDNA from Genomic DNA

RNA was extracted from homogenised adult *Drosophila*. Adult flies were flash-frozen in LN_2. Samples could then be stored at -80ºC until required. A pestle and 2ml eppendorf tube were used to homogenise *Drosophila* material. The RNAqueous Micro Kit (Ambion, Invitrogen cat. No. AM1931) was used to extract the RNA immediately following homogenisation. Initially 100µl lysis solution and 50µl 100% EtOH was added to 10mg of homogenate, the samples were then briefly centrifuged and repeatedly passed through a pipette tip to ensure that the tissue samples had been completely disrupted. The extraction procedure then followed the manufacturer's instructions. Briefly the lysis mixture was passed through a selective filter which binds RNA, the RNA was subsequently washed and eluted from the filter. DNase I was added to the elute to remove any trace amounts of genomic DNA. The RNA samples were stored at -20ºC for later use for generation of cDNA of *Drosophila* wild type proteins.

2.2.12 DNA synthesis

The Superscript III First-Strand Synthesis System for RT-PCR (Invitrogen Cat. No: 18080-051) was used to synthesise cDNA from RNA in accordance with the manufacturer's instructions. Briefly, RNA was incubated with oligo(dT) and dNTPs

at 65ºC for 5 min. The mix was placed on ice for 1 min before the cDNA synthesis mix, containing reverse transcriptase, was added. cDNA synthesis was allowed to proceed for 50 min at 50ºC before the reaction was terminated at 85ºC. To remove any RNA from the synthesised cDNA, RNaseH was added to the sample and incubated at 37ºC for 20 min. The cDNA samples were stored at -20ºC. These samples could then be used to amplify cDNA for functional proteins using flanking primers targeted to the protein of interest using identified consensus sequences from http://www.flybase.org (in this case SRF and Actin5C).

2.2.13 Gateway system and recombination

Gateway recombination reactions require a final quantity of 150ng for each reaction, and rely on the exchange of DNA through the recombination homologous att sites. Once both vectors were mixed together, 2µl of Clonase II enzyme was added (Invitrogen catalogue no. 11391-100). The mix was made up to a final volume of 10µl using filter-sterilised TE buffer and incubated at 25°C (incubator) for 3 h. The enzyme was then denatured by adding 1µl Proteinase K (included in Clonase kit), and incubated at 37°C for 15 min.

Recombination mixes where then transformed in the same way as described in 2.2.9 using 2µl of the reaction mixture, with the use of DH5α *E.coli*. This strain has no resistance to the CCDB cassette which improves selection for correctly recombined vectors. To check transformants the primers pENTR2a Fwd and Rev (Table 1) were used.

2.2.14 DNA Sequencing

DNA sequencing was carried out by GATC, Germany (gmbH) (http://www. gatc-biotech.com/en). DNA was provided for a total of 6 reactions at a concentration of 30-100ng/µl and a total volume of 20µl. DNA was suspended in ultra pure dH_20. General inhouse primers were provided for sequencing reactions (e.g. CMV-FWD); the option for custom primers was also available. Custom primers were provided for GATC as a total volume of 30µl and a concentration of 10µM. Primers. Sequencing primers were designed with a theoretical melting temperature of 60°C and a Guanine/Cytosine composition as close as possible to 50%. Sequencing analysis was performed with MegAlign software (DNA Star) using estimated references from *in silico* plasmid maps created using VectorNTI (Invitrogen). Additional confirmation of sequences was carried out by NCBI BLAST searches.

2.3 Cell culture

2.3.1 Subculturing cells

HeLa (ECACC No. 93021013) and SK-N-AS (ECACC No. 94092302) cells were chosen due to their low mobility and their ease of transfection compared to other cell types. Cells were cultured as a monolayer and grown in Minimal Essential Medium (MEM) with Earle's salts, supplemented with 10% fetal calf serum (FCS) and 1% non-essential amino acids and maintained at 37ºC with 5% CO_2. Cells ($0.5x10^6$) were passaged when the monolayer reached 80% confluency in a 75 cm^3 tissue culture flask in a final volume of 20 ml.

Cells were washed with Phosphate Buffered Saline (PBS) then incubated with 1 ml of 0.05% (w/v) trypsin in 0.53 mM EDTA detaching the monolayer from the flask. Cells were resuspended in 9 ml complete medium and centrifuged (1000 rpm for 5 mins) to remove the trypsin and cell debris. The supernatant was discarded and the cell pellet resuspended in 5 ml medium. Cells were counted using a Z2 Coulter counter (Coulter, UK), diluted in medium and seeded as required.

2.3.2 Transient Transfection and Imaging

For confocal fluorescence microscopy HeLa and SK-N-AS cells were plated on 35mm glass-bottom dishes (Iwaki, Japan) at $5.0x10^4$ and $1.8x10^5$ cells respectively in 3ml growth media. 100µl MEM was warmed to 37ºC to aid formation of micelles. 2µl fugene (Roche) was then added and left for 5 min. A total of 1µg of DNA was then added and to the mixture, and micelles were left to form over 20 to 40 min. Cells were seeded and transfected simultaneously with the appropriate plasmid(s) and were imaged 24h post transfection.

2.3.3 TNFα Treatment

Cells treated with TNFα to stimulate NF-κB response were treated with 3µl of a 10µg/µl concentration mixed in 100µl MEM (to enable faster diffusion) for a final concentration of 10ng/µl in 3ml of media. MEM was taken directly from Iwaki dishes being imaged, and applied after one cycle of imaging to obtain unstimulated data values before TNFα stimulation.

2.3.4 *Drosophila* S2R+ Cell culture

Drosophila melanogaster S2R+ cells were cultured in Schneider's Insect Medium With L-glutamine (Gibco cat no. 11720-034) with the addition of 10% FCS and 1% 1:100 Penicillin-Streptomycin (Gibco cat no. 15070-063). Cells were maintained at 25ºC seeded in a 75 cm^3 tissue culture flask in a final volume ($0.5x10^6$) of 15ml and were passaged every 3-4 days. Cells required constant selection to maintain adherent properties. Cells were transferred by removing detached cells through vigorous agitation of flask and washing with PBS. 10ml of new medium was then added to the flask and the remaining adherent cells were then vigorously agitated followed by repeated pipetting of cells (5-10 times) to ensure cells had not formed clumps. 5ml medium was then transferred to a new flask. 10ml medium was added to flasks.

2.3.5 S2R+ Transfection

For confocal fluorescence microscopy S2R+ cells were plated on 35mm glass-bottom plates pre-coated with poly-d-lysine (MatTek, USA cat no. P35GC-0-10-C). Cells were plated at 3.5×10^5 in 4ml growth media (approximately 60% confluency). Cells were then transfected with Effectene as per manufacturer's instructions (Qiagen, cat no. 301425). 0.4µg total plasmid DNA was condensed by interaction with the 3.2µl of Enhancer in EC Buffer to a final volume of 100µl and incubated for 5 mins. 10µl Effectene Reagent was then added to the condensed DNA to produce condensed Effectene–DNA complexes. The Effectene–DNA complexes were mixed with 1.4ml medium to aid faster diffusion and directly added to the cells. Cells were then imaged 48 h following transfection.

2.3.6 Stimulation with Latrunculin

Latrunculin A is an inhibitor of actin filaments which associates with actin monomers preventing the further formation of polymers (Wakatsuki, Schwab *et al.* 2001). Used to alter actin dynamics within S2R+ cells, a final concentration of 200ng/ml was used to stimulate changes in actin cytoskeleton dynamics. The master stock solution was reconstituted in anhydrous DMSO to a final concentration of 100mg/mL and stored at -20 ºC away from light sources.

2.4 Western Blotting

2.4.1 Preparation of Protein Samples

SK-N-AS cells were plated at a density of $5x10^5$ per dish in 60mm dishes and simultaneously transfected appropriately. 24h post plating, the cells were treated with 10ng/ml TNFα for the indicated times (as described in 2.3). Cells were washed with ice cold PBS. 1ml Lysis buffer (1% (w/v) SDS, 10% (v/v) glycerol, 10% (v/v) β-ME, 8% (v/v) 0.5M Tris pH6.8, 0.01% (w/v) bromophenol blue) was then added to dishes for 2 mins and cells were then scraped and lysates collected into 2ml micro-centrifuge tubes and held on ice until lysate collection was complete. Lysates could be stored at -20°C for later use or boiled at 100°C for 5min. Protein samples were then separated by SDS polyacrylamide gel electrophoresis (SDS-PAGE).

2.4.2 Preparation of SDS-PAGE Gels

SDS-PAGE gels were cast using the Mini-PROTEAN 3 System and glass plates with 0.75mm integrated spacers (Bio-Rad, UK). 10% polyacrylamide resolving gels were produced by combining 6.7ml of 30% (v/v) acrylamide/bis-acrylamide, 8.3ml of ddH2O and 5ml of main-gel buffer (1.5M Tris 0.4% SDS– HCl pH8.8) and polymerisation was initiated by adding 10ul of 100ng/ml APS 10% (w/v) ammonium persulphate (APS) and 25µl N,N,N′,N′-Tetramethylethylenediamine (TEMED). The gel solution was poured between the glass plates in the casting frames held in the casting stand allowing 3cm at the top for the stacking gel. The gel was overlaid with ~3mm of ddH_2O and allowed to set. The stacking gels were produced by combining 1ml of 30% (v/v) acrylamide/bis-acrylamide, 9.2ml of H2O and 1.75ml of stacking-gel buffer (0.5M Tris–HCl pH6.8) and polymerisation was initiated by adding 50µl APS and 25µl TEMED. The water was removed using blotting paper, the stacking gel solution was then poured on top of the main gel, the 10-well combs added and the gels allowed to set.

2.4.3 Protein Separation by SDS-PAGE

Gels were loaded into a Mini-PROTEAN 3 (Bio-Rad) clamping frame and electrode assembly then suspended in the Mini-PROTEAN 3 gel tank. The reservoir was filled with running buffer (25mM Tris, 192mM glycine and 3.4mM SDS). 18µl protein samples were loaded onto the gel along with 4µl of biotinylated protein ladder (Cell Signaling, USA). The samples were electrophoresed at 180V for approximately 60min until the bromophenol blue was close to the bottom of the gel.

2.4.4 Transfer of Electrophoresed Proteins to Nitrocellulose

After electrophoresis separation of protein samples, the stacking gel was removed and discarded, and the main gel was washed in (TBS, 0.1% (v/v) Tween-20). Proteins were transferred to nitrocellulose blotting membranes (Optitran BA-S85, Schleider & Schuell) using an ice-cooled Mini Trans-Blot Cell (Bio-Rad). The blotting tank was filled with transfer buffer (20% (v/v) methanol, 25mM Tris, 200mM glycine) completely submerging the gels and nitrocellulose. 100mA was applied across the membrane overnight.

2.4.5 Probing Membrane

Nitrocellulose membranes were soaked for 30min in Tris-buffered saline (TBS) (20mM Tris, 140mM NaCl, adjusted to pH7.6), then incubated at room temperature in 10ml blocking buffer (0.1% (v/v) Tween-20, 5% (w/v) non-fat milk powder in TBS) for 1h to prevent non-specific binding. The membranes were washed 3 times for 5min each in TBS-T (TBS, 0.1% (v/v) Tween-20) and incubated overnight with 10ml primary antibody diluted in TBS-T and 5% (w/v) BSA. All primary IgG antibodies were raised in rabbit, purchased from Cell Signalling and were used at a dilution of 1:1000. The following day, membranes were washed 3 times in TBS-T for 15 mins, and incubated for 2h with 8ml secondary antibodies (horseradish peroxidase- (HRP) conjugated goat anti-rabbit IgG and HRP-conjugated goat anti-biotin IgG (both Cell Signalling), diluted 1:2000 in blocking buffer. After further washing, membranes were incubated for 5min with 5ml chemiluminescent (CL) substrate (1:1 mix of CL solution 1 (100mM Tris-HCl pH8.5, 2.5mM luminol, 400µM paracoumaric acid) and CL solution 2 (100mM Tris-HCl pH8.5, 1.92% (v/v) H_2O_2)). The blots were wrapped in a single layer of cling-film and signal detected by exposure to Kodak Biomax Light films (Sigma).

2.5 Imaging Techniques

2.5.1 Live-Cell Imaging

Confocal fluorescence microscopy was carried out on transfected cells in glass-bottomed 35mm dishes (section 2.3.2) in a Zeiss XL incubator (37°C, 5% CO_2). Several different imaging systems were used for experiments.

A Zeiss LSM510 Axiovert confocal microscope with a Spectrophysics pulsed multiphoton MaiTai laser was used for multiphoton excitation of samples, in addition to a standard Argon ion laser and 561nm diode laser for imaging with standard wavelengths. A x40 1.3NA oil immersion apochromat objective was used for imaging. Standard filtersets were available for imaging using ECFP, EGFP, EYFP and DsRedXP as well as UV excitation such as DAPI.

A Zeiss LSM 710 Axiovert with Confocor FCS module was generally used for UV excitation and FCCS data collection. UV excitation was carried out using a 405nm laser while an Argon ion laser and 561nm diode laser were used for imaging with specified standard wavelengths. A Plan-Apochromat 40x/1.4 Oil DIC M27 objective lens was used on this system for imaging. A wide range of spectral options were available due to the 34 channel QUASAR detection unit. This allowed superior spectral separation of fluorophores.

A Zeiss LSM780 with GaAsp detectors was used for imaging as well as FCS and FCCS with the wavelength specified in each section. A Fluar 40x 1.4NA oil immersion objective lens was used on this system for imaging studies.

Live cell imaging was conducted using the zeiss Zen MTS macro which allowed the creation of complex imaging scenarios including multifield time series experiments with bleaching steps and autofocus to control for minor temperature changes causing focal changes through expansion and contraction of the dish. All of these functions would not have been available in both AIM and Zen2010B software suites without the use of this macro. Live cell time lapse imaging data sets were analysed using Cell Tracker, a program specifically developed for use with such datasets (Shen, Nelson *et al.* 2006). Both cytoplasm and nuclear compartments were tracked over multiple frames for each field in a time series experiment. Data sets were then exported to Excel for further analysis (Microsoft, USA).

2.5.2 FRET: Optimised Illumination Strategy

While optimisation of an illumination strategy is discussed at length in Chapter 3, two distinct illumination strategies were finalised for the majority of biological experiments. They differ by the use of either multiphoton excitation or UV excitation of Dronpa to promote activation. Switching Dronpa into the off state was achieved using the 488nm line of an Argon Ion laser to simultaneously image and switch Dronpa into the off state.

Table 2-2 Time lapse imaging parameters

	488nm Excitation	**458nm Excitation**	**Switch parameters**	**Image Properties**	**Lightpath settings**
LSM510E Multiphoton	4.5%	5%,	810nm 2.5% 25it	512x512 stack 12bit	458/466/810nm beam split 515LP I_{AA}/I_{DA} Band pass I_{DD} Band pass
LSM710 405nm UV	4%	3.5%	405nm 1% 5it	256x256 stack 8bit 2.55µs pixel dwell	458/488 vis beam splitter 405 invis beam splitter I_{AA} range I_{DD} Range I_{DA} range

Separation of ECFP and EYFP fluorescence was carried out using the linear unmixing algorithms in Ver. 3.0 of the Zeiss LSM510 software (Zeiss). This was carried out through comparison with reference spectra taken from cells expressing ECFP or EYFP alone or nothing (background reference). The fluorescence spectrum was separated into ECFP, EYFP and background signals. FRET was assayed by acceptor (EYFP) photo-bleaching. For bleaching the entire cell assayed was exposed to 50 iterations of 514nm laser light set at 100% power. Once signals were unmixed into respective channels, fold-change in donor fluorescence, relative to an unbleached cell in the same field of view, were used as a measure of FRET. Multiple cells were averaged and data were expressed as mean change in donor fluorescence +/- SD.

2.5.3 FCS and FCCS

FCS and FCCS was carried using either a Zeiss LSM780 with or Zeiss 710 with confocor 3 mounted on an Axio observer Z1 microscope with a 63x C-apochromat, 1.2 NA water-immersion objective. Zen 2010B was used for data collection and analysis. EGFP fluorescence was excited with 488 nm laser light and emission collected between 500 and 530nm dsRed-express was excited with 561 nm laser light and emission collected between 580 and 630nm. The protocols as outlined in Kim et al. (Kim, Heinze *et al.* 2007) were followed, with 10 x 10 s runs used for each measurement. The lateral beam dimension was estimated to be 229 ± 6.3 nm using Rhodamine 6G as a known calibration standard. A structural parameter value of 5, which is the ratio of the axial to lateral beam dimensions, was assumed. Free EGFP in cells was measured to have a diffusion rate of 27 ± 5.8 $\mu m^2 s^{-1}$, agreeing with previous measurements (Baudendistel, Müller *et al.* 2005).

The intensity fluctuations recorded and their auto and cross-correlation function calculated on ZEN 2010. Measurements (10x10s) were carried out in cytoplasm or nucleus, with binning time of 200ns. The data was fitted into a mathematical model describing one or two component diffusion; the appropriate model was selected based on the Chi^2 value describing each fit. The cross-correlation function included correction for triplet state transitions of fluorophores and assumes Brownian diffusion of molecules.

Chapter 3: Tools and Optimisation

3.1 Introduction

The aim of the work described in this chapter was to establish the methodology for real-time FRET using a switchable fluorescent protein. This required: 1) the identification of candidate switchable fluorescent proteins; 2) characterisation of their properties and the optical strategy for switching their fluorescence; and 3) the identification of appropriate donor or acceptor fluorescent proteins that could be used. The careful identification of these basic conditions for the assay was an essential first step to the establishment of a robust and quantitative assay.

3.2 Testing Methodology

Dronpa was singled out as the most likely candidate for a repeatedly switchable component in a FRET system due to its relatively high quantum yield and photostability compared to other available photoswitchable FPs (see Chapter 1). The three dimensional structure of Dronpa as a protein has only recently been elucidated x-ray diffraction of crystal structures. The working hypothesis for how photoswitching is achieved has only recently been proposed (Andresen, Stiel *et al.* 2007; Bourgeois and Adam 2012). It was deemed necessary to rigorously test Dronpa to ensure unexpected behaviour of the fluorophore did not invalidate its use as a FRET partner.

Characterising the behaviour of Dronpa and optimising the change in fluorescence using both multiphoton and UV excitation was considered important, since the availability of both methods of switching would increase the flexibility for the use of Dronpa on different microscope systems and indifferent experimental situations where varying fluorescent proteins are used in the same experiment. Following this, the rigorous testing of potential FRET partners using optimised illumination strategies was employed to ensure that partners behaved as expected and would not prevent detectable energy transfer or report false positives.

The final stage of this optimisation was to generate positive control constructs that would report the most efficient energy transfer between fluorophores to act as a benchmark for every system being used to both calibrate, and detect maximum FRET efficiency, and to compare to biological FRET partners.

3.3 Dronpa Photoswitching Optimisation

The Dronpa switchable fluorescent protein was introduced in Chapter 1. It was selected as the most appropriate candidate for this assay through prior work in the laboratory. The optimal illumination strategy for Dronpa is dependent on several factors which needed to be carefully considered. The optical switching behaviour of Dronpa is determined in part by the protein to which it is fused, the optical efficiency and parameters of the imaging system and the environment in which the fusion protein is being expressed. The combination of these factors means that ideally the behaviour of Dronpa should be characterised for a set of fusion proteins expressed in specific cell lines for any given imaging system, so that an optimised illumination strategy can be established.

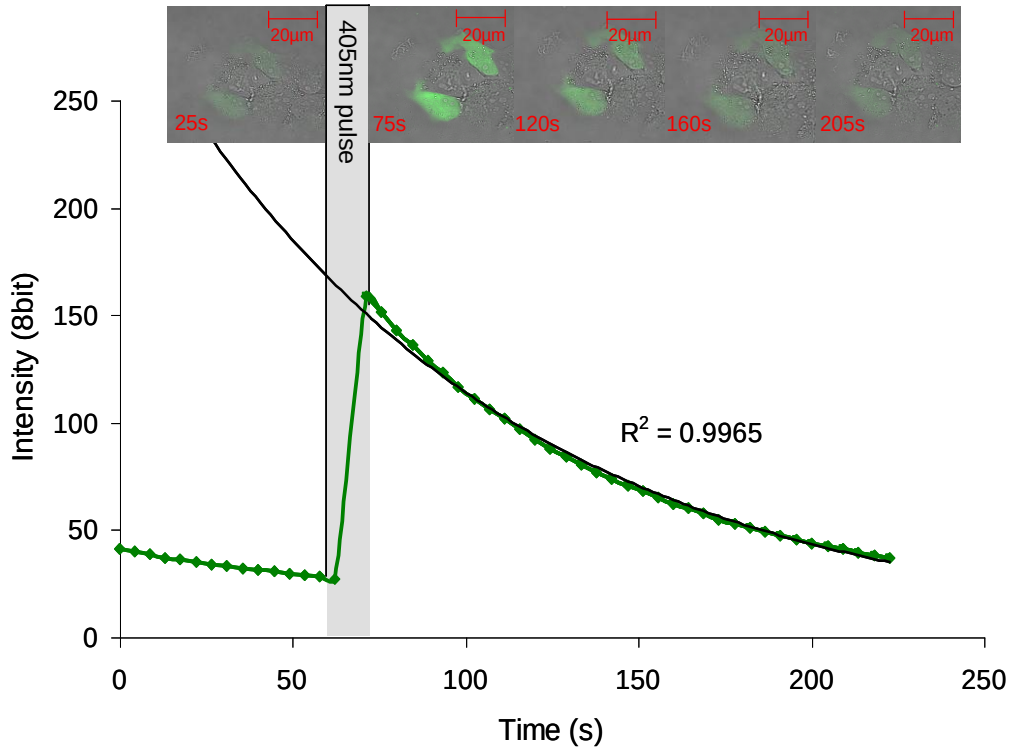

Figure 3-1- Illumination to activate and inactivate Dronpa fluorescence.
A single SK-N-AS cell expressing pG-CMV-Dronpa was imaged with a 488nm laser line for 225s every 5s and fluorescence levels analysed. Imaging simultaneously partially converted Dronpa to an off (protonated) state. Then Dronpa was switched to the on state (deprotonated) using a 405nm laser pulse at 62 seconds using 5 iterations at 1% laser power. An exponential fit was found to match decay following photoswitching.

Figure 3-1 demonstrates the strategy adopted to maximise photoswitching. The figure illustrates that deactivating Dronpa takes exponentially longer the closer to 0 the signal gets. As reported in Habuchi *et.al.* the switching of Dronpa follows a first order kinetic model (Habuchi, Ando *et al.* 2005). This implies that the switching off of Dronpa is impeded due to the raster scanning motion of the laser. As a result there is always some detectable fluorescence as it becomes too time intensive to completely switch off the fluorophore.

To that end, Dronpa photoswitching behaviour was characterised using the control construct pG-Free Dronpa (Table 3-1) expressed in both SK-N-AS and HeLa cells on three separate confocal laser scanning systems.

3.3.1 Multiphoton Excitation

It was initially decided to optimise Dronpa switching using a multiphoton laser light source. This was to minimise the potential damage that 405nm illumination is known to cause through generation of reactive oxygen species (Kvam and Tyrrell 1997; Lan, Nakajima *et al.* 2005). These experiments were carried out using a Zeiss 510E laser scanning confocal microscope with a Newport/Spectraphysics MaiTai multiphoton laser, The Dronpa photoswitching was optimised with an iterative process.

Three variables were adjusted to optimise the switching efficiency. These were: 1) laser attenuation (which was controlled by the AOTF); 2) the number of times (iterations) a ROI was repeatedly scanned using the X and Y galvanometer mirrors; and 3) the wavelength of light used for illumination. These parameters were changed one at a time in a logical sequence. Initially the switching wavelength was set at 810nm due to the reported optimal UV wavelength of 405nm which has been used to photoconvert Dronpa(Habuchi, Ando *et al.* 2005).

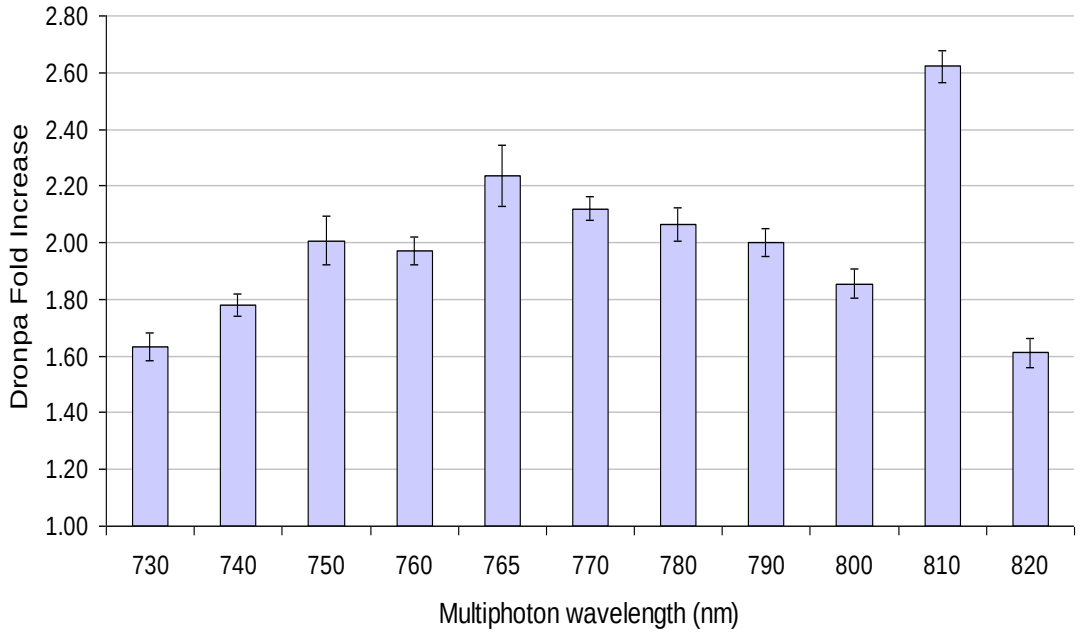

Figure 3-2 Effect of multiphoton wavelength on Dronpa switching.

A population of 10 SK-N-AS cells expressing pG-CMV-Dronpa. Using 20 iterations and AOTF at 3% attenuation, different far red wavelengths were used to establish the most effective wavelength for photoswitching. The fluorescence of Dronpa post-switching was normalised to the pre-switch fluorescence. The mean for each set of conditions was taken. Error bars show standard deviation between cells.

The use of different multiphoton wavelengths clearly showed that 810nm was the most efficient wavelength for photo-switching with a 1.4 fold better efficiency (+-0.06 SD) in fluorescence compared to the next best wavelength (Figure 3-2). Interestingly, the second highest peak was at 765nm implying that this may identify an alternative absorbance peak for switching Dronpa at a shorter multiphoton wavelength.

Increasing the number of iterations and the amount of laser light used to illuminate the sample had a measurable effect on switching efficiency (Figure 3-3). The most efficient switching was observed using 35 iterations and 3% laser power showing a 3.06 fold increase (+-0.16 SD). This illumination strategy took an average of 16 s. Using a reduced number of 20 iterations was favoured in order to prevent fluorophore damage and phototoxicity. It also had the added advantage of maximising the speed of switching (saving approximately 6 s). The use of 20 iterations at 3% laser power was 15% less efficient (+-2.3% SD) compared to using

35 iterations. The benefits of reduced illumination were considered to outweigh the small loss in switching efficiency. These conditions were used to observe differences in switching efficiency by changing activation wavelength.

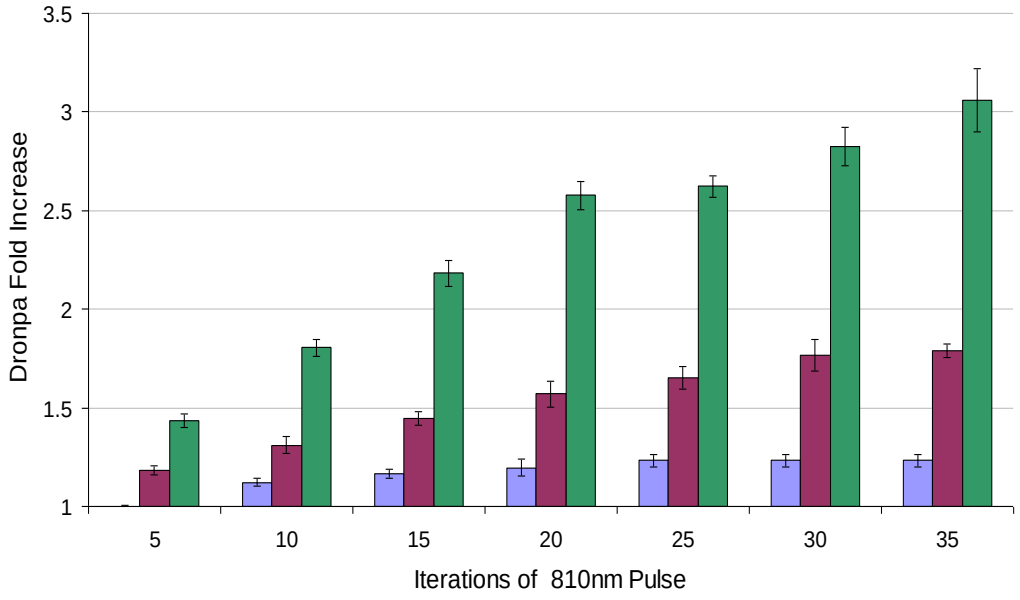

Figure 3-3 Effect of the number of iterations of illumination at 810nm on Dronpa switching.
A population of 10 SK-N-AS cells expressing pG-CMV-Dronpa. The x-axis indicates the increasing number of iterations of 810nm Dronpa switching pulses. Different bars represent different AOTF attenuations with blue at 1%, purple at 2% and green at 3% illumination. Post-switch Dronpa is normalised to the pre-switch fluorescence. (at time 62 s in Figure 3-1). This should represent Dronpa in its most protonated form. Therefore, the fold change in Dronpa represents the relative change in fluorescence from the lowest fluorescence value following an extensive period of imaging. The mean for each set of conditions was taken. Error bars show standard deviation between cells.

3.3.2 Switching Dronpa with 405nm Excitation

As an alternative to multiphoton excitation, illumination with the 405nm laser line was also investigated. This proved to be an effective way of switching Dronpa fluorescence on. Optimisation of the AOTF settings showed little variation, with increasing laser power showing no significant difference suggesting that very low level illumination could be used (Figure 3-4). 5 iterations were used switching Dronpa. This procedure took under 2.7 s (+- 0.3SD, n=10). A fixed value of 1% using 5 iterations was chosen to switch Dronpa in future experiments with 405nm illumination as it showed low variation.

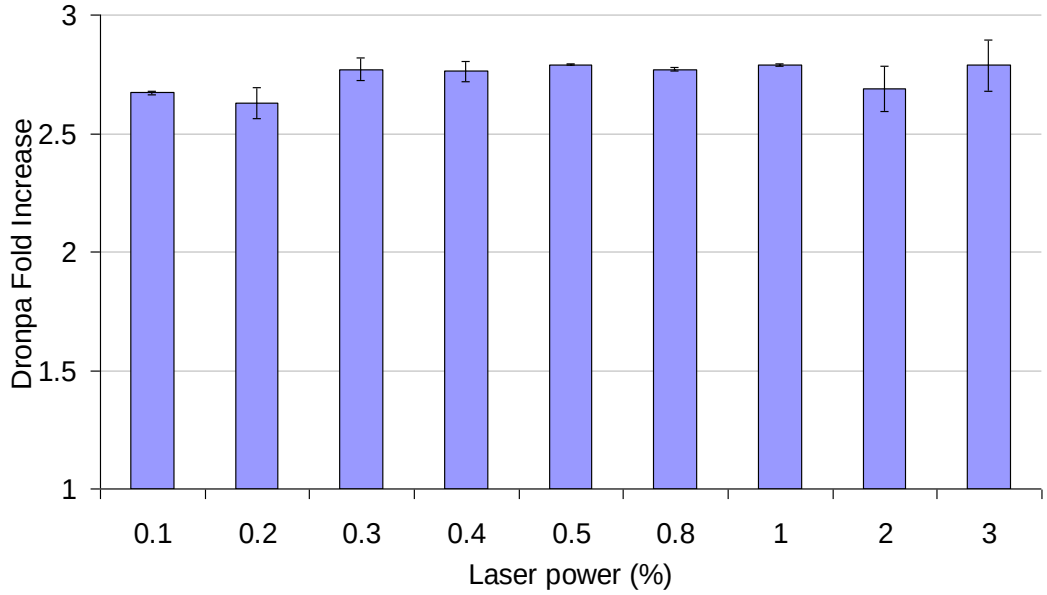

Figure 3-4 Effect of 405nm laser power on Dronpa switching.

SK-N-AS cells (N=3) expressing pG-CMV-Dronpa using 405nm diode laser and 5 scan iterations to switch Dronpa. Dronpa post-switching is normalised to the pre-switch fluorescence. The mean for each set of conditions was taken. Error bars show standard deviation between cells. AOTF settings were varied between 0.1% to 3% to establish the most for photoswitching.

3.3.3 Effect of extracellular pH on Dronpa Switching Efficiency.

Photoswitching efficiency appeared to vary from day to day at one point in the project and this was coincident to a fault in the CO_2 controller on the microscope. It was therefore postulated that a possible cause of the variation in photo-switching efficiency was due to pH changes in the media. This was tested by using 1M NaOH and HCL, to adjust the pH of the cell media across a range of pH values from 7.2-7.8 (Figure 3-5). Resting pH following incubation of media at 37^{o}C in 5% CO_2 was measured as being pH 7.4 using reference media samples. 1M NaOH and 1M HCL was then used to adjust the pH of reference media and the volume of NaOH and HCL required was recorder. The temperature of the reference media was kept at 37^{o}C.

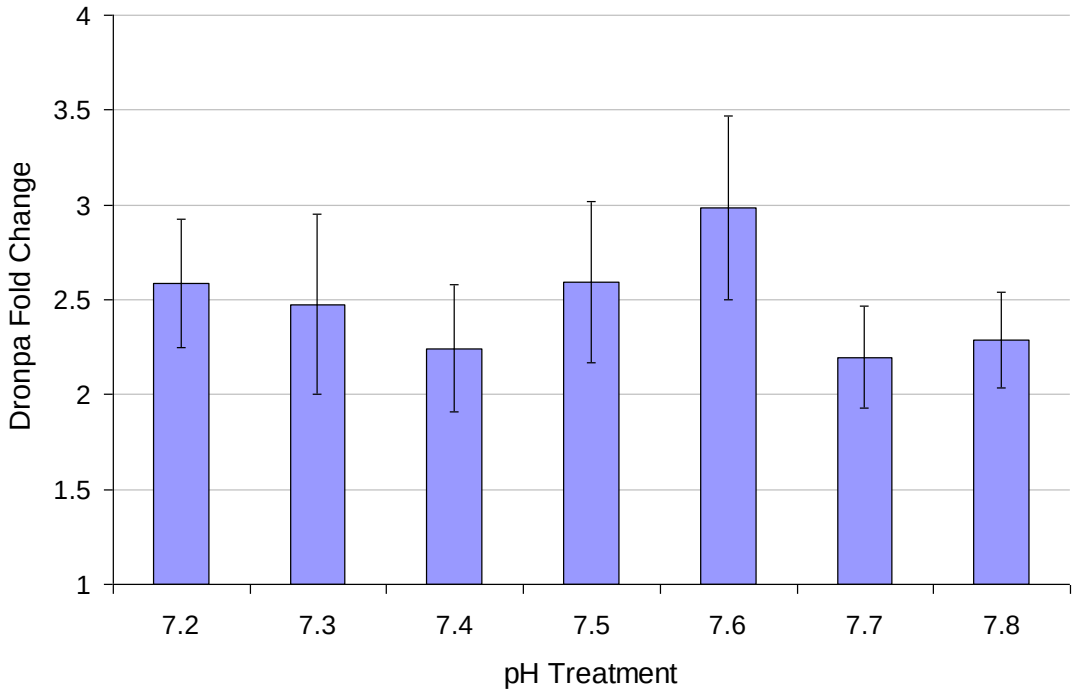

Figure 3-5 Effect of pH condition on Dronpa Switching.

A population of 10 SK-N-AS cells expressing pG-CMV-Dronpa. Using 20 scan iterations and AOTF set at 3% attenuation. Cells expressing Dronpa switched in different media pH conditions altered using NaOH and HCL. Dronpa post switching is normalised to the pre-switch fluorescence. The mean for each set of conditions was taken, and the standard deviation between cells plotted as error bars.

No significant trend in switching sensitivity across this pH range was observed. The increased standard deviation between cells observed in these experiments compared to those described earlier was found to be due to a multiphoton laser fault that was causing variable laser power.

3.3.4 Dronpa Fusion Characteristics

It was investigated whether the initial fluorescence intensity of Dronpa fusion proteins was dependent on the fusion partner (Figure 3-6). To ensure the largest modulation of Dronpa switching, a set of images using 488nm illumination were taken prior to any switching in order to reduce the fluorescence levels to their lowest levels. Due to the negative exponential decay of Dronpa (Figure 3-1) there comes a point of diminishing returns where switching Dronpa into its off state becomes too time-intensive. A fixed number of (15) images were taken before switching to maximise observable change following switching.

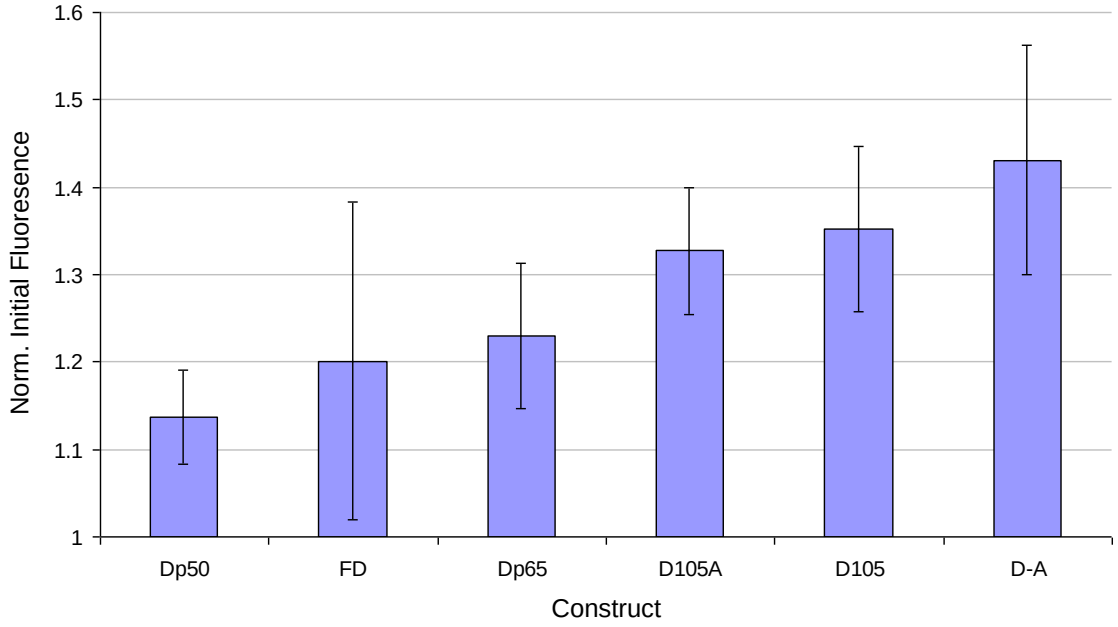

Figure 3-6 Variability of Dronpa fluorescence when expressed in various fusion proteins.
SK-N-AS cells expressing different Dronpa fusion constructs (n=10 for each construct). The figure shows initial Dronpa fluorescence which has been normalised to the lowest fluorescence value following a consistent period of imaging (15 frames). The mean for each set of conditions was taken, and the standard deviation between cells plotted as error bars. Constructs: Dp50 is pG-CMV-Dronpa-p50. FD is pG-CMV-Dronpa. Dp65 is pG-CMV-Dronpa-p65. Dp105A is pG-CMV-Dronpa-p105-AmCyan. Dp105 is pG-CMV-Dronpa-p105. D-A is pG-CMV-Dronpa-7aa-AmCyan. Data obtained using 405nm excitation. 1% AOTF and 5 scan iterations.

Different fusion proteins were found to have varying switching efficiencies as demonstrated in Figure 3-7. This complicates comparisons between constructs, and must be taken into account when using the photoswitching properties of Dronpa for quantitative purposes. However, looking across the functional constructs, the fold Dronpa change range is only 2.4-3 allowing for a greater degree of comparability.

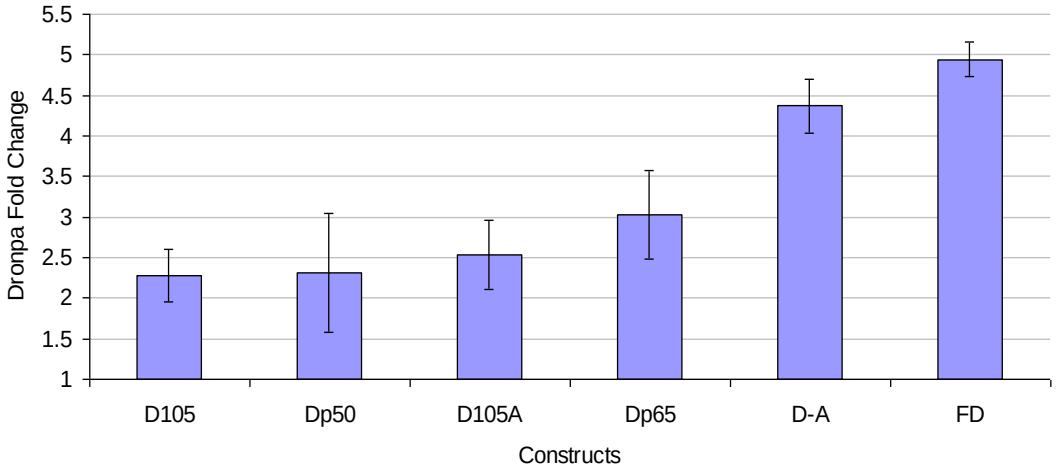

Figure 3-7 Efficiency of Dronpa switching in different fusion proteins.

SK-N-AS cells expressing different Dronpa fusion constructs (n=10 for each construct). Dronpa normalised to preswitch). Fold change in Dronpa represents the relative change in fluorescence from the lowest fluorescence value following an extensive period of imaging switching efficiencies of different constructs under the same imaging parameters. Constructs: Dp50 is pG-CMV-Dronpa-p50. FD is pG-CMV-Dronpa Dp65 is pG-CMV-Dronpa-p65. Dp105A is pG-Dronpa -105-AmCyan. Dp105 is pG-CMV-Dronpa-p105. D-A is pG-CMV-Dronpa-7aa-AmCyan. These experiments used 405nm excitation, 1% attenuation and 5 iterations.

3.4 FRET Partners

Dronpa is capable of acting as either a FRET donor or FRET acceptor. The most desirable pairing of fluorophores would be where Dronpa is an acceptor of energy transfer. In this instance, any modulation in the fluorescence of Dronpa would result in a corresponding reduction in the fluorescence of its donor due to quenching of the donor itself. As a result, any change in the sensitised emission ($\mathbf{F_c}$) can be confirmed by this interaction, thus confirming that a FRET interaction occurred. By contrast, in the instance where Dronpa is used as a donor, modulation in Dronpa would have no effect on the fluorescence of the acceptor. This means that FRET would have to be inferred purely through the sensitised emission, which is liable to false positives due to unaccounted contributions from the donor. For absolute confidence to be placed in the change in sensitised emission, rigorous controls must be carried out ideally using multiple microscopy techniques; FLIM FRET as well as spectral FRET.

The absorption spectra of Dronpa is more complex than a standard fluorophore due to its shifting absorption, dependent on its level of protonation (see Chapter 1) For practical purposes, the spectra of Dronpa can be considered as that depicted in Figure 3-8. A number of appropriate fluorophores were selected due to their spectral characteristics (See Table 2, Chapter 1). They were chosen to have an appropriate spectral overlap with Dronpa that suggested their potential as a FRET partner

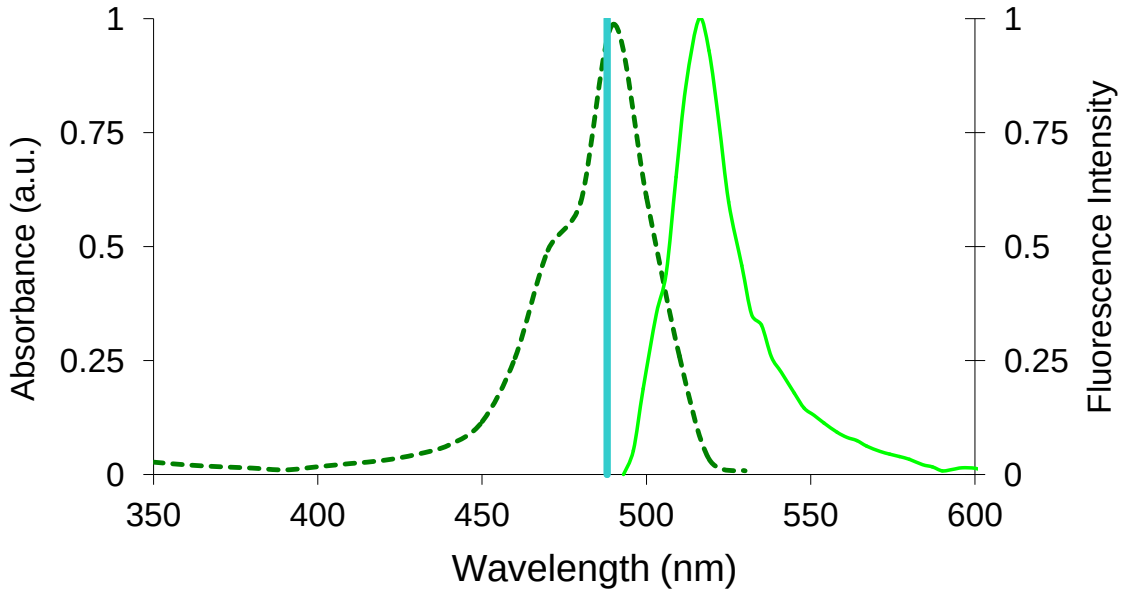

Figure 3-8 Excitation and emission spectra of Dronpa.

The excitation spectrum of Dronpa (dashed line) was obtained from the literature (Habuchi, Ando *et al.* 2005). The emission spectrum of Dronpa (solid line) was experimentally determined in SK-N-AS cells through transfection of pG-CMV-Dronpa and subsequent spectral sampling of the emission. wavelength. Blue line represents 488nm Excitation line.

3.4.1 Cyan Partners

Three Cyan fluorophores were earmarked and tested as suitable donors for Dronpa. These were Cyan Fluorescent Protein (ECFP), AmCyan and Teal Fluorescent Protein (mTFP). Each of these fluorophores has significant spectral overlap with the excitation spectra of Dronpa as shown in Figure 3-9.

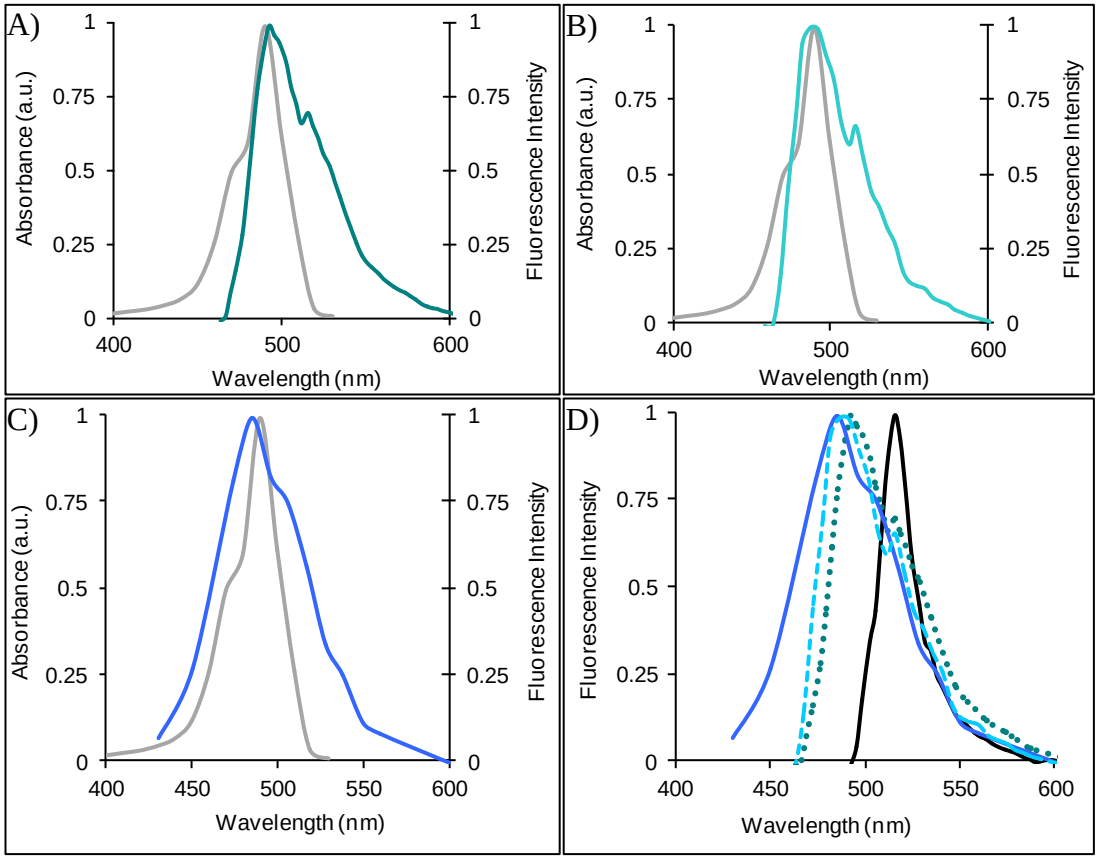

Figure 3-9 The spectral overlap of Cyan family fluorescent proteins with Dronpa.
The emission spectra were determined experimentally through expression in SK-N-AS cells of free FP CDS, and subsequent spectral sampling of the emission wavelength. A) mTFP (teal) and Dronpa excitation (gray). B) AmCyan Emission (Cyan) and Dronpa Excitation (Gray). C) CFP Emission (Blue) and Dronpa Excitation (Gray) D) CFP (Solid blue) AmCyan (Dashed cyan) and TFP (Dotted teal) emission spectra and subsequent spillover into the emission spectra of Dronpa (black).

3.4.2 Enhanced Cyan Fluorescent Protein

ECFP has been in use as a fluorescent dye for nearly two decades and is well characterised as the classical FRET donor to EYFP (Shaner, Steinbach *et al.* 2005). It is known for forming dimers with itself, being susceptible to photobleaching and has a relatively low quantum yield compared to that of EGFP (see Table 1, Chapter 1). These properties do not make it an ideal candidate for FRET. However, its long history as a FRET donor and good spectral overlap made it a good starting point for testing as a FRET partner for Dronpa.

As expected the relative brightness of CFP coupled with its low photostability proved a challenge to image with the pre-optimised imaging and photoswitching protocol. Adjustments were made to attempt to compensate, but bleaching proved to be unavoidable as shown in the data in Figure 3-10.

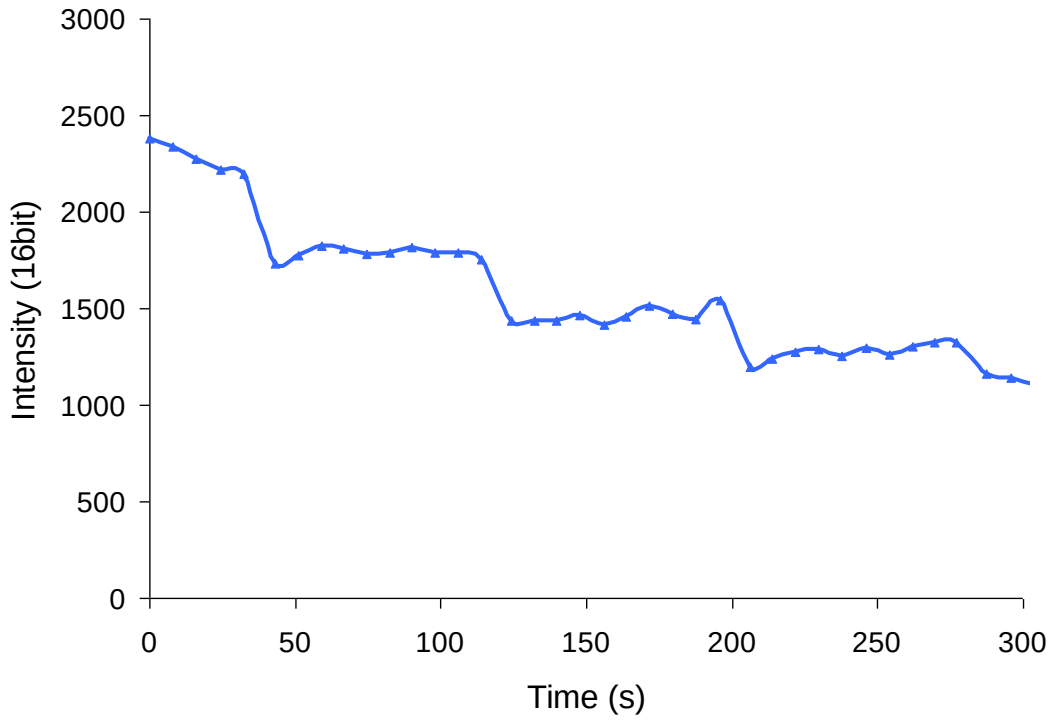

Figure 3-10 ECFP fluorescence and susceptibility to bleaching when subjected to the switching protocol for Dronpa.

pG-CMV-ECFP was expressed in SK-N-AS cells and the cells illuminated with the multiphoton laser for switching. Minimally invasive settings were used, in order to minimise bleaching (1.5% attenuation, 810nm illumination, 20 iterations). ECFP was bleached during photo-switching using 810nm excitation, initially pulsing with 810 nm laser line after 5 frames, then every 10 frames.

3.4.3 mTeal Fluorescent Protein

mTFP has several properties other than its spectral overlap that make it a good candidate for a FRET donor for Dronpa. Primarily it has a high quantum yield and proves to be relatively robust to photobleaching (see Table 1, Chapter 1). It also has the added advantage of being a monomer, reducing the likelihood of spurious FRET in high concentrations.

Testing of mTFP under experimental conditions yielded interesting results (Figure 3-11). While mTFP proved to be significantly brighter than any other cyan fluorophore tested, following illumination with 405nm, its relative fluorescence was found to increase, followed by a decay back to the starting level. This characteristic made mTFP unusable as a FRET partner with Dronpa as any quenching effect caused by FRET could be masked by this increase.

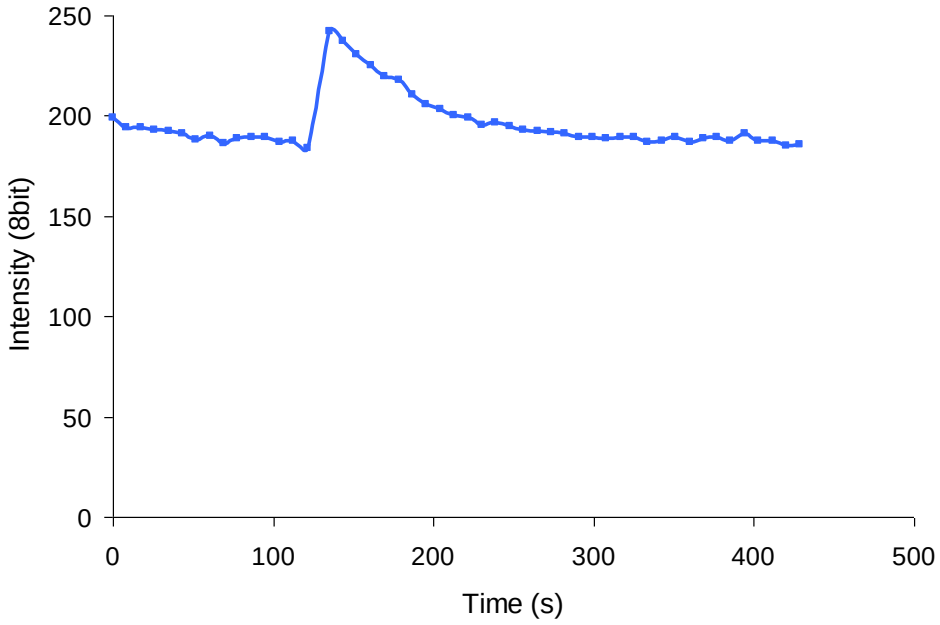

Figure 3-11 Evaluation of mTeal fluorescent protein.

The graph shows the fluorescence of mTFP following an optimised illumination strategy in a single cell (representative of 10 tested). pG-CMV-mTFP expressed in SK-N-AS cells imaged using an optimised illumination strategy on a Zeiss 710LSM confocal microscope using 405nm wavelength for switching. The data show the increased fluorescence of mTFP following illumination with a pulse of illumination at 405nm (~114s). These data indicated that TFP shares some of the switching characteristics of Dronpa.

3.4.4 AmCyan

AmCyan did not initially appear to have as desirable optical characteristics on paper as mTFP. AmCyan can dimerise, and while it has a higher quantum yield and extinction coefficient (see Table 1, Chapter 1) compared to that of ECFP, it is still considerably less bright compared to mTFP and Dronpa.

The data shown in Figure 3-12 represents the behaviour of AmCyan in three separate channels, the AmCyan channel (I_{AA}), the Dronpa Channel (I_{DD}) and the FRET channel (I_{DA}). These data demonstrate the behaviour of a representative cell following a pulse of 405nm illumination (with 1% attenuation, after 5 frames). No bleaching or changes were visually detectable in any channel. This suggested that AmCyan was the best fluorophore of those tested to use as a FRET donor for Dronpa.

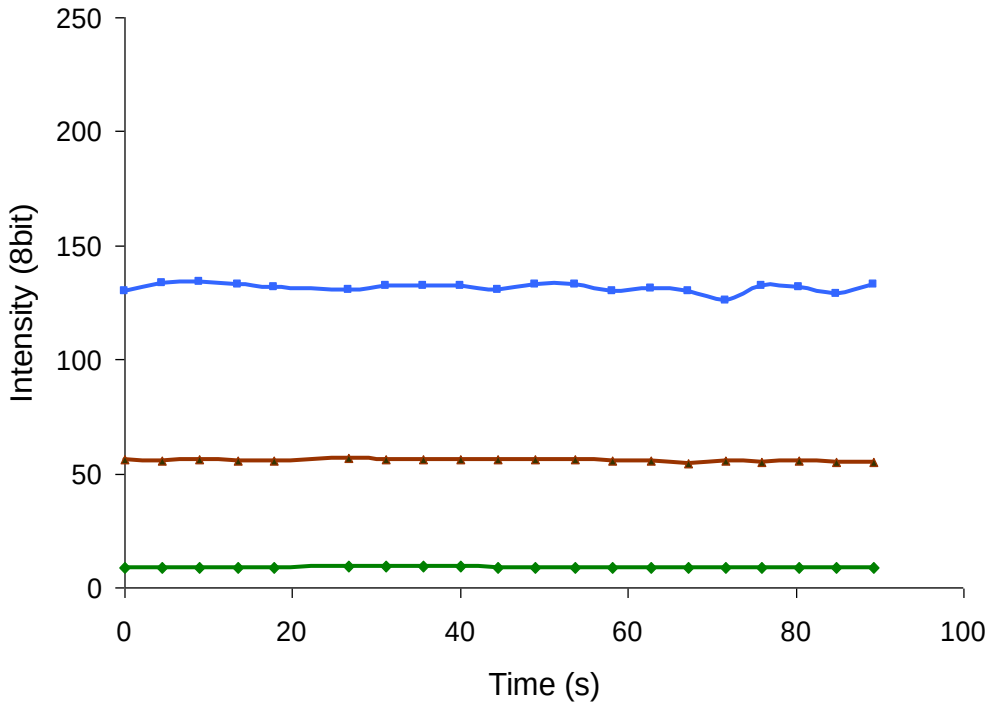

Figure 3-12 Effect of pulsing with 405nm illumination on the fluorescence from AmCyan in single cells.

AmCyan expressed in SK-N-AS cells imaged using optimised illumination strategy with Zeiss LSM710 confocal microscope. The representative cell shows behaviour of AmCyan following a pulse of 405nm illumination with 1% attenuation after 5 frames (18s). Three channels are shown: AmCyhan Channel (I_{AA}, blue), Dronpa channel (I_{DD}, green), and FRET channel (I_{DA}, red).

In a population of cells (n=20), a total of 2 cells showed a small increase in AmCyan fluorescence (represented in I_{DD}) and also the I_{AA} and I_{DA} channels following pulsing with 405nm excitation (Figure 3-13.B). Normalised changes in these two channels will be amplified due to their relatively small values in the raw data, which has the potential to interfere with sensitised emission (F_c). Controlling for this increase could be difficult due to its random nature. This potential effect should be minimised by using an adequate sample size to compensate for this effect. It must be considered that an increase in AmCyan fluorescence could be responsible for either negative reporting of FRET through donor quenching, or measurement of false positives in F_C.

A)

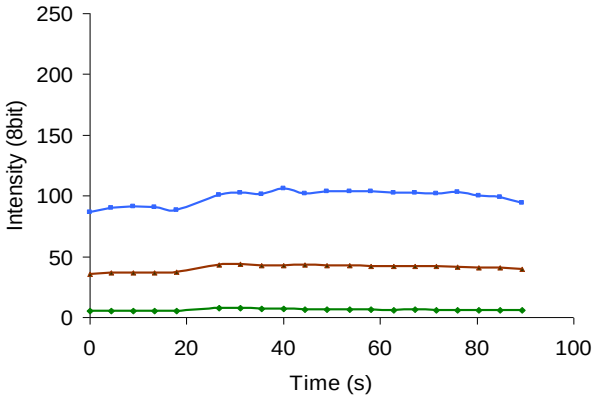

B)

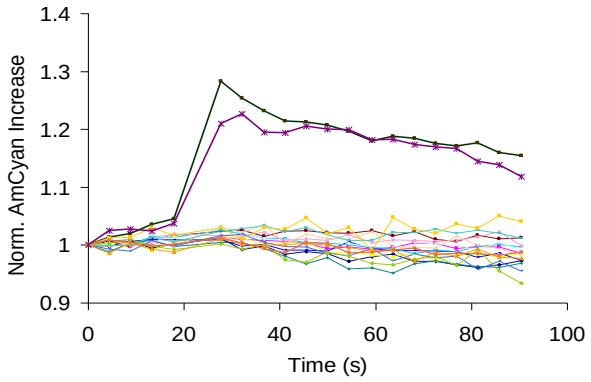

Figure 3-13 AmCyan can show a small increase in fluorescence following pulsing with 405nm excitation

(A) Single representative SK-N-AS cell expressing pG-CMV-AmCyan. showing relative increase in I_{DA} I_{DD} and I_{AA} channels following switching after 5 frames (19sec). (B) SK-N-AS cells expressing pG-CMV-AmCyan cells (n=20) showing normalised increase in fluorescence following pulsing with 405nm excitation in accordance with the optimised illumination strategy for 405nm switching of Dronpa. AmCyan intensity was normalised against the initial starting fluorescence.

3.4.5 Red Partners

Out of all readily available red fluorophores, five were singled out for testing as suitable acceptors for Dronpa. These were DsRedExpress, mStrawberry, mRaspberry, tdTomato and mCherry. Most of the absorbtion spectra of these fluorescent proteins have significant spectral overlap with the emission spectra of Dronpa as shown in Figure 3-14. The mRaspberry absorption spectrum was shown to have a poor overlap with Dronpa emission, combined with a low quantum yield (see Table 1, Chapter 1). It was therefore considered prudent that this florescent protein should not be used in further studies.

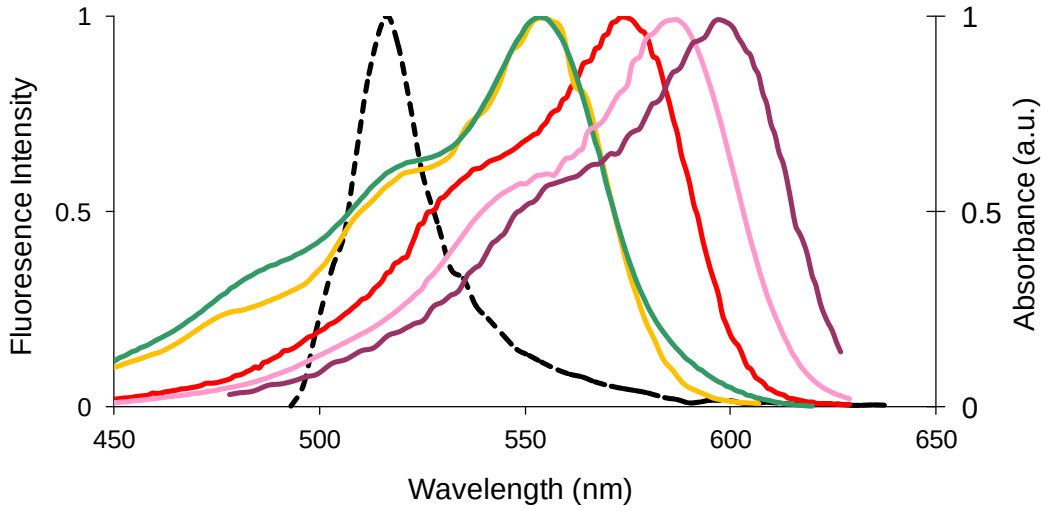

Figure 3-14 Emission spectrum of Dronpa (dashed line) overlaid with the absorbtion spectra of the red fluorescent proteins.

DsRedExpress (green), tdTomato (Orange) mStrawberry (red), mCherry (pink), and mRaspberry (purple).

3.4.6 DsRedExpress

DsRedExpress is a variant of the fluorophore DsRed, optimised for speed of maturation of the chromophore. DsRed has three separate forms before it reaches its mature conformation, including transient blue and green forms (although the behaviour of DsRedExpress has not been fully characterised).

DsRedExpress was tested under the same optimised illumination strategy that had previously been used for both Dronpa and Cyan fluorophores. All cells (n=20) responded as represented below in Figure 3-15. An unexpected increase in the I_{DA} channel was observed which could mask a genuine increase in sensitised emission, making DsRedExpress unsuitable as an acceptor. It was hypothesised that illumination with multiphoton and UV wavelengths caused one of the earlier maturation states of DsRedExpress to temporarily increase fluorescence following exposure to 405nm, like mTFP.

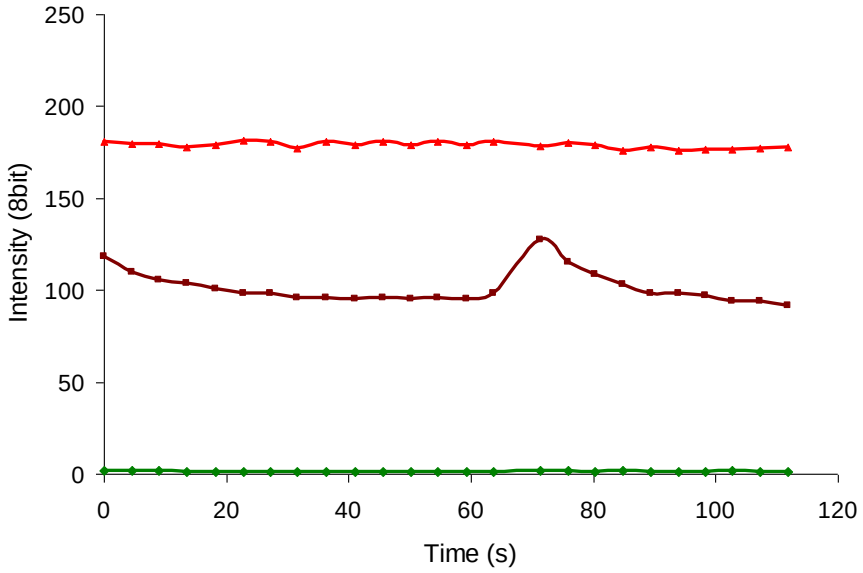

Figure 3-15 Analysis of the properties of DsRedExpress as an acceptor for Dronpa.
pG-CMV-DsRedExpress was transiently expressed in SK-N-AS cells and imaged using the optimised illumination strategy with a Zeiss LSM710 confocal microscope, using 405nm excitation with 1% attenuation and 5 iterations for switching. Red shows fluorescence, green shows contribution of DsRedExpress to I_{DD} (spillover into Dronpa), and dark red represents sensitised emission. The representative cell demonstrates an increased signal in the I_{DA} channel following switching with 405nm illumination.

3.4.7 mStrawberry

mStrawberry has an exceptionally high relative brightness and robust extinction coefficient for a red fluorophore (see Table 1, Chapter 1). It also has the added advantage of being a monomer. Although its excitation maxima is not as well placed as DsRedExpress as an acceptor to Dronpa, its relative brightness was considered as a strong advantage over DsRedExpress. Following switching no change in fluorescence was detectable over a population of cells, unlike DsRedExpress (Figure 3-16). This suggested that it was a more suitable candidate for a Red partner with Dronpa

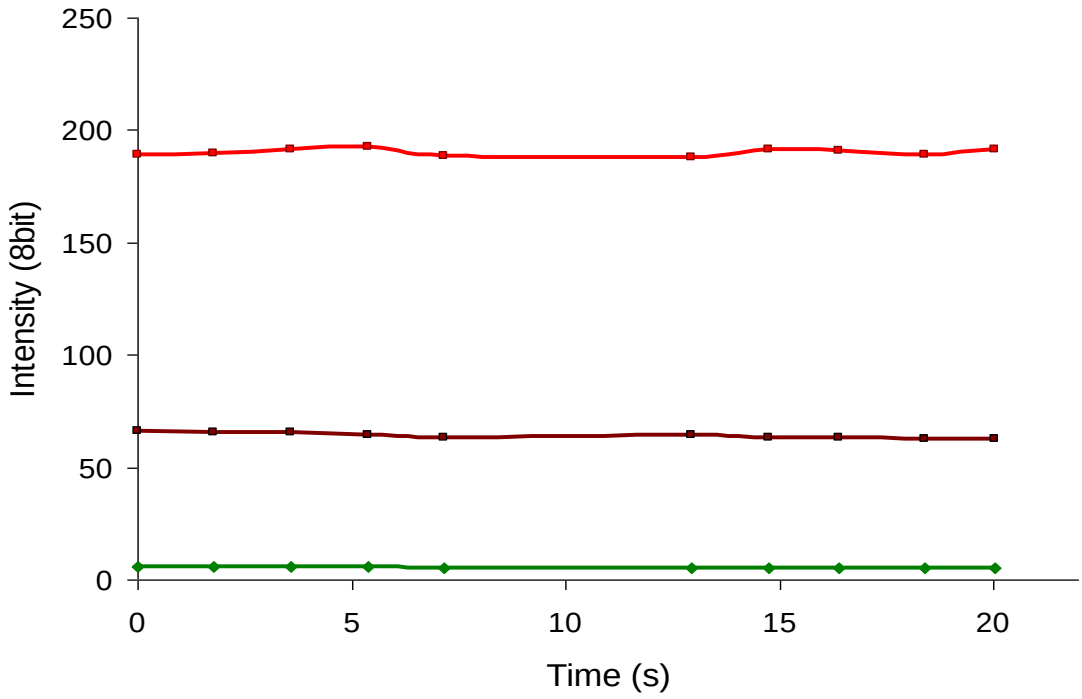

Figure 3-16 Characterisation of the properties of mStrawberry as a potential acceptor for Dronpa.

SK-N-AS cells expressing pG-CMV-mStrawberry were imaged using the optimised illumination strategy on a Zeiss LSM710 confocal microscope using 405nm illumination, 1%, attenuation and 5 iterations for switching. A representative cell is shown.

3.4.8 tdTomato & mCherry

Both tdTomato and mCherry were tested by Dr. Mohamed Awais. mCherry has come into popular use as a red fluorophore due to its more spectrally separate characteristics while maintaining a comparably high brightness to that of other spectrally similar fluorophores. This unfortunately makes it less ideal as an acceptor for Dronpa. tdTomato on the other hand has very good spectral overlap with Dronpa and an extraordinary brightness for a red fluorophore due to its tandem dimer formation (see Table 1, Chapter 1). This property raised questions about FRET efficiency however, as nonradiative energy transfer might be limited either partially or wholly to one part of the tandem fluorophore.

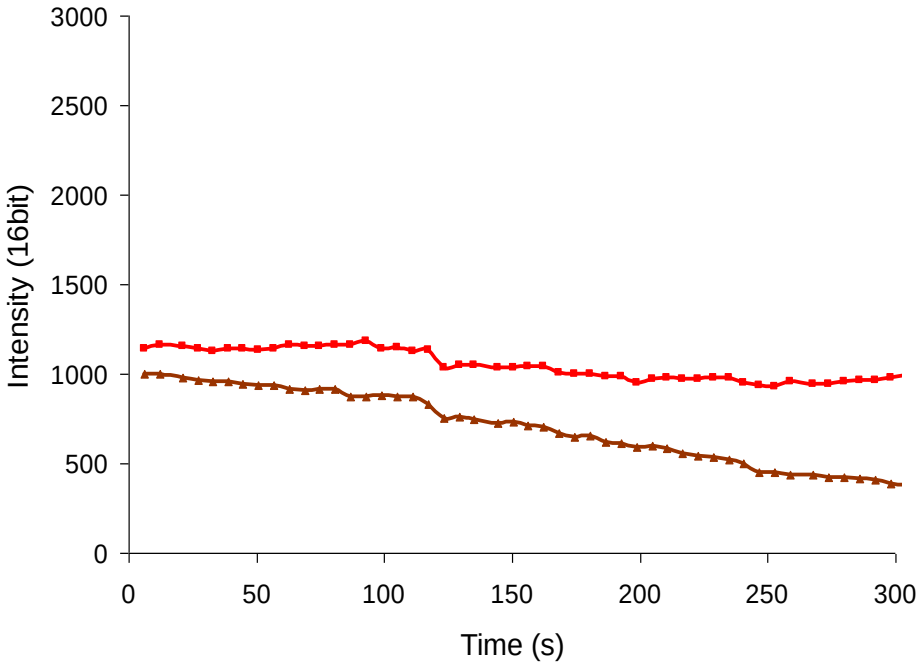

Figure 3-17 Properties of mCherry and tdTomato.

tdTomato (dark red) and mCherry (red) imaged using a multiphoton microscope with 2% 488nm and 1% 561nm illumination and a switching protocol which used 1.5% 810nm illumination with 25 iterations. Switching was performed after 105s (21 frames).

Testing carried out by Dr. Awais showed that both fluorophores bleached easily under Dronpa switching conditions using a multiphoton laser source. Although testing using 405nm excitation might in theory yield different results, tdTomato was found to bleach readily through continuous imaging of the fluorophore.

mCherry had the most separate spectrum from the emission profile of Dronpa of the FPs tested. It was therefore considered that it was unlikely to be a good partner for Dronpa. It was therefore decided to pursue the optimisation of mStrawberry as an acceptor for Dronpa.

3.5 Positive Controls and Construct Creation

Untagged florescent protein control constructs were used in the work described above to test empty fluorophore behaviour under imaging conditions. Positive control constructs where the two fluorescent proteins are linked by a short standard sequence were next needed in order to test the viability and efficiency of FRET between partners. They were also important for general system calibration and for quantitative characterisation of the FRET behaviour of Dronpa with its partner.

It was decided to use a small linker between the FP genes in order to generate a direct fusion between Dronpa and each partner. The linker structure is important to maximise energy transfer and linker length has been shown in numerous examples to be the key factor in determining FRET efficiency. The linker that was decided on was:

GGNGG

This was a flexible linker sequence that had previously been used by Dr. Awais which had yielded good results (personal communication). Constructs were generated through inserting PCR amplified linker-FP amplicons into empty Gateway CMV-Dronpa destination vectors at either the N or C terminal end of Dronpa. Cloning restrictions resulted in a slightly adapted linker being generated which had two additional amino acids:

LEGGNGG

All constructs (see Table 4) expressed the test protein from the hCMV promoter sequence. Each construct was and transiently transfected into the cells. This provided a wide range of expression levels which had the advantage that it helped to ascertain whether or not optical behaviour of the fused proteins was an artefact of over-expression of the fluorophores.

Table 3-1 List of control constructs
made for testing spillover, FRET efficiency and fluorophore behaviour.

Construct name	Components	Abbreviation
pG-Free mStrawberry	CMV_Strawberry(CDS)_stop	F-S
pG-Free DsRedxp	CMV_DsRedXP(CDS)_stop	F-xp
pG-Free Dronpa	CMV_Dronpa(CDS)_stop	F-D
pG-Free Amcyan	CMV_AmCyan(CDS)_stop	F-A
pG-Free mTFP	CMV_mTFP(CDS)_stop	F-T
pG-Free ECFP	CMV_ECFP(CDS)_stop	F-C
pG-Dronpa-7aa-Amcyan	CMV_Dronpa-LEGGNGG-AmCyan(CDS)_stop	D-A
pG-AmCyan-7aa-Dronpa	CMV_AmCyan-LEGGNGG-Dronpa(CDS)_stop	A-D
pG-Dronpa-7aa-mStrawberry	CMV_Dronpa-LEGGNGG-mStrawberry (CDS)_stop	D-S
pG-Dronpa-7aa-mTFP	CMV_Dronpa-LEGGNGG-mTFP (CDS)_stop	D-T

Emphasis was placed on testing AmCyan and mStrawberry constructs due to the promising results obtained following the single fluorophore testing results described above.

3.5.1 AmCyan Positive Control

Both orientations of the positive control for AmCyan were cloned. pG-Dronpa-7aa-AmCyan and pG-Amcyan-7aa-Dronpa. Interestingly some spots showed fast movement throughout the cell suggesting aggregated fluorophores had been packaged into vesicles, but stationary spots were also present. pG-Dronpa-7aa-AmCyan was ubiquitously expressed but was not necessarily expressed uniformly throughout the cell (see Figure 3-18 A&B).

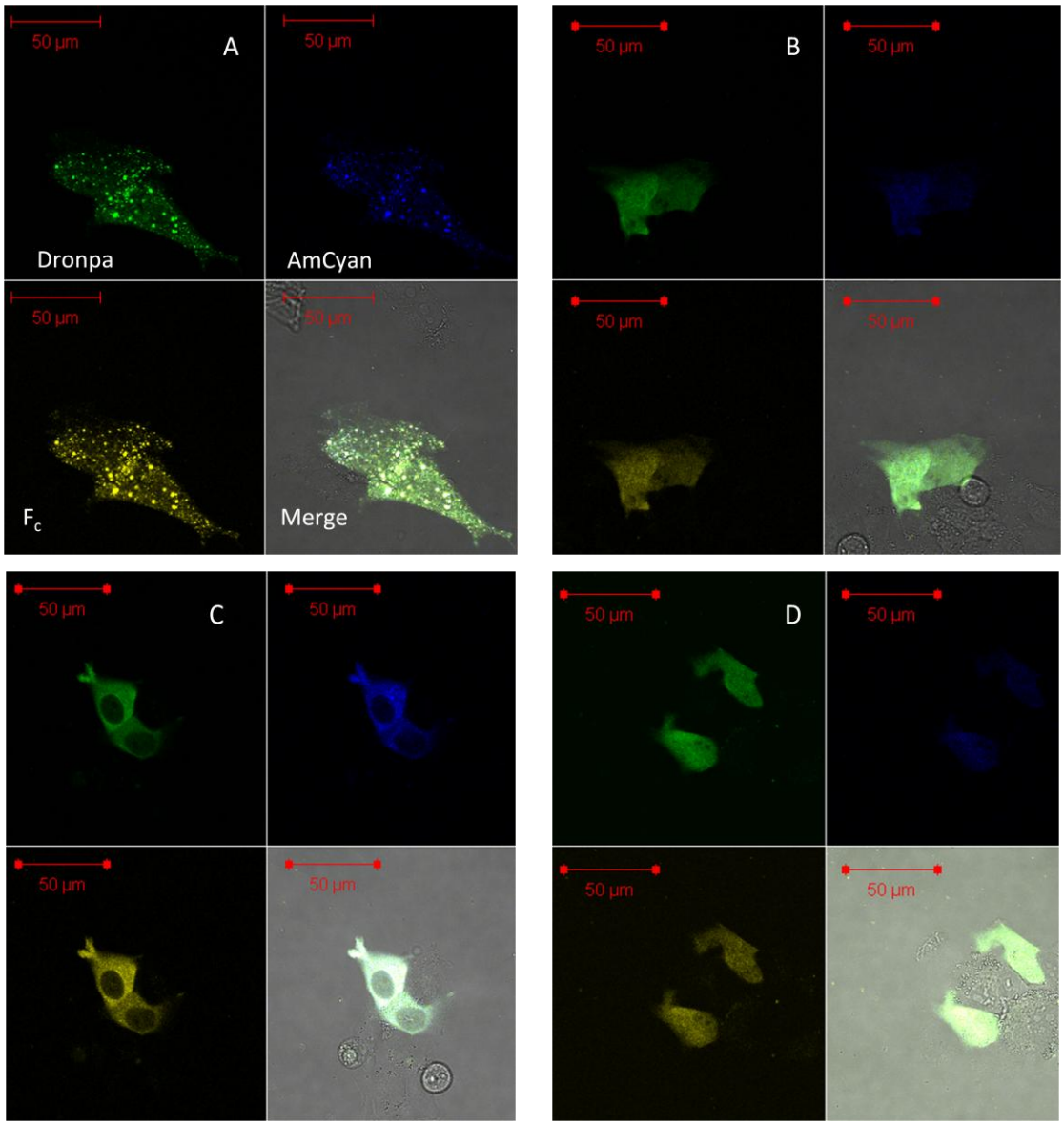

Figure 3-18 Imaging of control fluorescent proteins with AmCyan as acceptor and Dronpa as donor in two orientations.

AmCyan-7aa-Dronpa (**A** & **B**) and Dronpa-7aa-AmCyan (**C** & **D**) were expressed in SK-N-AS cells and imaged using the optimised illumination strategy with a Zeiss LSM710 confocal microscope using 405nm wavelength for switching. Green pseudocolour represents Dronpa fluorescence, blue represents AmCyan and yellow represents sensitised emission. For AmCyan-Dronpa construct, **A)** 50% of cells showed speckled phenotype, and **B)** 50% of cells showed uniform phenotype. For Dronpa-AmCyan construct, expression could be either **C)** cytoplasmic, **D)** or uniform.

Both fusion proteins showed a good response to photoswitching (Figure 3-18), although visible differences in efficiency were apparent. D-A produced a reliable FRET signal with little variation. A-D however produced two distinct profiles of FRET. When the protein was uniformly expressed (Figure 3-18. B) there was a relatively low FRET response, whereas cells with a speckled phenotype (Figure 3-18.A) yielded a much stronger FRET response. This may imply that more energy exchange occurs between the control D-A, where as the conformation of fluorophores in A-D is not ideal for FRET. Higher degrees of FRET were seen in cells with speckles possibly due to fluorophores aggregating into clumps. It can be speculated that this speckling may have caused an artificially high concentration of both fluorophores which could have resulted in intermolecular energy exchange rather than intramolecular FRET.

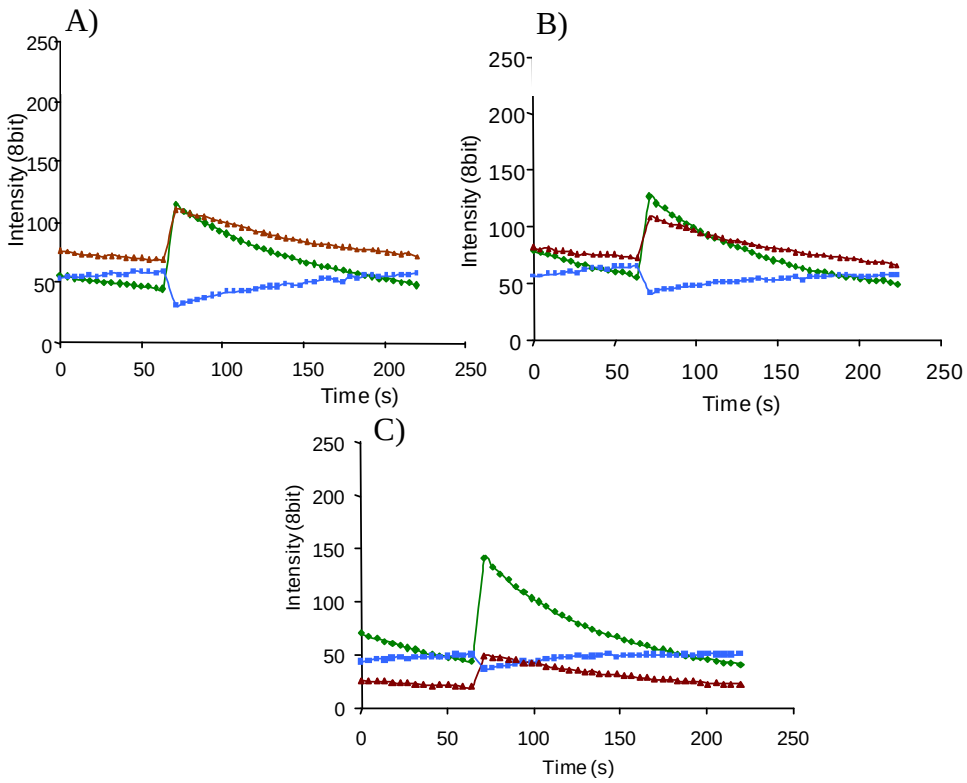

Figure 3-19 FRET between AmCyan and Dronpa in the control fusion proteins.

SK-N-AS cells expressing both pG-CMV-Dronpa-AmCyan and pG-CMV-AmCyan-Dronpa were imaged using the optimised illumination strategy using a ZeissLSM710 confocal microscope using 405nm illumination for switching. **A)** D-A fusion protein showing strong quenching in I_{DD} and an increase in I_{DA} following switching on of Dronpa. **B)** A-D uniformly expressed with no aggregates. This fusion protein showed markedly weaker FRET compared to D-A. **C)** FRET in cells with aggregated A-D fluorescent protein showing visibly stronger FRET response compared to uniformly expressed protein.

Although the I_{DA} channel shows somewhat of an agreement with AmCyan quenching in the different degrees of FRET between constructs, and spillover can be somewhat discounted due to the 1:1 ratio of fluorophores, until a method of removing spillover from F_c is implemented this measure of FRET is of limited use.

3.5.2 Strawberry Positive Control

Only one orientation of the strawberry positive control was successfully cloned. pG-Dronpa-7aa-mStrawberry was tested and Dronpa fluorescence was successfully modulated with no bleaching of mStrawberry following Dronpa switching. The main issue with these data is that spillover of Dronpa cannot be separated from a genuine FRET signal until a method of removing spillover from F_c is implemented. Donor quenching could not be used as an inference of FRET as this was the signal that was being modulated with light.

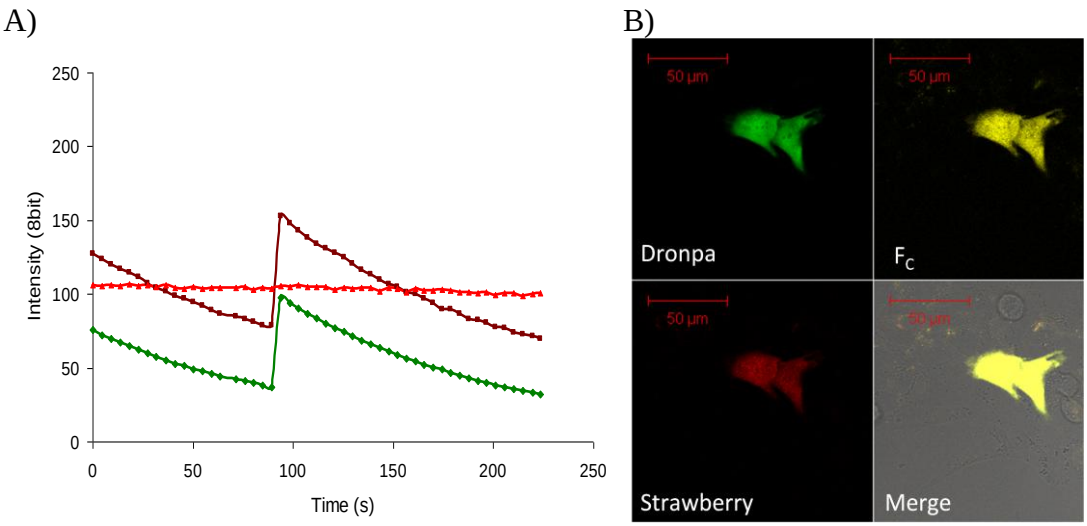

Figure 3-20 FRET between Dronpa and mStrawberry in positive control.
pG-Dronpa-7aa-mStrawberry (D-S) expressed in SK-N-AS cells imaged using the optimised illumination strategy on a Zeiss LSM710 confocal microscope using 405nm wavelength for switching. **A)** The fusion protein showed undetectable bleaching and a good response following Dronpa switching. **B)** Imaging of construct.

3.6 Reverse Dronpa Switching Strategy

To enhance the speed of switching, and thus the time resolution between steps of changing I_{DA} and $I_{DD,}$ an alternative switching strategy was investigated to switch Dronpa. This involved the sudden 'switching off' of the flurophore as opposed to the activation of Dronpa followed by a steady exponential decline to the off state (see Figure 3-1).

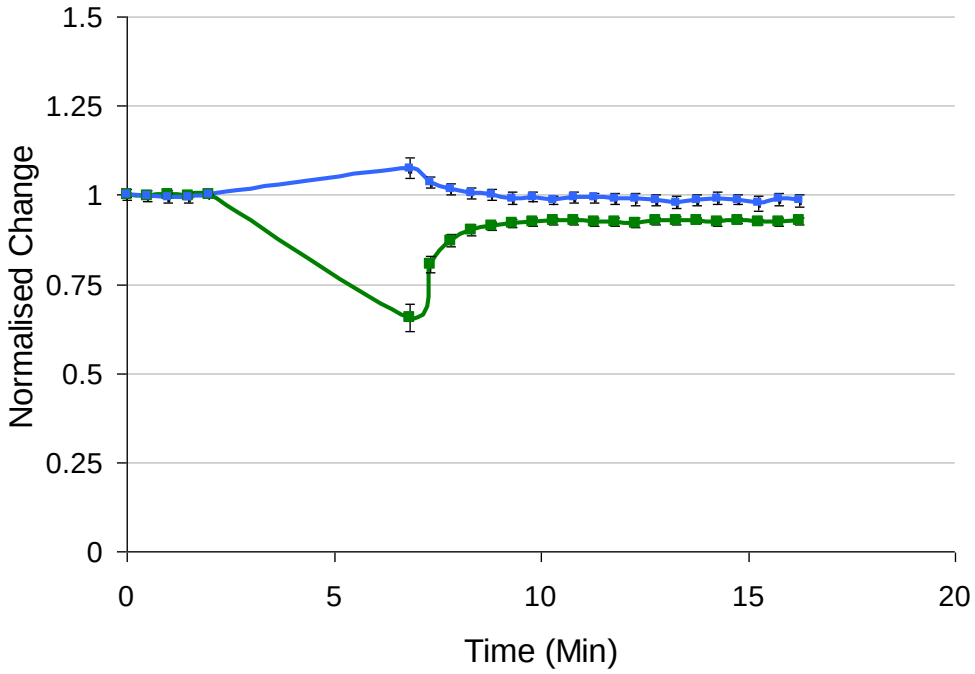

Figure 3-21 Reverse Dronpa switching strategy results in less efficient change in Dronpa fluorescence.

SK-N-AS cells expressing pG-CMV-Dronpa-AmCyan were imaged using a Zeiss LSM710 confocal microscope (n=15) using intense 488nm pulsing to switch Dronpa off. 405nm excitation was attenuated to 0.1% to maintain Dronpa at maximum fluorescence. The resulting protocol resulted in switching of Dronpa and a subsequent increase in AmCyan emission. This technique resulted in reduced overall fluorescence of Dronpa following switching, implying bleaching of the fluorophore. Furthermore the overall change in Dronpa fluorescence was 50% less efficient compared to the previously established optimised protocol.

This method was not pursued further, as it resulted in less substantial switching of Dronpa due to minor bleaching of the fluorophore and less switching efficiency in the Dronpa fluorophore.

3.7 Conclusion

The work described in this Chapter optimised the approach for Dronpa switching and selected appropriate FRET pairs for use with Dronpa. The generation of direct fusion controls provided a vital benchmark for the optimisation of microscope settings to maximise sampling resolution of FRET. This work was vital in establishing Dronpa as a viable tool for switchable FRET. There were some unexpected results, such as an increase in the fluorescence of certain fluorescent proteins following illumination with 405nm light resulting in increased spillover into sensitised emission channels and masking potential quenching of donor fluoresence. This was an important observation because it could confound FRET modulation with Dronpa switching. The next aim of the work described in Chapter 4 was to test the FRET behaviour further using a known protein interaction model.

Chapter 4: Qualifying and Quantifying FRET

4.1 Rationale for Quantification

Once appropriate pairs had been found for Dronpa that minimised reporting of spurious interaction, and an appropriate imaging strategy (optimising reporting of FRET with Dronpa) had been developed. The behaviour of FRET between donor and acceptor FPs needed to be qualified to ensure that FRET behaved in a repeatable and quantifiable way. This was not predictable because of the structural changes Dronpa undergoes to facilitate changes in fluorescence (Andresen, Stiel *et al.* 2007). Following this, a standardised protocol for qualifying and quantifying FRET needed to be established. FRET efficiency and FRET indices are generally tailored to their specific application. Therefore for the target application the correct methods needed to be established for accurate quantification of FRET (Berney and Danuser 2003). Not all of the methods in the literature make use of acceptor photobleaching, but most make use of some form of cross talk correction. To that end, available options were tested to quantify energy transfer, and the most suitable approach established in order to analyse biologically relevant applications.

4.2 Zeiss Spectral Deconvolution

The quantification of FRET can be established purely through observed changes in the quenching of a donor provided changes in acceptor fluorescence are consistent. Alternatively, FRET can be quantified by establishing true sensitised emission (F_c) and its relationship with donor quenching (Gordon, Berry *et al.* 1998). Spectral overlap of fluorophores demands that spillover of spectra be accounted for to observe true F_c. To that end, two options were available for spectral separation of datasets; the pre-existing Linear unmixing algorithm as provided in the Zeiss AIM and Zen software or manually subtracting spillover components following ROI analysis of cell fluorescent intensities.

Established techniques in use in house for observing FRET signals involved the use of spectral deconvolution of spectral data through Zeiss AIM software. While this was an option for analysis, the size of data sets that would be produced if timelapse imaging were implemented meant that long multi field time courses could easily

reach sizes of 50-100GB for a single experiment (compared to 5-10GB of data collected through standard filter based PMT imaging).

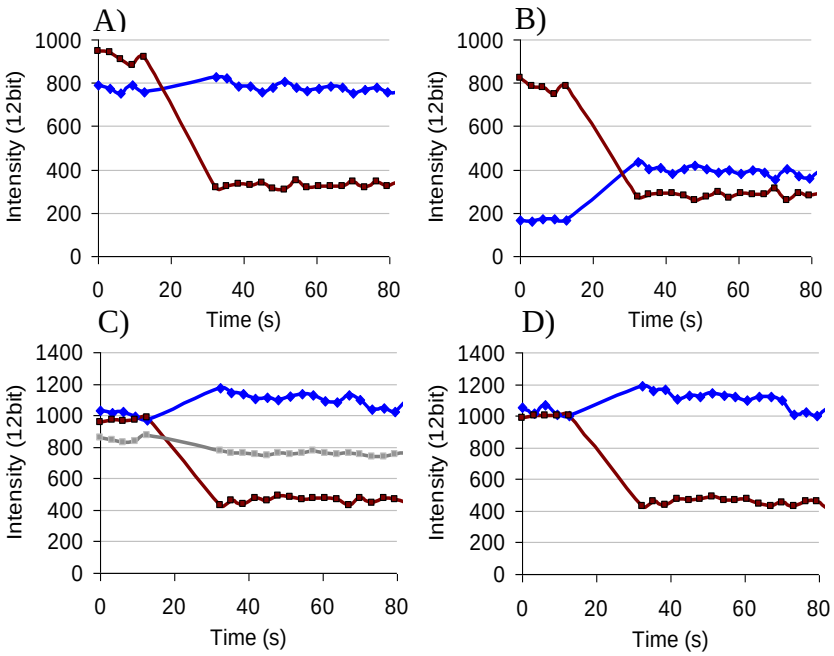

Figure 4-1 Problems encountered using Zeiss AIM linear unmixing algorithms.

Cells transfected with pGCMV-p65-EYFP and pG-CMV-ECFP-GR. Blue is ECFP dark red is EYFP and gray is unassigned light. A and B compare the same image series unmixed with two different spectra from different levels of expression. This shows a clear difference in the detected fluorescence indicating genuine FRET efficiency is not being wholly reported. C and D are from the same image series using the same reference spectra to unmix the data. C has specified the use of 'residuals' where as D has not. The exclusion of residuals from unmixing does not force the software to assign all detected fluorescence, unmixed light will remain.

Apart from the problems involved in handling and analysing such large data sets, Figure 4-2 highlights the main issue with this method for quantification of FRET. The algorithms incorporated into the Zeiss AIM and ZEN2010b employed to unmix spectra assigns a certain degree of the total signal in each channel based on the reference spectra, rather than the direct subtraction of unwanted spillover from a channel. It also appeared to exclude a certain degree of fluorescence that could not be assigned. As the software was supplied "as is" it was unclear how spectral fluorescence data was assigned to certain channels. The software appeared to be very sensitive to changes in the amplitude of the reference spectra compared to that in the data series and to the options selected for channel separation. For these reasons this method was not used to quantify the FRET response as the aim was to achieve data that was as quantitatively accurate as possible.

4.3 Manual Linear Unmixing

Manual linear unmixing relies on two assumptions of the properties of fluorophores: 1) That the relative spillover of a fluorophore into different channels remains linear in relation to the emission maxima; 2) That acceptor fluorescence does not bleed into the donor (I_{DD}) channel. The first assumption means that all microscope and laser settings must be fixed once a linear relation is established. This is due to detectors/PMTs operating on a nonlinear scale depending on the voltage applied to them and their spectral bias ((Maréchal, Asano *et al.* 2012)). The second assumption is important as it gives a point of reference for unmixing fluorophores. Fluorescence in the I_{DD} channel can be used as a starting point to establish the genuine fluorescence of the acceptor when both fluorophores are present (Figure 4-2).

4.3.1 Unmixing AmCyan

There was a clear linear relationship between spillover into different channels (Figure 4-2). Furthermore these data indicated that Dronpa spillover was linear regardless of its degree of protonation which means that F_C can be established regardless of the degree of protonation of Dronpa providing energy transfer is linear.

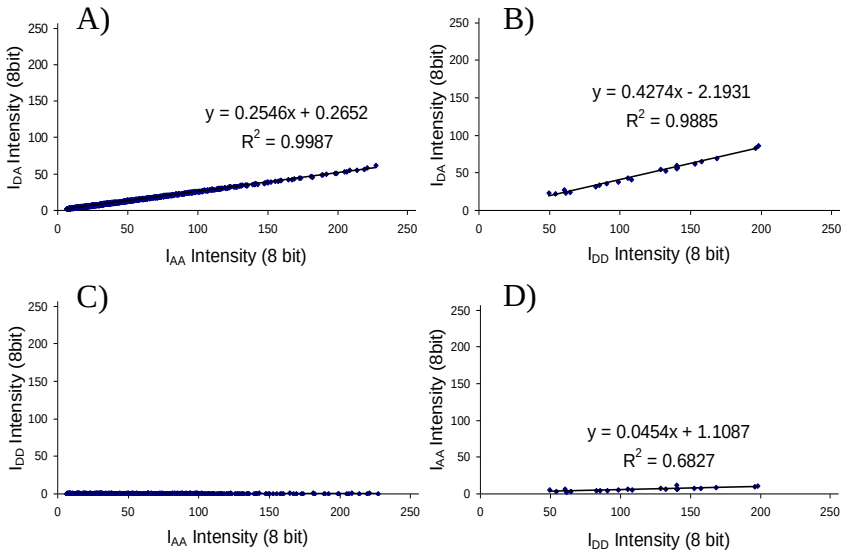

Figure 4-2 Relative fluorescence spillover in single cells

Cells expressing pG-CMV-AmCyan and pG-CMV-Dronpa into I_{DD}, I_{AA} and I_{DA} channels. A) spillover of acceptor into I_{DA} B) Spillover of donor into I_{DA}. C) spillover of acceptor into $I_{DD.}$ D) spillover of donor into acceptor. There was very strong linear relationship in each instance.

Using these linear relationships, true F_c was estimated by simple subtraction. Initially the fluorescence of Dronpa (I_{AA}) was corrected due to AmCyan (I_{DD}) spillover. Following this the intensity of each channel was substituted into each corresponding linear equation (Figure 4-2) and subtracted from the I_{DA} Channel. This method was tested on the negative control of SK-N-AS cells expressing both pG-CMV-AmCyan and pG-CMV-Dronpa (Figure 4-3). Microscope Settings were initially calibrated using the D-A positive control as this construct was assumed to have a 1:1 ratio of both fluorophores.

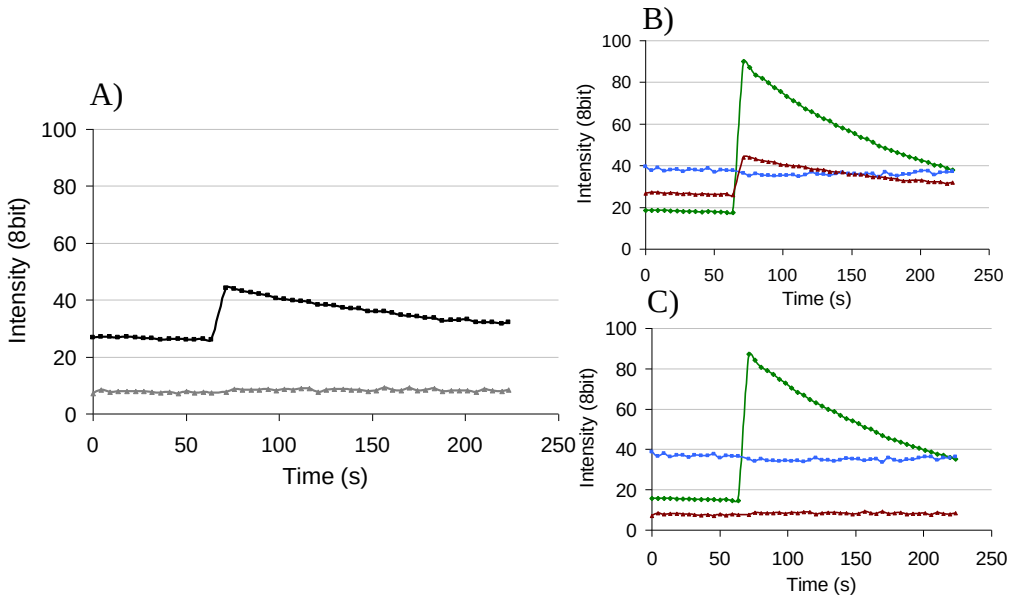

Figure 4-3 An example of spillover correction with Dronpa acceptor

Data from a single SK-N-AS cell expressing pG-CMV-AmCyan and pG-CMV-Dronpa control constructs using optimised illumination strategy for 710LSM. **A)** both raw (black) and processed (grey) I_{DA} channels plotted on same axis. **B)** unprocessed data showing increase in F_c (Red) **C)** processed data showing corrected F_c.

Most importantly, these methods allowed the effective removal of the spurious switch in the sensitised emission (F_c) caused by spillover (Figure 4-3). However, some residual signal remained in the I_{DA} channel even after accounting for spillover. As the photoswitching showed no quenching of the AmCyan signal or any change in F_c corresponding with the switch, it was decided that this residual I_{DA} signal might safely be ignored. If this was the case then this aspect of the technique could be of considerable advantage as artefacts such as these should not interfere with quantification.

To test this hypothesis a larger population of cells expressing pG-CMV-AmCyan and pG-CMV-Dronpa were imaged and analysed to determine the possible range of spurious FRET signals in the I_{DA} channel. A small number of cells were shown to display a minor increase in $I_{DA.}$ after photoswitching. This increase might be attributed to the properties of AmCyan as spillover correction could not remove this spontaneous change (Figure 4-4 A). Normalisation of the data (Figure 4-4 A and C) tended to make this change more apparent. The change in I_{DA} did not appear to be related to residual level of fluorescence. (Figure 4-4).

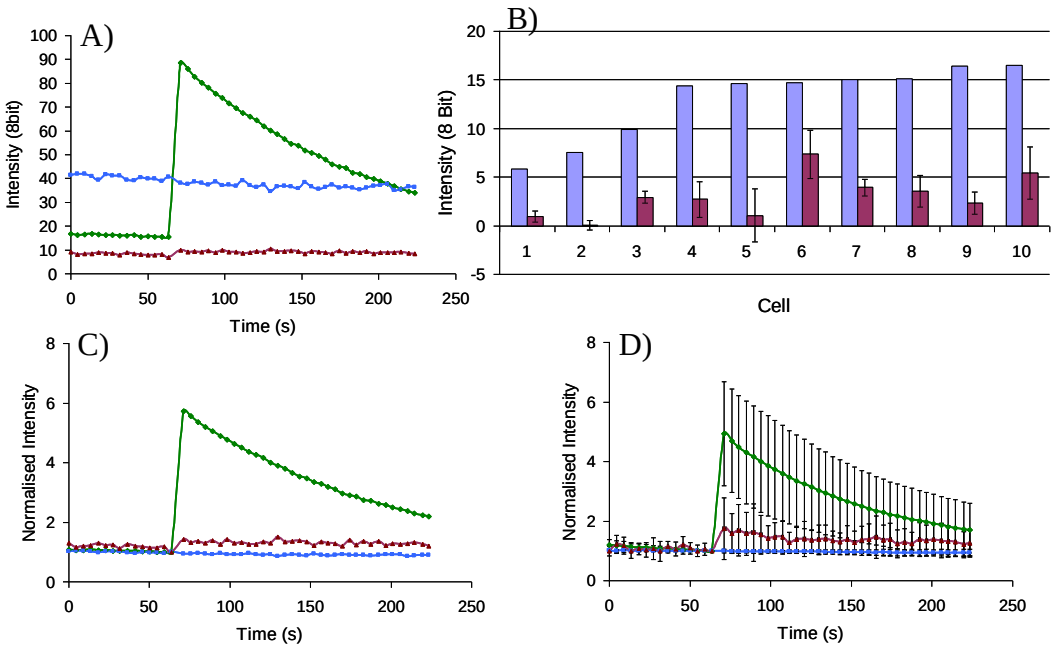

Figure 4-4 Spillover in a cell population with Dronpa acceptor.

Single SK-N-AS cells expressing pG-CMV-AmCyan and pG-CMV-Dronpa displayed spontaneous increase in I_{DA}. **A)** a: single cell showing a small increase. **B)** 10 cells showing total remaining fluorescence in I_{DA} (Blue) and change in I_{DA} with error bars showing noise in the channel (purple) **C)** Single cell normalised showing increase. **D)** Average population (n=10) of normalised cells showing variance between cells.

Using this approach to analyse cells expressing the positive control vector showed a reduction in the overall intensity of F_c but ΔF_c showed no apparent change (Figure 4-5). Comparing the positive to the negative control, the linear subtraction of spillover worked well for preserving sensitised emission in positive interactions.

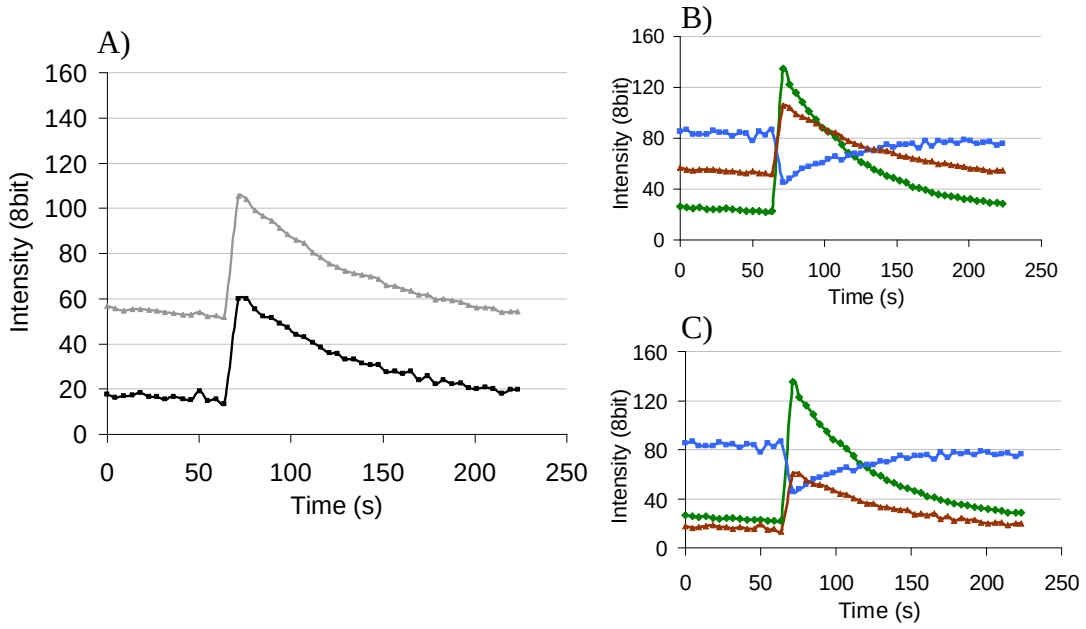

Figure 4-5 Spillover correction of the Signal from a positive control for FRET.

Single SK-N-AS cell expressing positive control (pCMV-Dronpa-7aa-AmCyan) construct. **A)** both raw (black) and processed (grey) I_{DA} channels plotted on same axis. **B)** unprocessed data showing increase in F_c (Red) **C)** processed data showing corrected F_c.

4.3.2 Unmixing mStrawberry

Using the method established in section 4.3.1, Dronpa and mStrawberry were similarly tested to ensure spillover between detectors was linear. Using the optimised illumination strategy for mStrawberry for LSM710, relative spillovers were measured. As expected spillover between channels occurred within the linear range of PMTs (Figure 4-6).

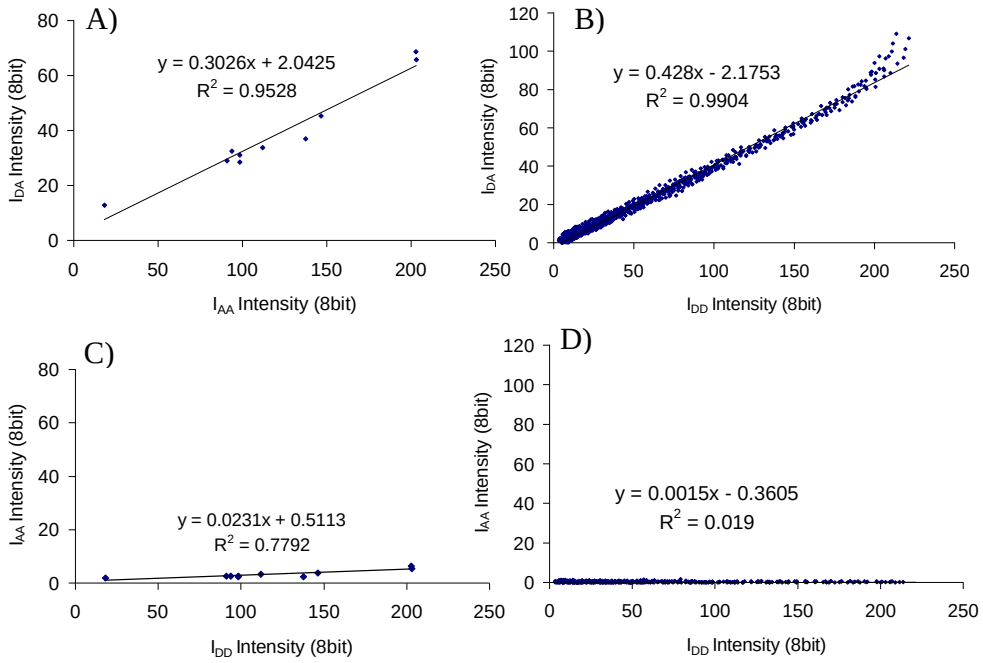

Figure 4-6 Spillover between Dronpa and mStrawberry.

The relative spillover of cells expressing the acceptor pG-CMV-mStrawberry and the donor pG-CMV-Dronpa into I_{DD}, I_{AA} and I_{DA} channels. A) spillover of acceptor (mStrawberry)into I_{DA} B) Spillover of donor (Dronpa) into I_{DA}. C) spillover of Acceptor (mStrawberry) into $I_{DD.}$ D) spillover of donor (Dronpa) into I_{AA}. Shows very strong linear relationship in each instance.

Cells expressing a Dronpa mStrawberry positive control construct showed promising results with a relatively high energy transfer detected through change in sensitised emission (Figure 4-7). However, the pair Dronpa and AmCyan did not require spillover correction to observe quenching of AmCyan fluorescence on Dronpa switching so this was chosen for further study.

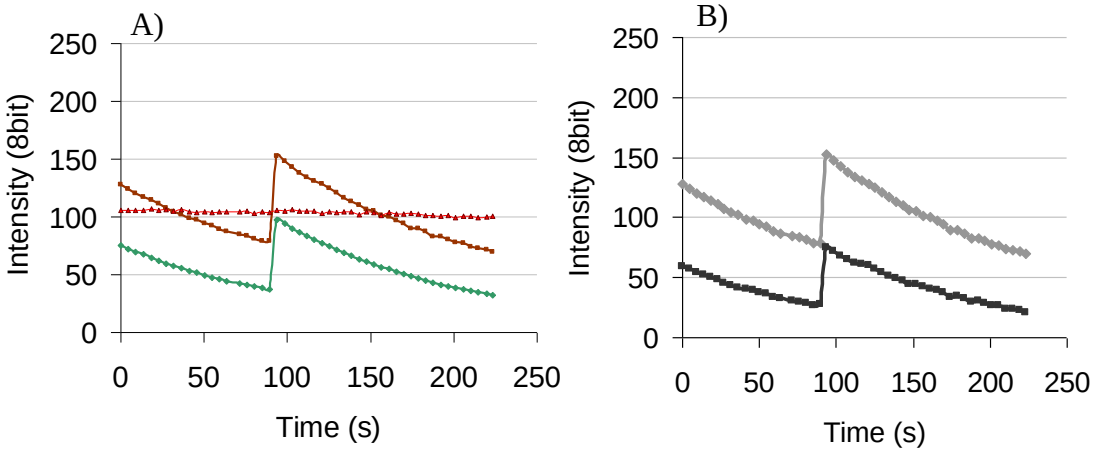

Figure 4-7 Spillover correction of Dronpa mStrawberry FRET

Single SK-N-AS cell expressing positive D-S control construct. A) unprocessed data showing increase in Fc (Red) processed data showing corrected Fc. B) both raw (black) and processed (grey) IDA channels plotted on same axis.

4.4 Donor Relationship with Sensitised Emission

The relationship between the change in donor and F_c was shown to be a linear relationship independent of expression level (Figure 4-8). This relationship is known as G (Zal and Gascoigne 2004) (Gordon, Berry *et al.* 1998). A non linear relationship could infer that FRET could be caused through over-expression and dimerisation of fluorophores at high concentrations. It was also possible that the conformational change that gives Dronpa its spectral characteristics may cause aberrations in energy transfer due to physical changes in chromophore distance (Andresen, Stiel *et al.* 2007). To investigate these questions cells expressing protein from a Dronpa-Amcyan positive control vector were investigated using an optimised illumination strategy for LSM710 using a 405nm laser for Dronpa switching (Figure 4-8).

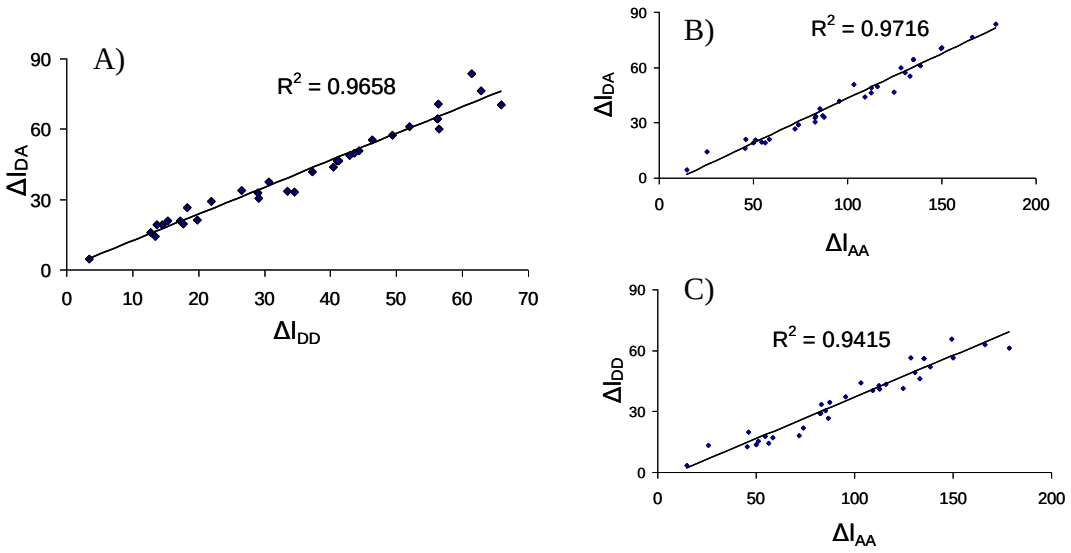

Figure 4-8 The relationship between sensitised emission (F_C) and donor quenching

SK-N-AS cells (n=32) exhibiting different expression levels from pG-CMV-Dronpa-7aa-AmCyan were examined for relative changes in fluorescence level following switching using the standardised imaging protocol on LSM710 with 405nm switching. A) change in sensitised emission vs. change in donor B) change in sensitised emission vs change in acceptor. C): change in donor vs. change in acceptor. There were linear relationships regardless of expression levels.

The relationship between sensitised emission (F_C) and donor quenching showed a strong linear correlation (R^2=0.9658) implying no dimerisation of fluorophores at high concentrations, and efficient FRET over a standardised change in fluorescence of Dronpa. Certain aberrations were present in certain cells. It was postulated that these aberrations were due to the previously observed unstable characteristic of AmCyan. G is only proportional if both fluorophores are at a 1:1 ratio, or more specifically if the population of available acceptor exceeds that of the donor, provided sensitised emission has been processed to remove spillover.

While the relationship between ΔF_c and ΔI_{DD} showed a linear constant with regard to expression level, 'G' strongly correlated in a linear relationship with the protonation state of Dronpa (R^2= 0.9857) (Figure 4-9). Though the relationship was linear with the standardised imaging protocol, incomplete switching (introduced in chapter 3) could be a source of error for detecting FRET efficiency. This possible error is equivalent to incomplete acceptor photobleaching in acceptor photobleaching assays of FRET efficiency (Berney and Danuser 2003).

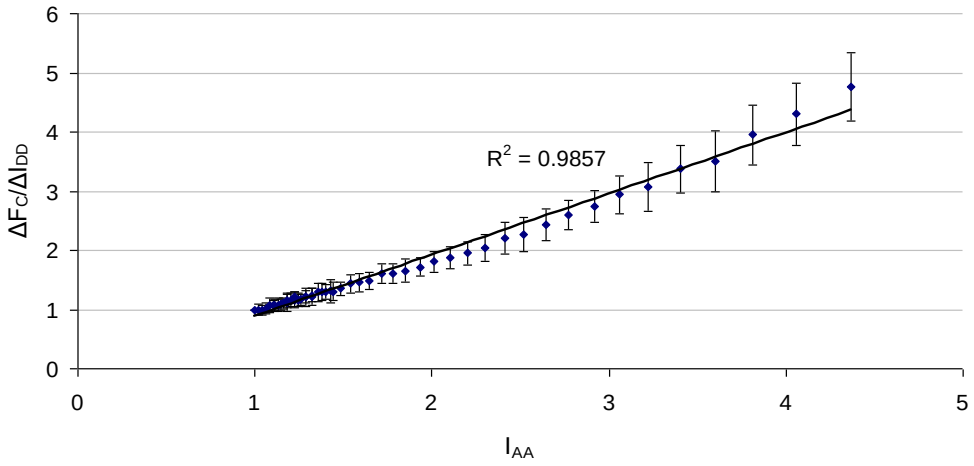

Figure 4-9 The relationship of 'G' with Dronpa protonation state.

A population of SK-N-AS cells (n=10) expressing positive control construct pG-CMV-Dronpa-7aa-AmCyan switched with 405nm excitation on LSM710 confocal using optimised illumination strategy. Each channel was normalised before Dronpa was switched. The relative fold change of F_c /I_{DD} was plotted against I_{AA} for each time point of the time series (imaged over 3min 40sec). Error bars represent SD of this relationship between normalised cells.

This relationship is promising for instances where donor and acceptor ratios are known to exist in a 1:1 stochiometry. Any inconsistencies in Dronpa switching affecting reported FRET may be corrected for simply by using the relative change of Dronpa. In instances where 1:1 stochiometric ratios deviate, this simple correction is not possible as the linear relationship between these values breaks down.

4.4.1 Donor and Acceptor Saturation

Donor concentration is known to be of importance with regards to concentration and competition. If donor concentration exceeds that of acceptor concentration, competition between donor molecules become a determining factor in energy exchange. This means that once saturated, a subpopulation of non-interacting donor molecules will be present. This means that past the point of saturation the linear relationship between sensitised emission and donor quenching breaks down. Although quenching will still be present, the total relative change will be masked by this subpopulation.

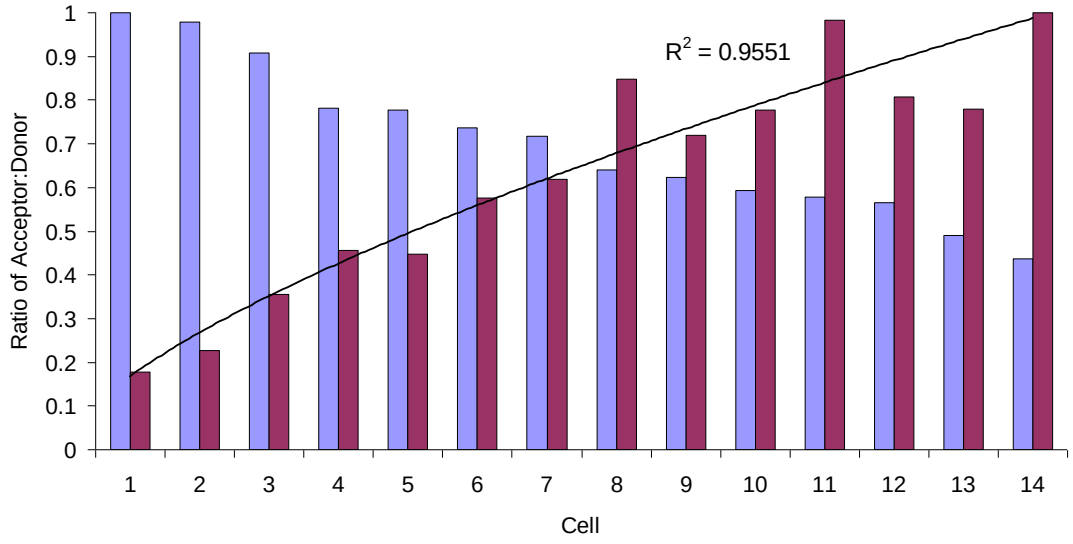

Figure 4-10 The relationship between F_C and acceptor:donor ratio.

Fluorescence levels were measured from unstimulated SK-N-AS cell expressing the FRET pair Dronpa-p65 (acceptor) and p105-Amcyan (donor). Fc (purple bars for each cell) is shown alongside increasing acceptor:donor Ratio (blue) for the same cell. The closer to 1 the more acceptor compared to donor is present in the cell.

Figure 4-10 illustrates that when acceptor molecules outnumber donor molecules changes in F_C are smaller. However 'G' remained linear, indicating that energy transfer between donor and acceptor was unaffected. While this relationship should plateau, not enough data points with higher donor concentrations were available in this dataset to conclusively show this. It should also be made clear that fusion proteins were functioning NF-κB proteins and as such may have been subject to stochastic differences between cells affecting sensitised emission. In conclusion scaling FRET response to positive controls should only be reserved in cases where donor fluorophores numbers are equal to or exceed the numbers in the acceptor population. The significance of this to endodgenous expression is that provided both sensitised emission.

4.5 Quantification

First and foremost, changes in sensitised emission are a visual representation of FRET and its relative efficiency. Figure 4-11 shows spillover corrected traces for four different experiments. Dronpa-p105-AmCyan, Dronpa-p105 p65-AmCyan, Dronpa-p105 and p105-AmCyan raw data while relative ratios of donor and acceptor have been kept as consistently similar as possible, sensitised emission is shown to not only have different changes, but also has different overall intensity values. Both of these factors are important indicators of FRET.

This can be most effectively demonstrated comparing Dronpa-p105-AmCyan and Dronpa-p105 p105-AmCyan (Figure 4-11 A & C). Both cells have similar ratios, switching efficiency and expression levels. F_c presence and increase is stronger in the double-tagged construct compared to that of the intermolecular interaction.

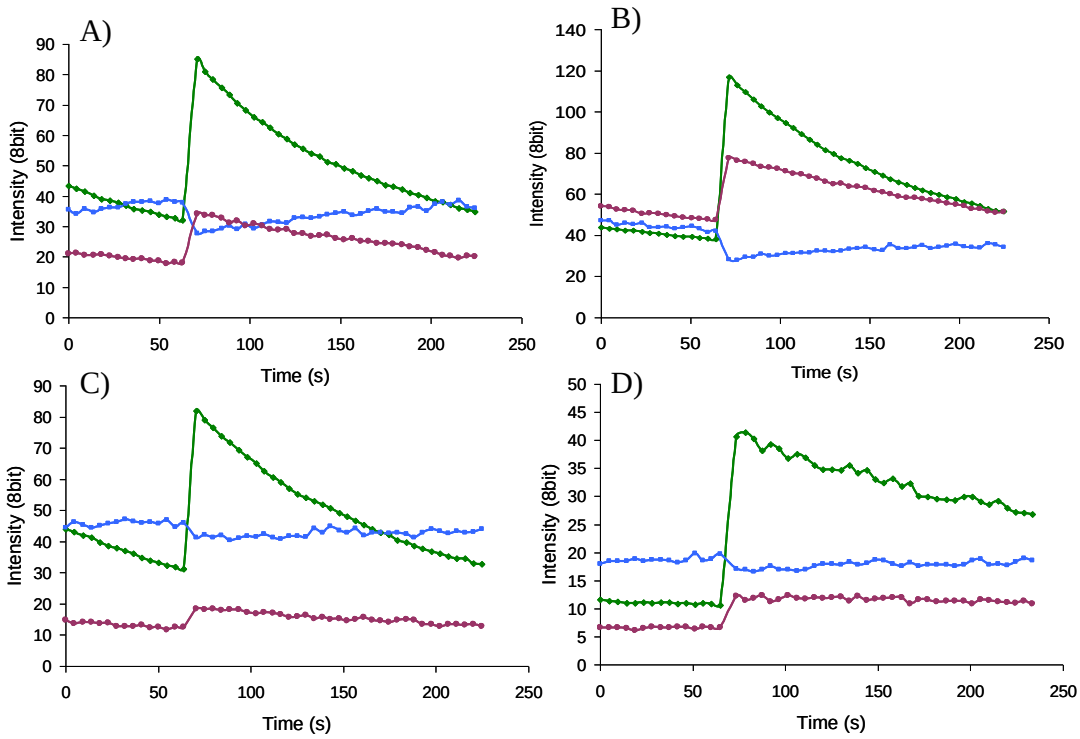

Figure 4-11 Example data from cells expressing different fusion pairs.

Four separate pairs of fusion proteins were expressed in single SK-N-AS cells and fluorescence levels analysed before and after Dronpa switching. I_{DA} channels were crosstalk corrected. A) Dronpa-p105-AmCyan B) Dronpa-p105 p65-AmCyan. C) Dronpa-p105 p105-AmCyan D) Dronpa-p50 p65-AmCyan. Green represents Dronpa fluorescence, blue represents AmCyan fluorescence, purple represents sensitised emission (Dronpa fluorescence through AmCyan excitation).

To make use of sensitised emission to visualise total remaining FRET, the ImageJ plug in 'Fret-analyzer' was employed to generate pixel by pixel representations of sensitised emission in cells. The software is based on corrected sensitised emission calculations from Youvan *et.al.* (Youvan, Silva *et al.* 1997). Generated images were non-normalised F_C images which were processed for spillover as previously described in section 4.3.

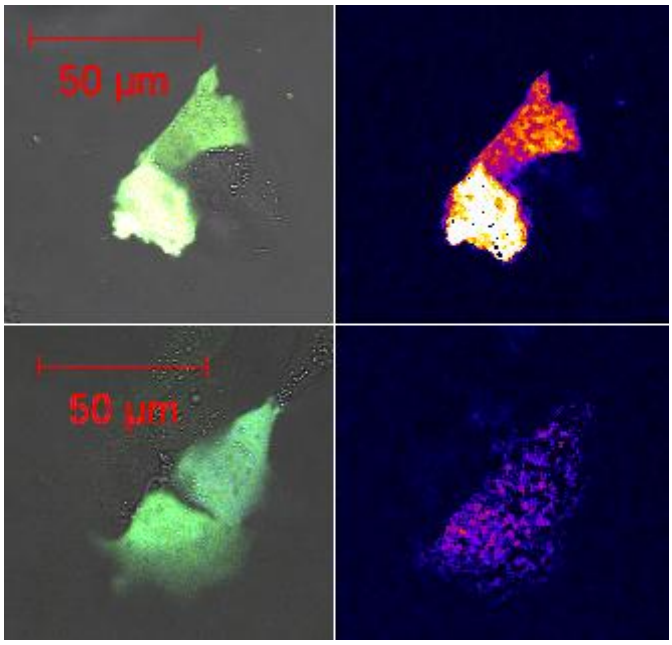

Figure 4-12 A comparison of outputted FRET images from Image J Plug in Fret Analyser.
A) pG-CMV-Dronpa-7aa-AmCyan Positive control and output from the plugin**. B)** Negative FRET control pG-CMV-AmCyan and pG-CMV-Dronpa coexpression and output from the plugin. The software uses spillover corrected sensitised emission to generate non-normalised images which infer total level of sensitised emission on a pixel by pixel basis.

This pixel by pixel measure gave an overall picture of remaining FRET in the system, but did not allow the visualisation of interacting FRET pairs independent of concentration and expression. These images were used in conjunction with FRET equations which allowed the quantification of FRET regardless of fluorophore concentration.

4.5.1 Normalisation of Populations

By normalising the fluorescence of cells, different expression levels could be compared directly to one another. Figure 4-13 shows both negative and positive control were each channel is normalised to the time point before photoswitching. Any change is then observed as a fold change. The standard deviation of each time point is plotted as error bars. Standard deviation gives an indication of variance between cells, with smaller error bars indicating more consistent FRET interactions and photoswitching of Dronpa.

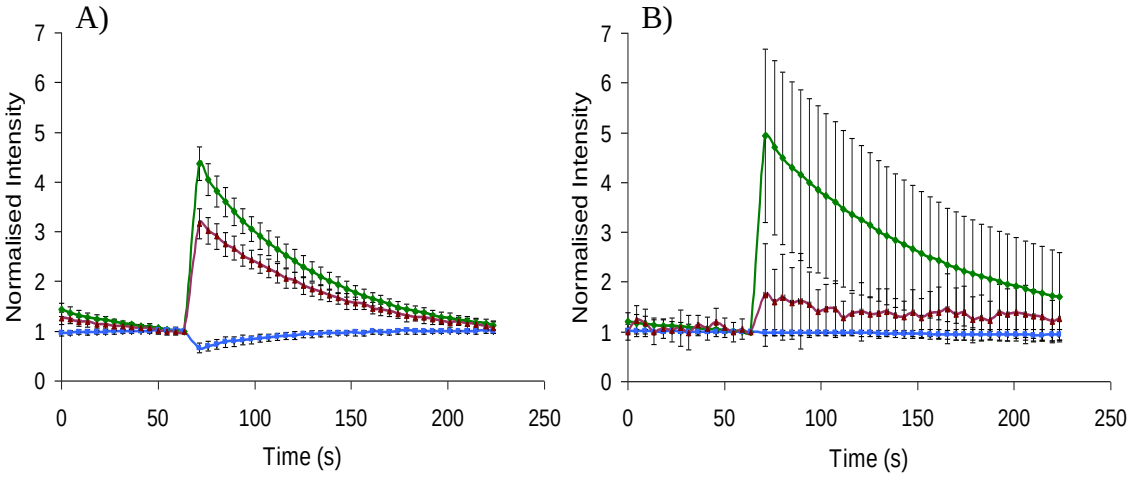

Figure 4-13 A comparison of Dronpa switching in cell populations expressing positive and negative FRET control constructs

Normalised population of cells (n=10) after image analysis and data processing. SK-N-AS cell expressing from a pG-CMV-Dronpa-7aa-AmCyan Positive control construct (A) and Negative FRET control pG-CMV-AmCyan and pG-CMV-Dronpa coexpression (B). Green is I_{AA} (Dronpa) Blue is I_{DD} (AmCyan) Brown is I_{DA} (F_c). Error bars represent standard deviation of each channel between normalised cells. The Optimised illumination strategy for on LSM710 was used.

ΔF_c represents the measurable energy transfer to the acceptor from the available donor, where as ΔI_{DD} represents the quenching effect on the donor by increased acceptor fluorescence. Normalisation in this way affects an important characteristic of the data; the expression levels of the fluorophores. As section 4.4.1 demonstrates, fluorophore ratios can have an adverse effect on relative change in both F_c and I_{DD}. Another important characteristic of this average population is discrimination between different FRET behaviours. Variation will become apparent in the degree of deviation between cells, and can be visualised by plotting relative change in each cell

individually.Both of these factors pointed to this method of analysis being best suited for cases where fluorophores are at a constant ratio. This would ideally be a biosensor which will change conformation depending on phosphorylation, ligand or protein concentration. However provided fluorophore populations remain at a consistent level, FRET should be internally consistent.

4.5.2 Calculating FRET Efficiency

A number of methods exist to calculate FRET efficiency in the literature (Berney and Danuser 2003). The Majority of these methods employ changes in sensitised emission in relation to donor and acceptor ratios to measure FRET to bypass destructive acceptor photobleaching. Used by Turcatti *et. al.* and many other publications, acceptor photobleaching can be used as a much more straightforward means of measuring differences in FRET efficiency (Turcatti, Nemeth *et al.* 1996; Wouters, Bastiaens *et al.* 1998) proposed the following equation:

$$\boldsymbol{E} = 1 - \frac{\boldsymbol{I}_{\boldsymbol{DD}}}{\boldsymbol{I}_{\boldsymbol{DD}}'} \qquad [1]$$

This results in the normalised change in quenching of the donor fluorophore following a corresponding change in acceptor fluorescence, allowing the comparison of FRET efficiencies reported between cells. Provided donor fluorescence does not exceed acceptor fluorescence, comparisons should be relatively simple. Using equation 1, FRET efficiency from different cells could then be easily compared as below using non parametric Kruskal–Wallis one-way analysis of variance to compare datasets for significant differences from one another.

Two other equations were tested which rely upon the use of sensitised emission to distinguish between FRET efficiencies. The first, proposed by Gordon et.al.(Gordon, Berry *et al.* 1998) is as follows:

$$FRETN = \frac{F_C}{I_{AA} \times I_{DD} \times G} \qquad [2]$$

This equation uses spillover corrected sensitise emission (Fc) divided by the levels of acceptor fluorophore and donor fluorophore. The second proposed by Zal *et.al.*(Zal and Gascoigne 2004) used the following equation:

$$E_{app} \frac{F_C}{I_{DA} + I_{AA} + (G \times I_{AA}) \times I_{DD}} \qquad [3]$$

These equations make use of total sensitised emission and its relationship with the level of both acceptor and donor fluorophores to account for donor occupancy. They also make use of the term G the relative change in donor excitation following acceptor photobleaching which should be a linear function of chosen donor and acceptor fluorophores in an idealized system (discussed in section 4.4).

Using these equations, existing positive control constructs were compared with molecules of the positive control construct pG-CMV-Dronpa-7aa-AmCyan, and the co expression pG-CMV-Dronpa-p105 and pG-CMV-p105-AmCyan which were shown to have less efficient energy transfer using acceptor photobleaching to qualify this.

Table 4-1 Comparison of different methods for Quantifying FRET
using positive control construct pG-CMV-Dronpa-7aa-AmCyan (n=8), biologicacl example of Dronpa-p105 p105-AmCyan (n=7) and negative control pG-CMV-AmCyan pG-AmCyan-Dronpa (n=14).

Measure of FRET	I_{DD}/I_{DD}'	FRETN	E_{app}
Positive Control			
Mean	0.29	0.0076	0.39
SD	0.13	0.0051	0.12
Low FRET			
Mean	0.09	0.0039	0.23
SD	0.03	0.0022	0.09
Negative Control			
Mean	-0.04	0.00089	0.09
SD	0.054	0.000286	0.028

Each method demonstrated the ability to discriminate between different degrees of FRET in samples (Table 4-1). Donor quenching however had the added advantage of being free from any unaccounted spillover and providing a good dynamic range with relatively small degree of deviation from the mean compared to other methods (specifically compared to FRETN). These additional methods were used as an additional method to quantity FRET efficiency.

4.6 Conclusion

The process of qualifying and quantifying the FRET response of Dronpa was of specific importance. It was of concern that Dronpa would behave non-linearly across a range of protonation states. This proved not to be true as Figure 4-9 demonstrates. Furthermore, FRET between different protonated states of Dronpa also behaved linearly indicating that the possibility of Dronpa behaving as a 'dark acceptor' of fluorescence was either trivial, or not of importance. A potential acceptor for Dronpa was also identified for further development in the form of mStrawberry but there was some uncertainty of the utility of this pair without crosstalk correction of sensitised emission.

Finally the quantification of FRET through means of sensitised emission for pixel by pixel analysis, and quenching of donor fluorescence proved an effective means for analysing the efficiency of energy exchange between fluorophores. Other efficiency equations that utilised sensitised emission also worked well when comparing changes in donor quenching efficiency. The next step was to apply this system to a biological example where changes in FRET could be measured over time to infer the dynamics of protein interaction.

Chapter 5: FRET in the NF-κB System

5.1 Context

Once the behaviour of Dronpa as a FRET partner had been confirmed to be as expected and appropriate optimised fluorophore partners had been tested to qualify partner behaviour. Different Dronpa fusion proteins were tested, in pairs and in long time course experiments. NF-κB was considered a good system to investigate due to the large number of potential time dependent protein interactions shown to occur as part of the pathway and availability of relevant cDNAs (Hayden and Ghosh 2004; Nelson, Ihekwaba *et al.* 2004).

p105 was singled out as a protein of interest due to its dual functionality as both an IκB and an NF-κB, providing twice the number of opportunities to bind to interacting proteins. Furthermore p105 is reported to inhibit the nuclear translocation of its N-terminal RHD through conformational inhibition of the NLS by the IκB like C-terminal, so the possibility of observing intramolecular FRET between both ends was considered a strong possibility (Moorthy and Ghosh 2003; Savinova, Hoffmann *et al.* 2009). A search of the literature of p105 for FRET studies also appeared to indicate that this area had not been studied. These factors combined suggested the possibility that FRET studies of this protein might give interesting insights into p105 biology and its interaction with other NF-κB family member proteins in live cells would be informative.

A double tagged Dronpa-p105-AmCyan fusion was initially generated by Dr. Sheila Ryan. This was used to test intramolecular FRET in p105, and for use in conjunction with other known interacting NF-κB family members such as p65 and p50. Resulting experimentation showed strong intra and intermolecular interactions with p105 and other NF-κB family members. FCCS was also used as an additional method to give context to findings using FRET. FCCS does not require the exchange of energy between fluorophores as in FRET (discussed at length in Section 1.2.4), but the cross correlation of fluorescence fluctuation in a small confocal volume (Section 1.2.5). As a result FCCS gives a measure independent of steric and conformational limitations and provides clear supporting evidence as to whether FRET is due to conformational or localisation changes of fluorophores.

5.2 The Characterisation of p105

As previously discussed, p105 was shown to undergo processing following TNFα stimulation. Lysates from SK-N-AS cells treated with 10μg/ml TNFα over a 24h period were subject to Western blotting using the Cell signalling antibody for N-terminal p105 (Cell signalling #3035) The data indicated that endogenous levels p105 were relatively unaffected by the treatment, with only a small increase in p50.

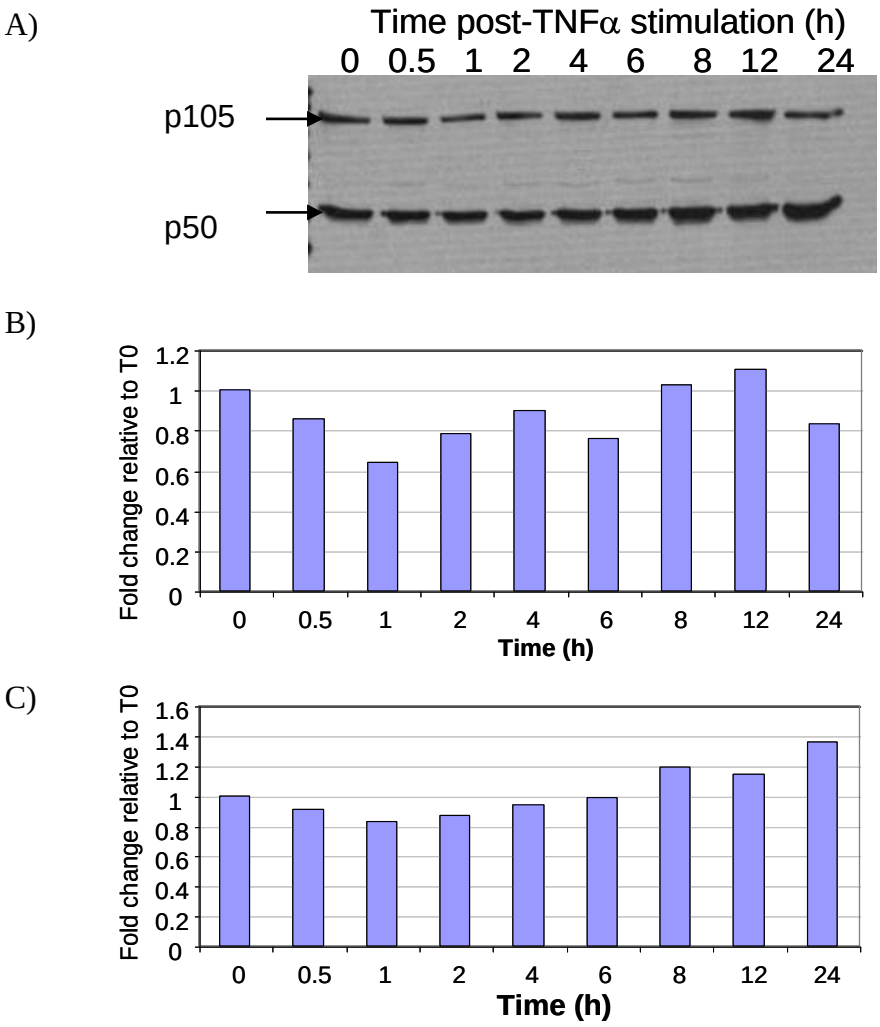

Figure 5-1 Western blot of endogenous N-terminal p105 levels

SK-N-AS cells stimulated with TNFα. Cells were treated with TNFα (10ng/ml) and lysed at the time points indicated. **A)** An antibody specific to the N-terminus of p105 (Cell signalling 3035) was used to detect both full-length p105 and p50. **B)** Quantification of shows relatively conserved level of p105 following stimuli over 24h period. **C)** Quantification of p50 showing small increase following stimulation. Data provided by Sheila Ryan

The construct pG-CMV-DsRedxp-p105-EGFP generated by Sheila Ryan for imaging of p105 behaviour in live cells was initially transiently transfected into cells and monitored for changes in expression following TNFα stimulation by western blot. This was to confirm fusion protein size and behaviour was consistent with endogenous protein behaviour.

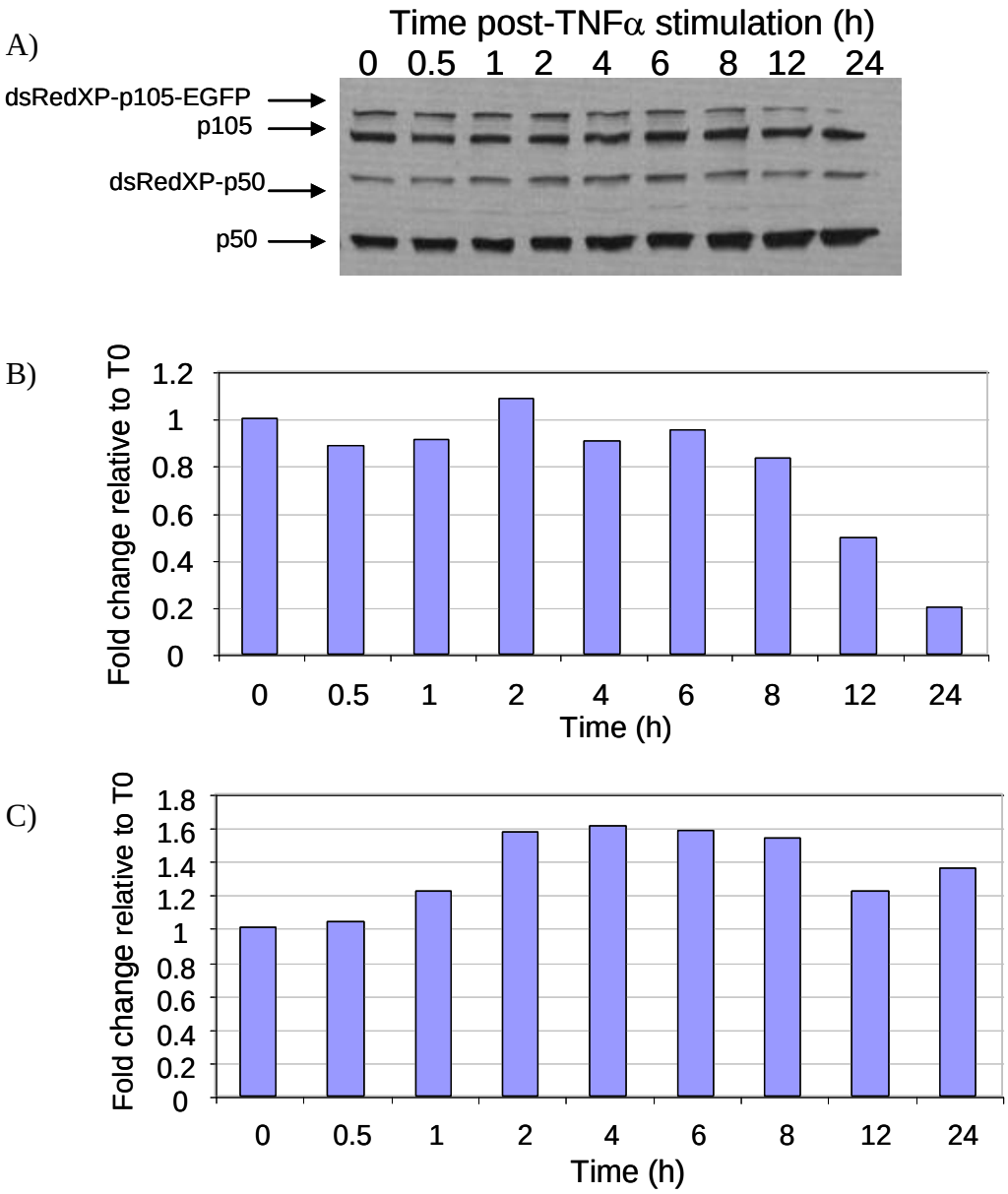

Figure 5-2 Western blot of endogenous and transiently transfected N-terminal p105

pG-DsRedXP-p105-EGFP in SK-N-AS cells stimulated 24h post transfection with TNFα. Cells were treated with TNFα (10ng/ml) and lysed at the time points indicated. (A) An antibody specific to the N-terminus of p105 (Cell signalling 3035) was used to detect both full-length p105 and p50. (B) Quantification of bands showed transient DsRedXP-p105-EGFP was slowly processed following stimulation of cells over a 24h period. (C) Quantification of p50 indicated a small increase following stimulation consistent with endogenous increase. Data provided by Sheila Ryan

Western blot analysis of the transient fusion expressed in SK-N-AS cells revealed that p105 processing of the fusion was consistent with that of the endogenous in that levels of p50 increased following stimulation. The construct also mimicked endogenous p105 behaviour via constitutive cleavage of the fusion protein at T0.

Following the testing of p105 fusion proteins through the use of bulk cell molecular assays, the single cell dynamics of p105 were characterised for later comparison against Dronpa constructs and use in FCCS experiments.

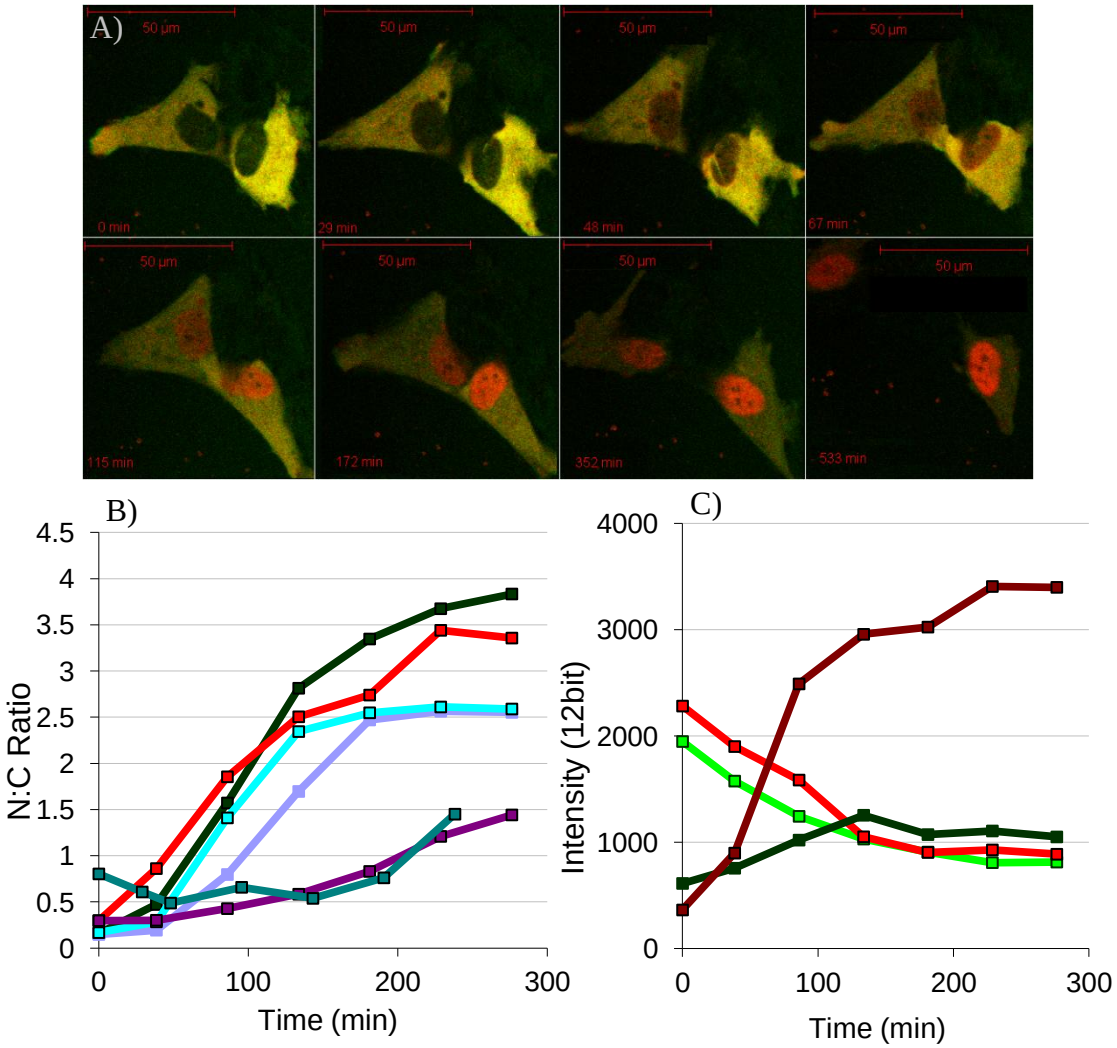

Figure 5-3 The behaviour of p105 fusion proteins in live cells following TNFα stimulation.
SK-N-AS cells expressing fusion proteins from pG-CMV-DsRedExpress-p105-EGFP were imaged and analysed using CellTracker. TNFα Stimulation post T0. A) Time series images following TNFα stimulation and resulting changes in fluorescence localisation. B) Change in Nuclear:Cytoplasmic ratio the red signal (n=6). C) Fluorescence levels of representative cell expressing DsRedxp-p105-EGFP following TNFα stimulation. Bright Green; Cytoplasmic green signal, Red: Cytoplasmic red signal. Dark Red: Nuclear red signal, Dark Green; Nuclear green signal.

TNFα induced a process of slow loss of the green fluorescent signal and the simultaneous slow nuclear translocation of red fluorescence to the nucleus which appeared to be reaching a plateau after approximately 180-240min. This is in stark contrast in comparison to the degradation of IκBα and subsequent translocation of p65 which can be observed within as little as 10min (Nelson, Ihekwaba *et al.* 2004). The apparent cleavage and translocation of p50/p105 is a comparatively slow process. Questions were raised as to whether constitutive cleavage of the construct was occurring in cells prior to the addition of stimulus. To that end, FCCS was used to assess the molecular ratio of DsRedXP to EGFP. Results showed a 2:1 ratio DsRed to EGFP, thereby indicating a 1:1 ratio of p50 to p105 (Figure 5-17).

5.3 FRET in p105

As previously discussed, p105 is thought to inhibit the nuclear translocation of its N-terminal RHD through conformational inhibition of the NLS by the IκB like C-terminal domain. A double tagged Dronpa-p105-AmCyan fusion was initially generated by Sheila Ryan. This was used to test intramolecular FRET in p105. The FRET response of pG-CMV-Dronpa-p105-AmCyan compared to negative (pG-CMV-Dronpa and pG-CMV-Amcyan) and the positive control constructs (pG-CMV-Dronpa-7aa-AmCyan) were examined following light modulated Dronpa switching in living SK-N-AS cells (Figure 5-4). By observing AmCyan quenching following Dronpa activation in ‘resting cells’ (i.e. those cells showing no translocation of n-terminal p50 into the nucleus), using quenching equation [1] established in Chapter 4: a reliable FRET response was observed in a population of 18 cells. Some cells that were not responding to Dronpa switching were excluded from the analysis to estimate FRET efficiency more accurately.

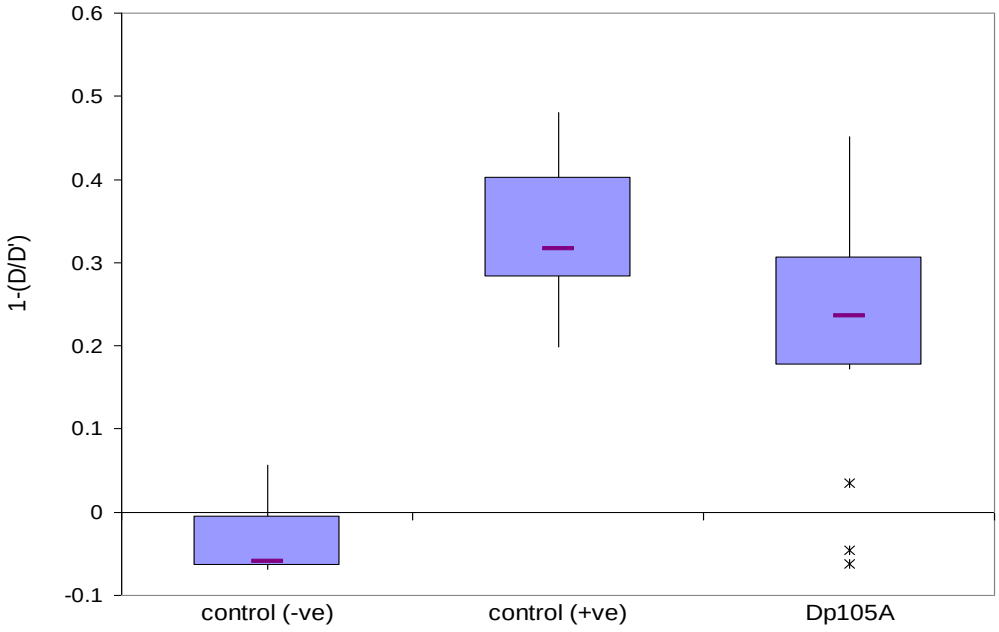

Figure 5-4 A comparison of the Intracellular FRET response from different transfections.
The FRET response of pG-CMV-Dronpa-p105-AmCyan (Dp105A n=18) compared to negative control (pG-CMV-Dronpa and pG-CMV-Amcyan) (n=10) and the positive control constructs (pG-CMV-Dronpa-7aa-AmCyan) (n=10) were examined following light modulated Dronpa switching in living SK-N-AS cells.

This indicated that the N and C termini of p105 interact strongly in cells. This leaves two possibilities. Either p105 remains a full length protein and prevents nuclear translocation through conformational inhibition of the NLS or p105 is cleaved and C terminal IκBγ associates with p50 following this event. The data also indicated that FRET between N and C termini was variable between cells. It was unknown if this observed difference was due to conformational changes of p105 or if p105 was being processed during the 16 h period between transfection and analysis.

To test if the measured FRET signal was purely intramolecular within p105, single tagged constructs with identical linker sequences to that of the double tagged construct were cloned using LR gateway recombination of pENRT2a-p105 and pg-B-AmCyan, and mutagenesis on the pG-D-p105-A construct to mutate a stop codon at the 3' end of the p105 CDS pG-CMV-Dronpa-p105 and pG-CMV-p105-AmCyan. These vectors were then transfected into cells to test intermolecular FRET efficiency and compared to the signal from the double labelled p105 fusion protein (Figure 5-5).

5.3.1 Intermolecular p105 interactions

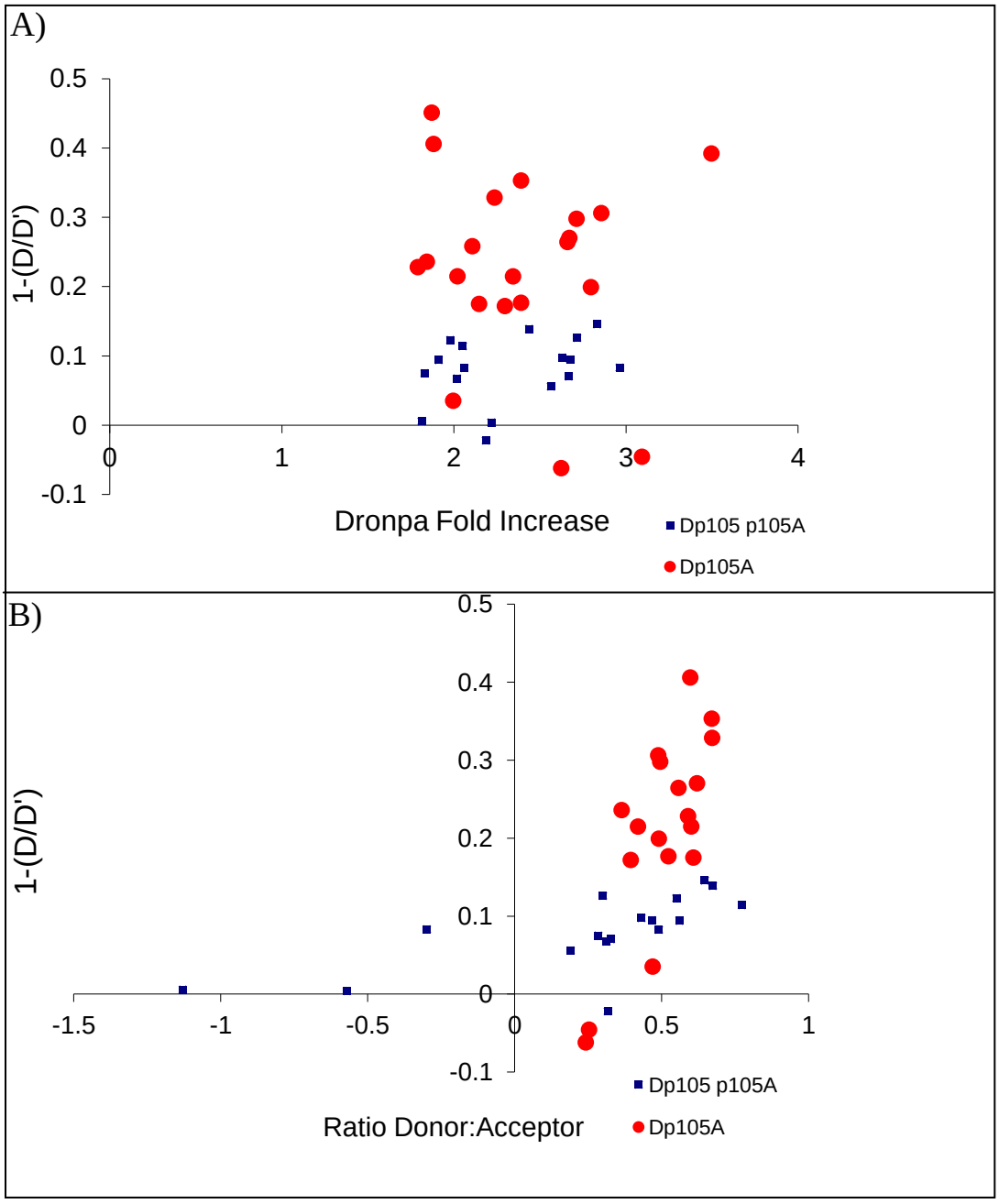

Figure 5-5. A comparison of the FRET efficiency between and within p105 proteins.

SK-N-AS cells expressing pG-CMV-Dronpa-p105-Amcyan alone (n=18) and cells expressing pG-CMV-Dronpa-p105 and pG-CMV-p105-AmCyan (n=15) using donor quenching to infer FRET efficiency. A) Change in donor fluorescence for intramolecular (red) and intermolecular (blue) interactions plotted against fold change in Dronpa. This shows FRET is generally unaffected over a range of switching efficiencies. B) FRET efficiency measured using donor quenching in double tagged (red) and intermolecular (blue) constructs. Plotted against arbitrary ratio of donor:acceptor fluorescence relative to PMT gain, normalised to maximum acceptor fluorescence.

Figure 5-5 shows the differences between intermolecular and intramolecular FRET in p105. Using non-parametric Kruskal-Wallis ANOVA, a statistically significant difference between intramolecular and intermolecular experiments was uncovered ($<p=0.05$, $Chi^2=10$). Intermolecular interactions between p105 were less efficient than intramolecular interaction, indicating that the FRET signal measured and displayed in Figure 5.2 was probably due to both binding between p105 oligomers and within p105 at N and C terminal regions. However, the data does not rule out the possibility that there was cleavage and re-association of N and C terminal regions. There also appears to be a small population of cells where there was no measurable FRET signal where either double tagged or both single tagged fusion proteins were expressed. These were excluded from statistical tests.

To test if there were other orientations of single fluorescence labels on p105 that had a higher FRET efficiency (an indicator of intermolecular interactions), a number of different p105 EYFP and ECFP fusion proteins were coexpressed pairwise in cells and FRET assessed by acceptor photobleaching. Due to the difficulty of detecting changes in fluorescence due to poor quantum yield of ECFP, FRET was assessed by spectral scanning using the META detector of a Zeiss LSM510 confocal microscope. Followed by linear unmixing using reference spectra (Zimmermann, Rietdorf *et al.* 2002) Efforts were made to keep conditions (such as fluorescence levels, detector gain and laser excitation) as similar as possible so that reasonable semi-quantitative comparisons could be made. Due to the significantly different approach to measuring FRET efficiency this way compared to Dronpa switching it is unsafe to directly compare the values of FRET efficiency from the data in Figure 5-6 to others in this Chapter.

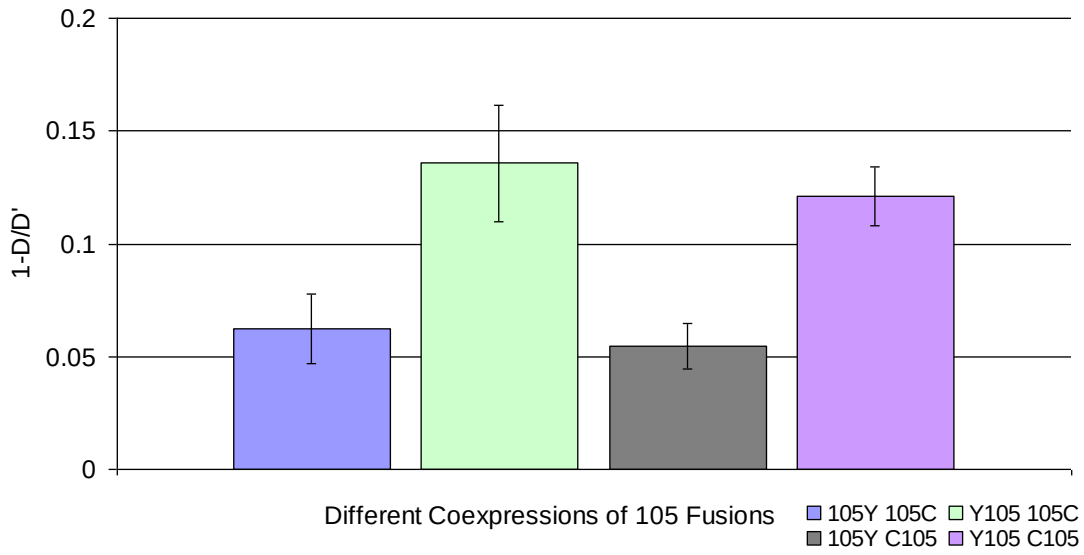

Figure 5-6 Change in donor fluorescence following acceptor photobleaching

SK-N-AS cells coexpressing different orientations of p105 fusion proteins to monitor differences in FRET efficiency between N and C terminals of p105 (n=10 for each pair). EYFP(Y) and ECFP(C) used. Data spectrally deconvolved using reference spectra from pG-CMV-p105-EYFP and pG-CMV-p105-ECFP.

There were only small differences between p105 co-transfection FRET measurements of any label orientation but notably the signal from the coexpression pG-CMV-EYFP-p105 pG-CMV-p105-ECFP (equivalent to pG-CMV-Dronpa-p105 and pG-CMV-p105-AmCyan) was the most efficient. These data, reinforce the idea that some of the FRET signal from expressed p105 fusion proteins can be from intramolecular associations. They also hint that intermolecular interactions through FRET are primarily from dimerisation of Rel regions of either constitutively cleaved p50 or full length p105.

The next step was to test the Dronpa AmCyan fusion proteins in a long time course to establishing the viability of the FRET pair over extended periods of imaging to assess potential photodamage, and in establishing any changes in intramolecular p105 FRET efficiency.

5.3.2 Changes in p105 over time

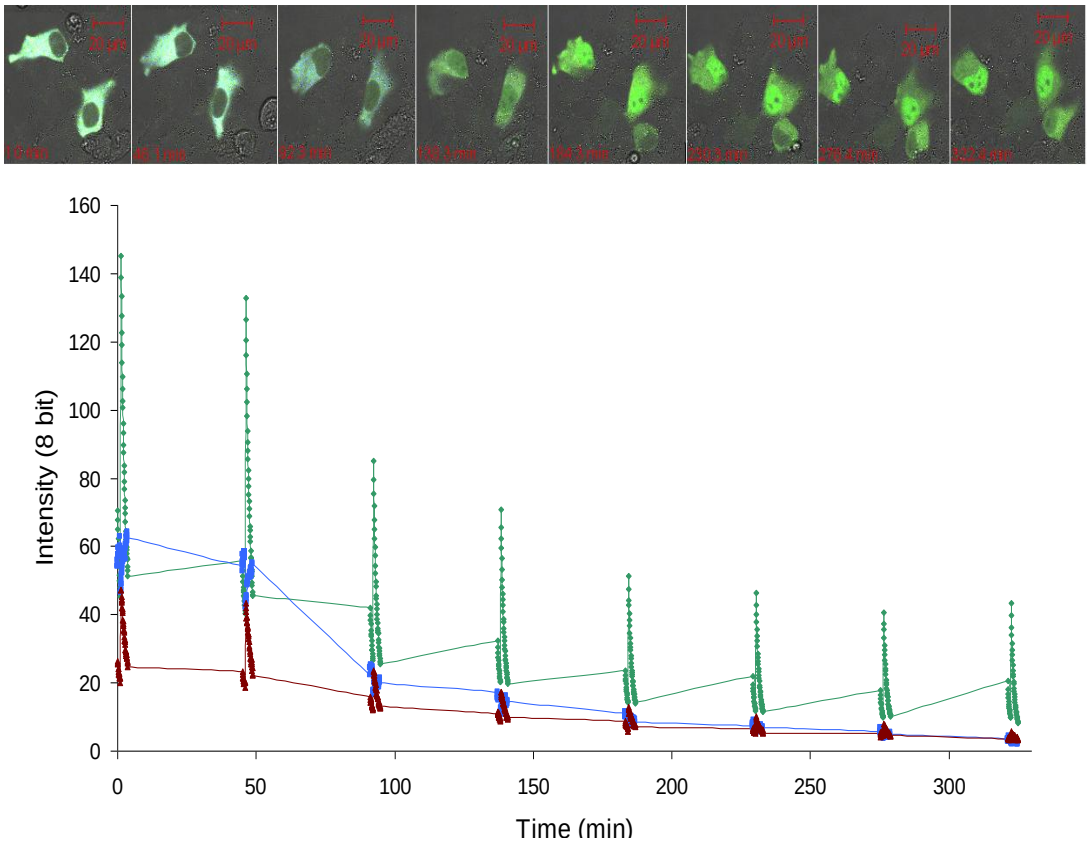

Figure 5-7 Changes in p105 fluorescent signals in a single cell over time.

Data was analysed from a ROI in the cytoplasm of a representative cell during a 5 h time series taken of SK-N-AS cells expressing pg-CMV-Dronpa-p105-AmCyan. Cells were stimulated with TNFa after each location had been imaged once (45 mins). Green represents Dronpa, Blue represents AmCyan and Red represents sensitised emission (crosstalk subtracted). Each cluster of time points represents a 50 frame contiguous image series. Gaps between the image series represent time lag between scanning each of 8 fields imaged sequentially.

The Optimised illumination strategy using whole field ROI switching ('bleaching') was used repeatedly in multifield time-series experiments. Due to the time taken to switch Dronpa from maximum to minimum fluorescence, each field required approximately 5 mins to image resulting in a lag between fields of 45 mins in an 8 field experiment. To obtain pertinent information from the raw data output that is illustrated in Figure 5-7 these data required processing. This was achieved by obtaining pre-switch and post-switch values of fluorescence levels which were normalised to the maximum Dronpa intensity for each field. This signal should be unaffected by any changes in FRET, and represents the relative expression level of

Dronpa (minimal variance was shown to occur between cells when switching of Dronpa to its most protonated form).

As previously discussed in the introduction p105 undergoes phosphorylation and proteolysis following TNFα stimulation at the glycine rich region (GRR) and the subsequent nuclear translocation of the N terminal p50 end to the nucleus. This process results in the slow nuclear accumulation of p50 in the nucleus reaching maximum translocation following several hours (Figure 5-3 and Figure 5-10). This is comparatively slow compared to p65 translocation into the nucleus following stimulation (Nelson, Ihekwaba *et al.* 2004).

A combination of FCS and FRET was used to observe changes in the conformation and affinity of p105 both before and after stimulation with TNFα. Over a 6 h time series, p105 was monitored for changes in FRET.

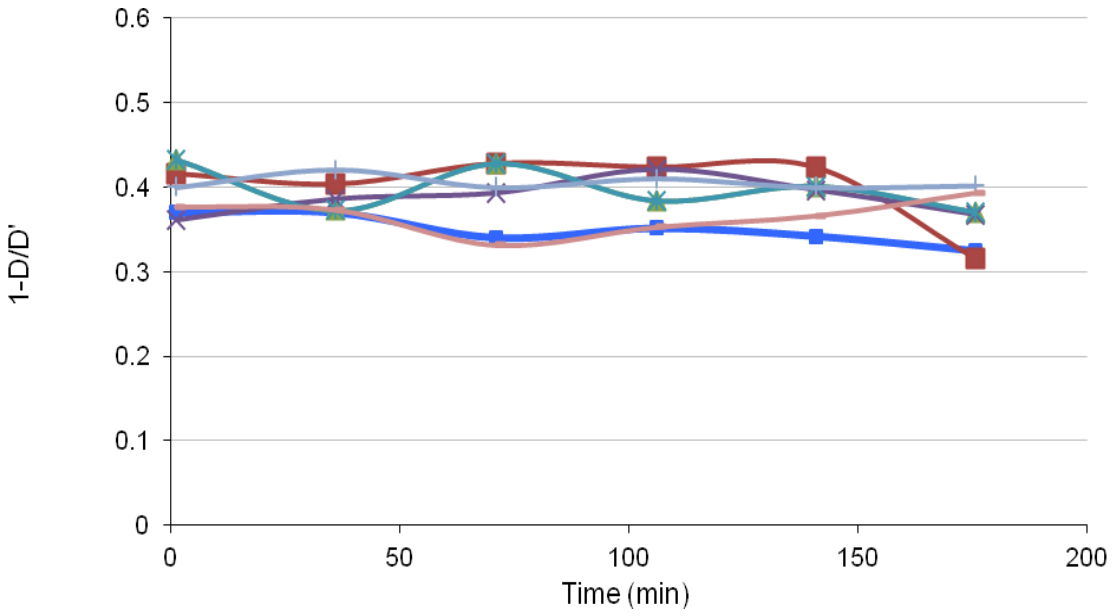

Figure 5-8 The Changes in fluorescence signal in Single cells over time.

The positive control construct pG-CMV-Dronpa-7aa-AmCyan was expressed in SKNS cells (n=6), in multiwell dishes to allow simultaneous imaging of p105 to ensure fluorophore brightness and FRET response remained consistent following repeated switching. Each line represents donor quenching and in a single cell. Cells expressing positive control were treated with TNFα at T=0 to monitor any possible changes in FRET efficiency due to cell to stimulation as expected no changes were observed.

Initially, the positive control construct pG-CMV-Dronpa-7aa-AmCyan was expressed in SK-N-AS cells to observe FRET behaviour of a potentially stable FRET fusion construct during a long time course. As expected, the fluorophores in the positive control fusion construct behaved consistently and maintained consistent FRET response over the 200min time course experiments in cells stimulated with TNFα at T=0, with changes in F_C and I_{DA} remaining consistent. (Fugure 5-8). This indicated that the imaging protocol and the illumination strategy were suitable for assessing FRET in live cells repeatedly over an extended period of time sufficient to capture potential changes in p105 behaviour.

The behaviour of the fusion construct pG-CMV-Dronpa-p105-AmCyan was characterised following 10ng/ml TNFα stimulation. Figure 5-10 shows a small population (n=7) of cells treated with TNFα and the change in localisation of n-terminally labelled p105 from cytoplasmic to nuclear compartments. The figure shows a slow accumulation of Dronpa-p105 (p50) beginning to reach a plateau after ~200min. (This correlates well with data from pG-CMV-DsRedExpress-p105-EGFP Figure 5-3).

An unstimulated control group of cells was examined to observe potential changes in p105 dynamics in resting cells. Cells showed minor variability in FRET efficiency over time in an asynchronous manner. While this could indicated that p105 was changing conformation regularly as part of cellular processes no visable difference could be seen between postitive control constructs and the unstimulated representative cell (Figure 5-9). More data points would need to be collected over longer time course experiments to confirm any conformational changes on the part of p105.

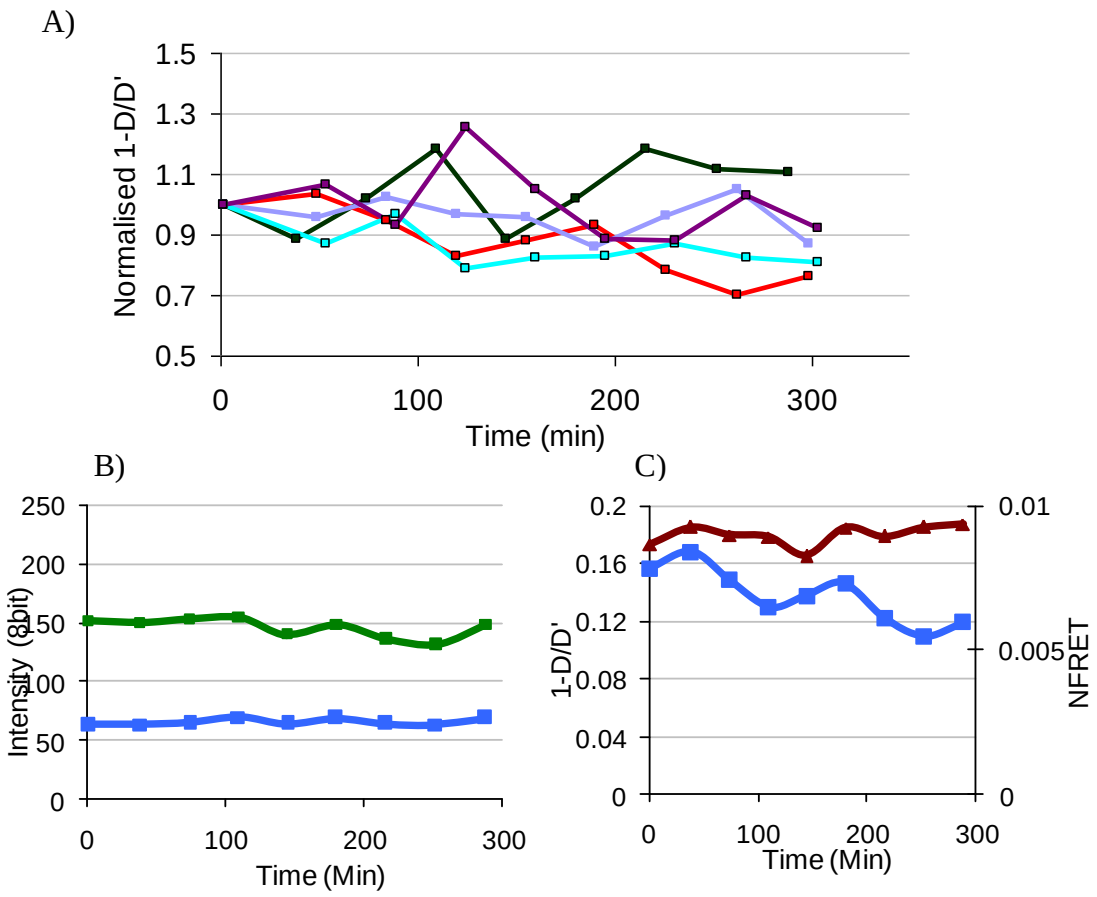

Figure 5-9 Changes in FRET over time.

SK-N-AS expressing pG-CMV-Dronpa-p105-AmCyan. representing cytoplasmic FRET dynamics in unstimulated cells.(n=5) A) Normalised change in quenching efficiency (T0) in Change in quenching efficiency has been normalised to the quenching efficiency for the first time point in each cell. This was to allow comparison of FRET changes in cells without identical FRET efficiency values. B) and C) Representative SK-N-AS expressing pG-CMV-Dronpa-p105-AmCyan (red in A). B) Fluorescence intensity over time showing consistent expression and little variation C)FRET efficiencies measured through donor quenching (blue) and NFRET (Red).

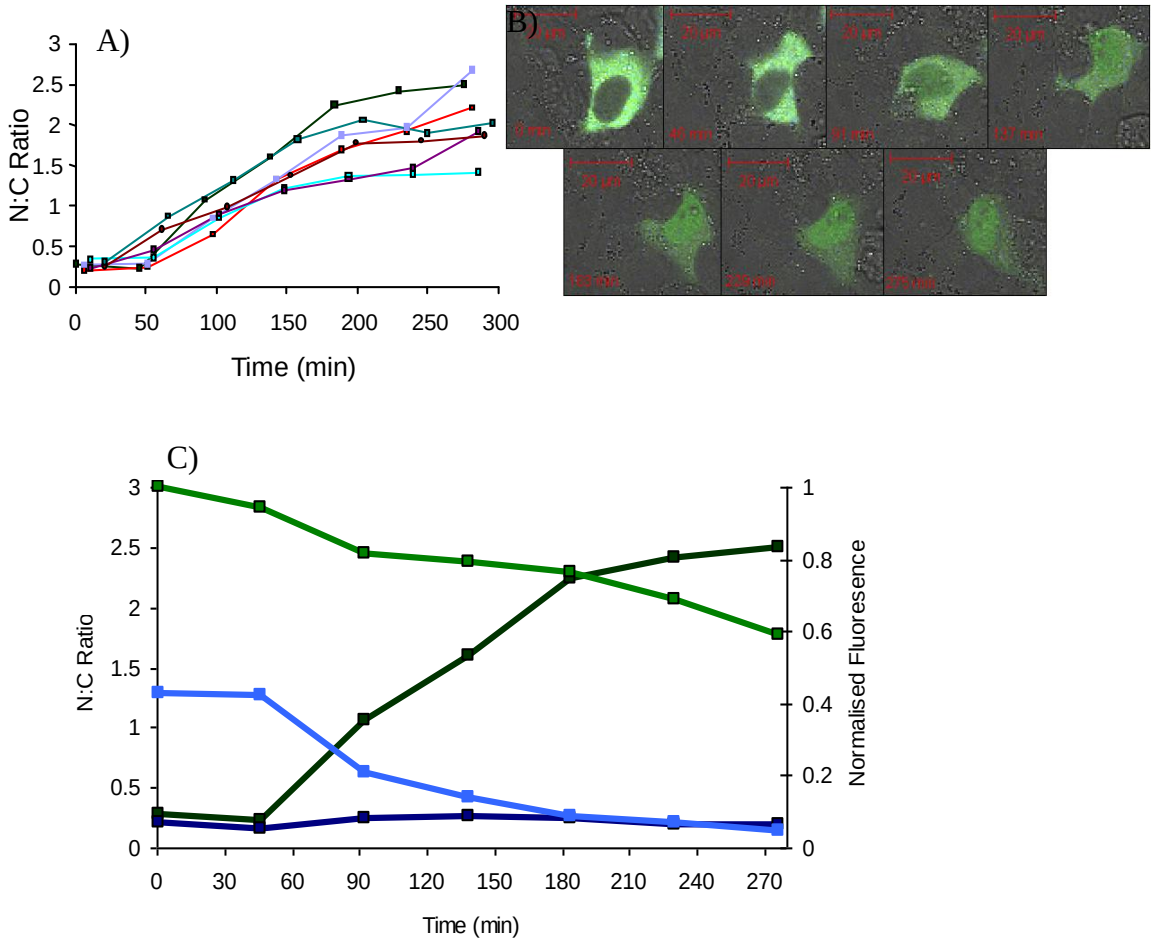

Figure 5-10 Time-dependent changes in Dronpa fluorescence localisation.

The effect on p105 following stimulation by TNFα. A) The change in nuclear to cytoplasmic ratio of Dronpa over time following stimulation in a population of cells (n=7), showing increased accumulation within the nucleus. B) Representative times series images (represented on population N:C as dark green). C) Changes in fluorescence of representative cell; dark Green represents N:C ratio change over time of Dronpa, dark blue similarly shows N:C ratio change in AmCyan, green represents decreasing fluorescence of Dronpa of the whole cell over time normalised to starting Dronpa intensity. Light blue represents fluorescence of AmCyan over time normalised to starting Dronpa intensity

A single representative cell was observed in more detail, (Figure 5-10) this showed a slow accumulation of Dronpa signal within the nucleus with no observable nuclear localisation of AmCyan fluorescence. Decreasing fluorescence of both Dronpa and AmCyan implied processing of the fusion construct consistent with Western blot data (Figure 5-2). The decrease in AmCyan fluorescence levels with the subsequent nuclear translocation of Dronpa signal following stimulation corroborates the literature and existing experimental data that suggests that p105 processing must occur before N-terminal translocation.

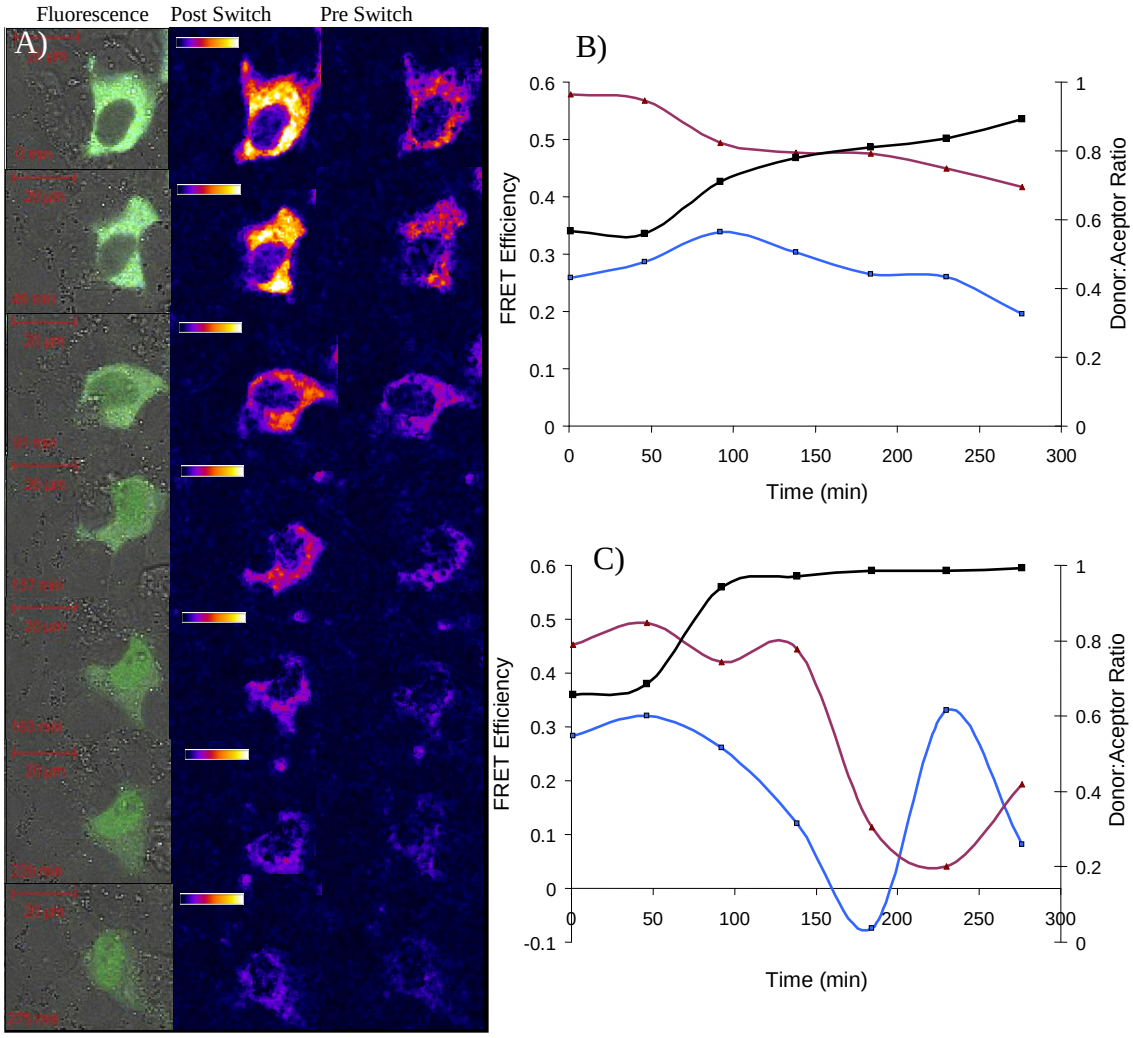

Figure 5-11. Changing FRET efficiency of an example cell over time.

A): pixel by pixel analysis of FRET using sensitised emission to acceptor to infer FRET using imageJ plugin as described in Chapter 4. Dronpa on (post switch) and off (pre switch). Shows decreasing FRET efficiency as p105 is processed. B) ΔF_C and ΔI_{DD} following switching of Dronpa in cytoplasm. Blue is change in donor quenching, red is change in sensitised emission. C) ΔF_C and ΔI_{DD} following switching of Dronpa in Nucleus. Blue is change in donor quenching, red is change in sensitised emission. Black is increasing ratio of acceptor to donor- calculated by normalising fluorescence to maximum Dronpa fluorescence and subtracting donor from acceptor; the closer to 1 the less donor remains in the cell.

The same representative cell was observed for changes in FRET efficiency.
Figure 5-11 shows the overall change in FRET represented by FRET maps using sensitised emission. This shows the decline in FRET response (as expected) due to the degradation of AmCyan through partial proteolysis of p105. Furthermore it shows the change in FRET efficiency of the remaining AmCyan population through

repeated donor quenching and corresponding changes in F_c emission. Interestingly, there seems to be a detectable FRET response in the nuclear compartment of the cell, and quenching efficiency exists within the same range as Dp105A (Figure 5-5) indicating the presence of full length p105 within the nucleus. Both ΔF_C and ΔI_{DA} show a rapid decline in the nucleus following stimulation. It should also be noted that the sudden increase in I_{DD} quenching ~200min is due to detector noise becoming greater than any measurable change in fluorescence; an issue due to diminishing AmCyan signal. Cytoplasmic changes in FRET efficiency show a small increase of 20% at ~100 mins followed by decrease in quenching efficiency of 50%. Although full length p105 appears to have been degraded through fluorescence analysis, a small population of interacting N and C terminal regions of p105 still appears to be present well past 4 h following TNFα stimulation (where p50 nuclear translocation has begun to plateau). This indicates that p105 is not completely processed following cell stimulus. This is similar to endogenous levels of p105 expression following TNFα shown in Figure 5-1.

A comparison of Nuclear and Cytoplasmic FRET efficiencies using data from Figure 5-10 show that FRET efficiency within the nuclear compartment is stronger. This indicates that there is full length p105 present in cell nuclei.

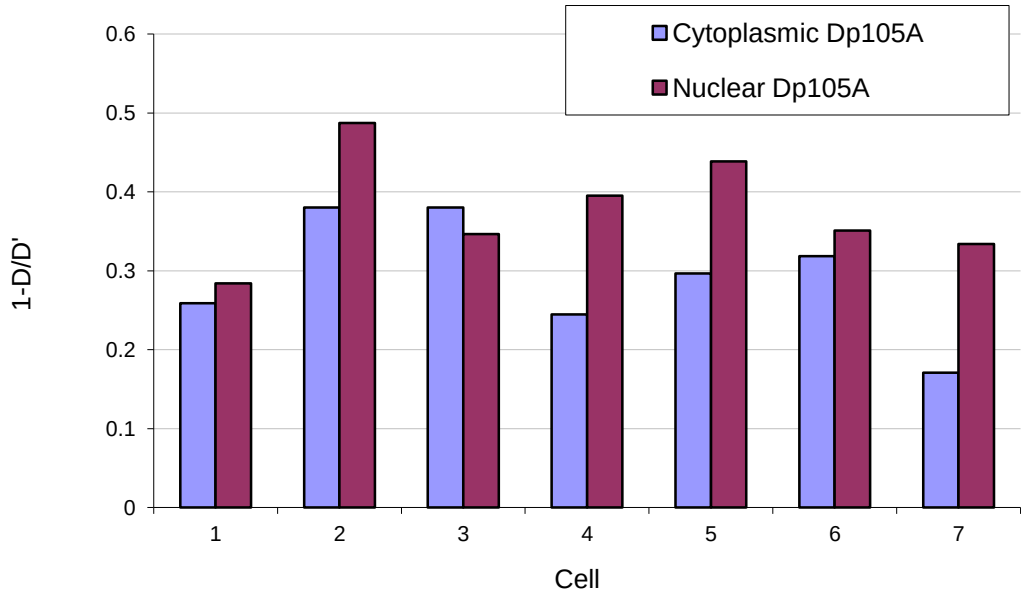

Figure 5-12 Comparison of FRET efficiency between nuclear and cytoplasmic compartments
Using cell data from Figure 5-10. On average, shows a stronger FRET efficiency within the nuclear compartment indicating full length p105 in cell nuclei, and closer N-C terminal association of fluorophores.

Population data from cells transfected with pG-CMV-Dronpa-p105-AmCyan was gathered by normalising changes in donor quenching to T0 for each cell in the population (n=7). The general trend of the population data showed a reduction in FRET efficiency in both nuclear (100% reduction in donor quenching) and cytoplasmic (50% reduction in donor quenching) compartments in both F_C and I_{DD} following stimulus with TNFα. This would indicate a gradual change in conformation or association of N and C terminal regions. FRET efficiency in the nuclear compartment showed a loss of any detectable AmCyan quenching at ~270mins. The cause of this was likely due to loss of detectable AmCyan as opposed to the breakdown of conformational or association of N and C terminal interactions. It should be noted that due to lag time between each field, more subtle protein dynamics may have been lost due to the process of averaging p105 behaviour over a 45 min period per field.

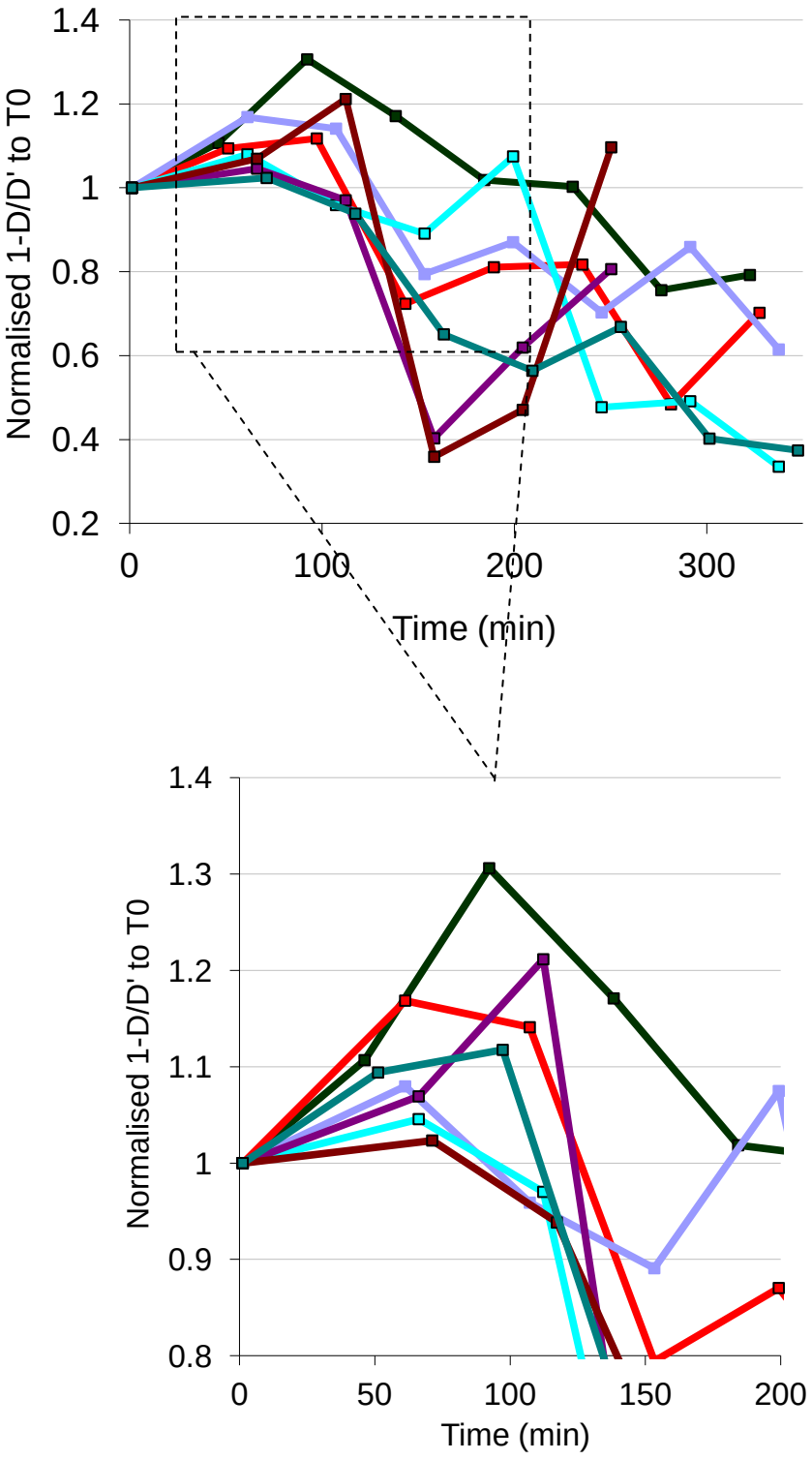

Figure 5-13 Normalised change in quenching efficiency in single cells

SK-N-AS cells expressing protein from pG-CMV-Dronpa-p105-AmCyan. Cytoplasmic FRET dynamics following TNFα stimulation. Responding cells in the population (n=7) Change in quenching efficiency has been normalised to the quenching efficiency for the first time point in each cell. This was to allow comparison of FRET changes in cells without identical fluorescence efficiency values.

A comparison of the FRET efficiency in cells following TNFα stimulation is presented in figure 5-13. All cells showed some increase in FRET efficiency following stimulation. While the fold change in FRET efficiency appears negligible in certain cells, these cells are often placed later in imaging series. There can therefore be up to 25-30mins difference between fields. Increasing the time resolution of stacks could show greater changes in FRET efficiency following stimulation. This dataset indicates a transient increase of FRET efficiency in p105 following TNFα stimulation synchronising the behaviour of p105 which had proved to be asynchronous prior to stimulation (Figure 5-8).

As already established in Figure 5-4 p105 can interact in both intermolecular and intramolecular fashion. This indicates either a conformational change of p105 following phosphorylation by the IKK complex (Salmeron, Janzen *et al.* 2001; Lang, Janzen *et al.* 2003) or increased association of p105 with p50 due to cleavage of p105 following stimulation. FCS data indicated molecule numbers at roughly 1:1 ratios in the cytoplasm following treatment and improved cross correlation between N and C terminal ends indicating mostly full length p105 remains in cytoplasm following stimulation.

While stimulation of most cells resulted in the proteolysis of c-terminal AmCyan followed by the slow nuclear accumulation of the n-terminal region of p105 and gradual degradation of Dronpa tagged p105, two additional cells exhibited different behaviour following stimulation. While the proteolysis of IκBγ and the subsequent slow accumulation of p50 still occurred, AmCyan fluorescence was maintained at a much higher level, and Dronpa was not slowly degraded and remained relatively constant following stimulation. The resulting cells showed a gradual increase in FRET efficiency in both ΔF_C (red) and ΔI_{DD} (blue). It is possible that this behaviour is due to active transcription of pG-CMV-Dronpa-p105-AmCyan. It could be argued this behaviour is more physiologically consistent with endogenous p105 which shows minimal effect on protein level in full length p105 following stimulation (Figure 5-1). While Figure 5-11 show increase and subsequent decrease in FRET efficiency, where p105 is not replenished, the more consistent efficiency of p105 could be due to new p105 being translated (Figure 5-14).

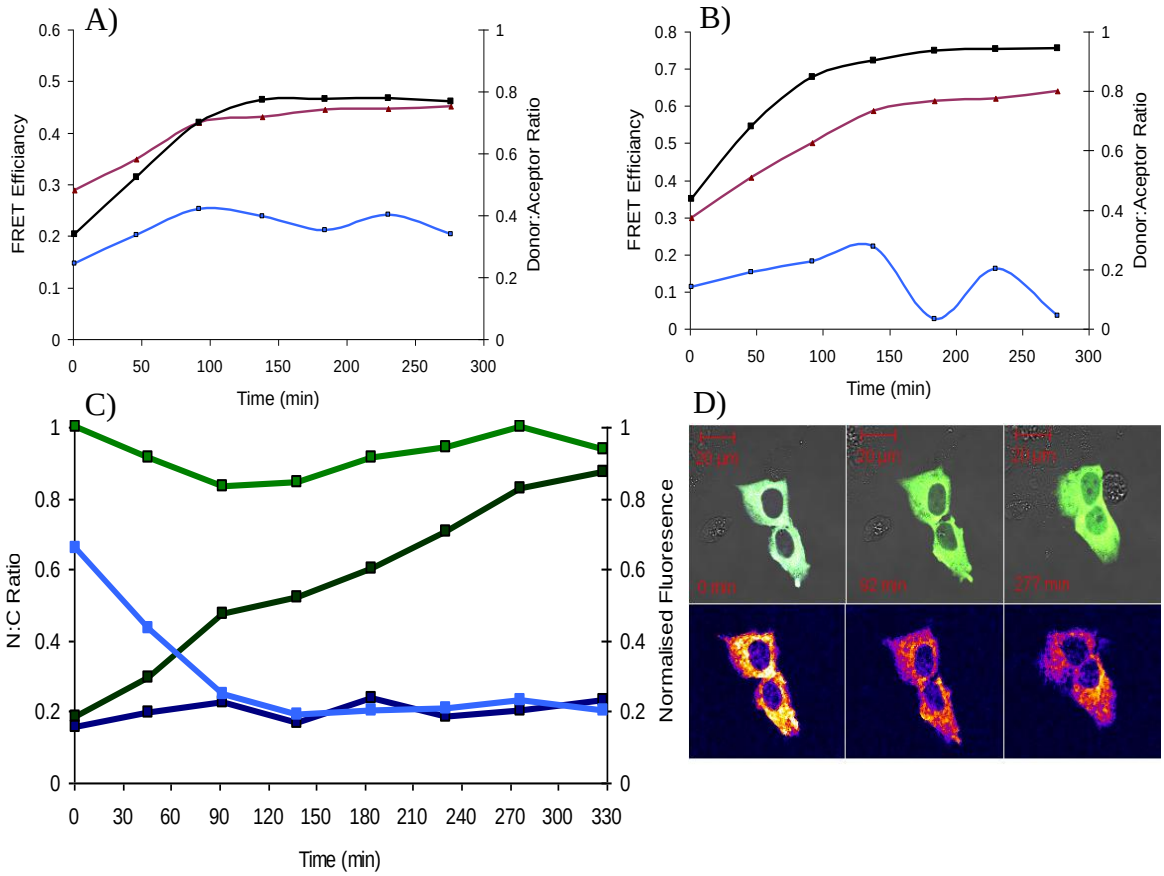

Figure 5-14 Changing FRET efficiency of a cell over time.

A) pixel by pixel analysis of FRET using ratio of sensitised emission to acceptor signal using imageJ plug in. Shows decreasing FRET efficiency as p105 is processed. A) (cytoplasmic) and B) (nuclear): ΔF_C and ΔI_{DD} following switching of Dronpa in cytoplasm. Blue is change in donor quenching, red is change in sensitised emission. Black is increasing ratio of acceptor to donor- calculated by normalising fluorescence to maximum Dronpa fluorescence and subtracting donor from acceptor; the closer to 1 the less donor remains in the cell. C) changes in fluorescence of representative cell; dark Green represents N:C ratio of Dronpa, dark blue similarly shows N:C ratio of AmCyan, green represents decreasing fluorescence of Dronpa of the whole cell over time normalised to starting Dronpa intensity. Light blue represents fluorescence of AmCyan over time normalised to starting Dronpa intensity.

5.4 Dynamics of p105 using FCCS

Fluorescence cross correlation spectroscopy is a highly quantitative technique used to measure minute changes in fluorescence fluctuation and correlate these fluctuations with the diffusion and subsequent fluctuation in signal as individual molecules move through the measured confocal volume. It was intended to use this technique to help confirm results observed through FRET using pG-Dronpa-p105-AmCyan.

Initially the construct pG-CMV-DsRedXP-p105-EGFP was used to measure the changes in dynamics before and after TNFα stimulation. Cross-correlation of DsRedXP-p105-EGFP increased following TNFα stimulation, with corresponding increase in autocorrelation of DsRed indicating lower molecular number.

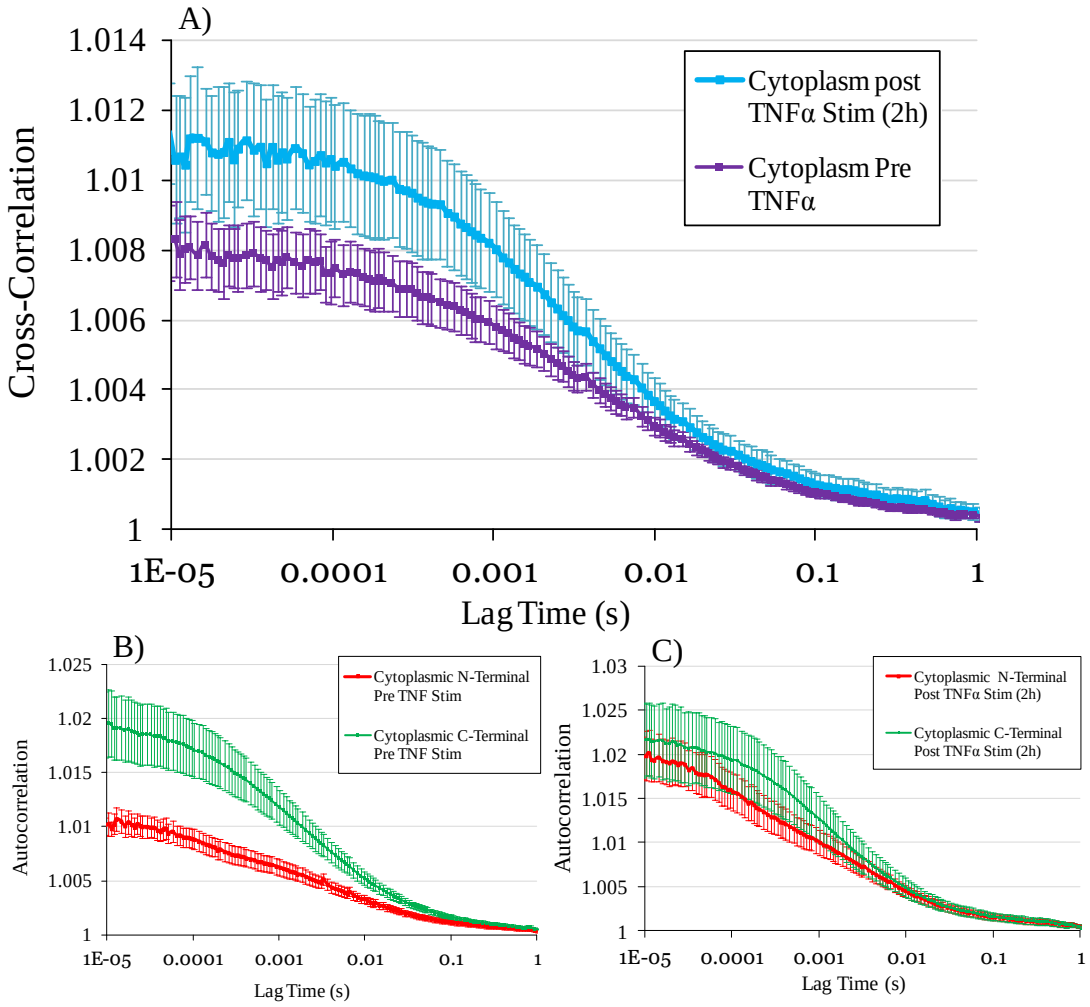

Figure 5-15. Cross-correlation and autocorrelation curves for SK-N-AS cells expressing protein from pG-DsRed-p105-EGFP

A) Cross-correlation of pG-CMV-DsRedExpress-p105-EGFP before TNFα stimulation (purple) and 2h following stimulation (blue) B) Autocorrelation curves for n-terminally tagged region (red) and c-terminally tagged region (green) prior to stimulation with TNFα C) Autocorrelation curves for n-terminally tagged region (red) and c-terminally tagged region (green) following stimulation with TNFα at 2hmin. 10x10s measurements taken per cell. Error bars represent S.E.M. between measurements (N=15)

Nuclear measurements showed an exceptionally high cross correlation of p105 in the nucleus in pre-stimulus conditions. This strongly indicates that full length p105 was present in the nucleus prior to stimulation and mirrors the FRET data which showed a higher FRET efficiency in the nuclear component of cells. Due to the 2fl confocal volume used in FCS and significantly different correlation between nuclear and cytoplasmic compartments, it was concluded that full length p105 was present in the nucleus prestimulation but at low concentrations. Following stimulation, a radical reduction in cross-correlation was seen. This implied full length p105 was exported from nuclear compartments following stimulus.

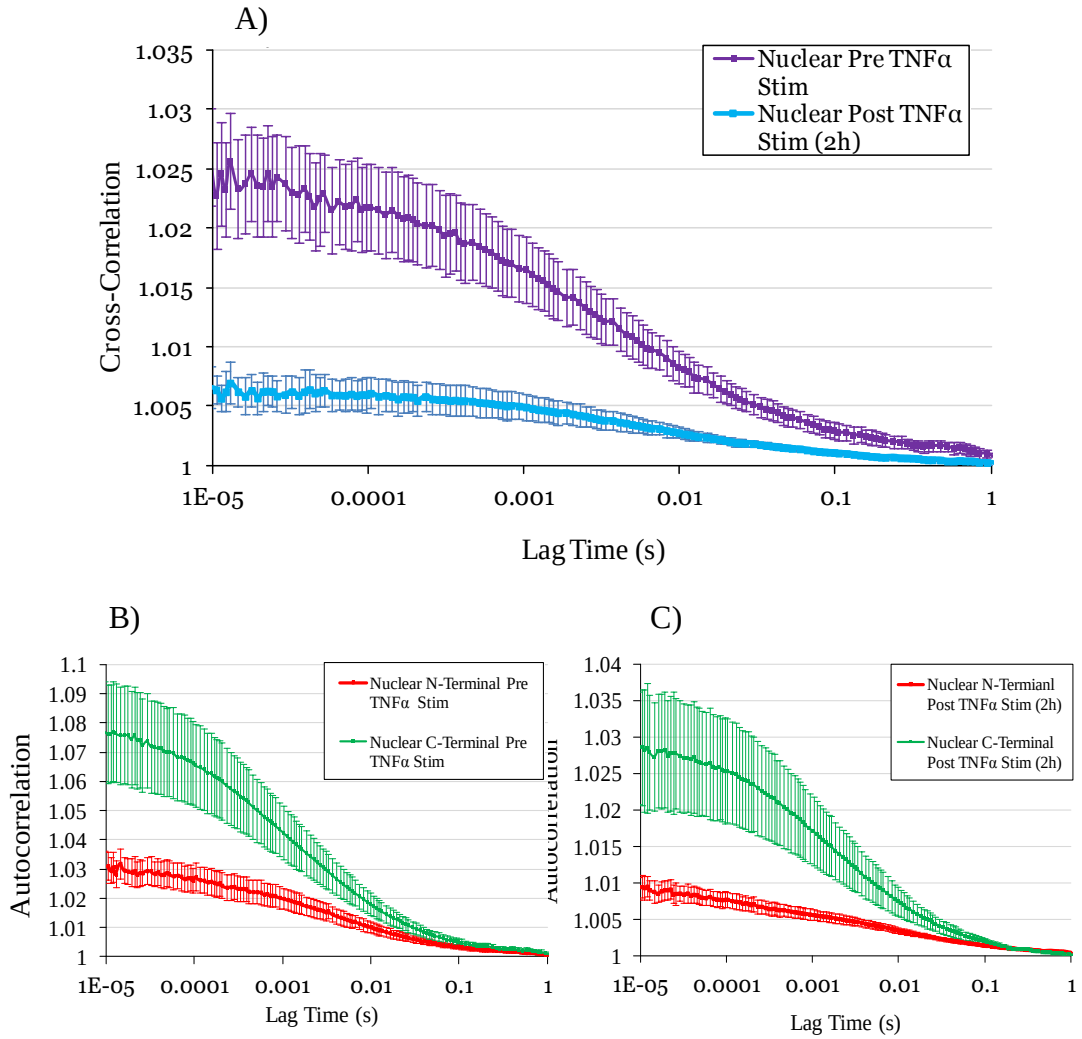

Figure 5-16 - Cross-correlation and autocorrelation curves for SK-N-AS transfected with pG-CMV-DsRed-p105-EGFP

A) Cross-correlation DsRedExpress-p105-EGFP before TNFα stimulation (blue) and following (purple) B) Autocorrelation curves for n-terminally tagged region (red) and c-terminally tagged region (green) prior to stimulation with TNFα C) Autocorrelation curves for n-terminally tagged region (red) and c-terminally tagged region (green) following stimulation with TNFα at 2h. Error bars represent S.E.M. between measurements (N=15).

Using the amplitude and number of particles from fluctuations, a direct estimation of molecular number in the confocal volume could be made for the two fluorophores. This has particular relevance to physiological levels of N and C terminal components and subsequent processing by the cell due to the synthesis of a single product rather than the transient cotransfection of two separate components. Data showed approximately a 2:1 ratio of DsRed to EGFP molecules prior to stimulation in cytoplasmic compartments, changing to a 1:1 ratio following stimulation. This implies a 1:1 ratio of free p50 to full length p105, and movement of p50 molecules into the nucleus following stimulation, leaving full length p105 in the cytoplasm explaining increased cross correlation of p105 in cytoplasm and decreased nuclear cross-correlation of p105 following stimulation.

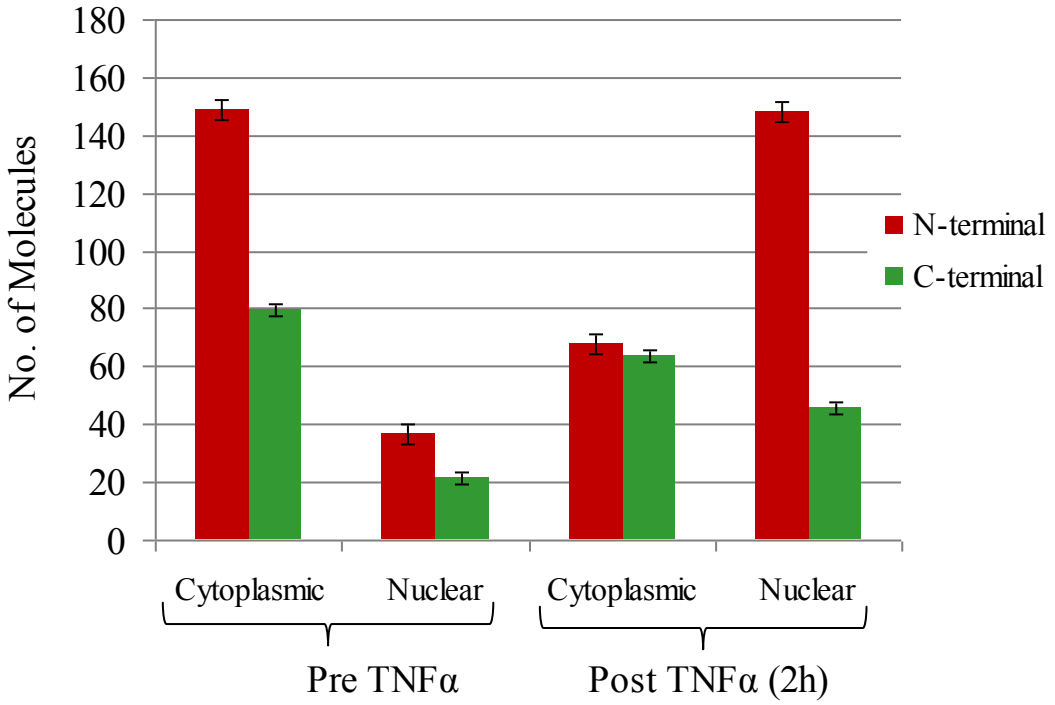

Figure 5-17. Quantification of DsRed-p105-EGFP fluorescence expressed in SK-N-AS cells.
Molecular number of N and C terminally tagged components using particle amplitude number to infer molecular number. Data shows approximately 2:1 ratio of DsRed to EGFP molecules prior to stimulation, changing to a 1:1 ratio following stimulation. This implies a 1:1 ratio of free p50 to full length p105, and the retention of full length p105.

5.4.1 Effect of p65 on full length p105

In the published scientific literature p65 and p50 are known as the archetypical NF-κB dimer (Hoffmann, Levchenko *et al.* 2002). Although p65 is shown to associate with full length p105 via co-immunoprecipitation (Savinova, Hoffmann *et al.* 2009), the effect of p65 on the conformation of p105 is unknown. A simple experiment where pG-CMV-Dronpa-p105-AmCyan was co-transfected with mCherry-p65 was used to assess the effect of p65 on the conformation of unstimulated full length Dronpa-p105-AmCyan. Figure 5-18 shows cells expressing both full length D-p105-A and mCherry-p65 show reduced quenching efficiency compared to that of cells transfected exclusively with pG-CMV-Dronpa-p105-AmCyan, possibly indicating that binding of p65 effects N and C terminal interactions of full length p105. Non-parametric Kruskal-Wallis ANOVA, showed a statistically significant difference between pG-CMV-Dronpa-p105-AmCyan and co-transfected Dronpa-p105-AmCyan mCherryp-65 (<p=0.05, Chi^2=11.56). Interestingly, there was no statistically significant difference between Dp105 p105A and Double tagged p105 co-transfected with mCherry-p65 (P= 0.53 Chi^2=0.38). This indicates that p65 causes p105 to change conformation to accommodate p65, but still interacts intermolecular with other p105 molecules.

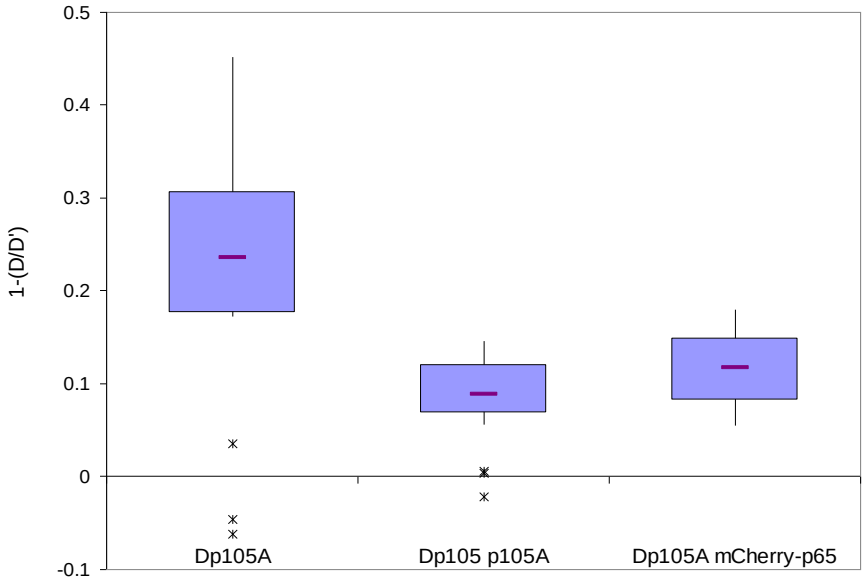

Figure 5-18. Effect of p65 on p105 FRET efficiency.

Comparing FRET efficiency using normalised AmCyan Quenching of pG-CMV-Dronpa-p105-AmCyan (n=18) co-transfected Dronpa-p105 p105-AmCyan (n=15) and co-transfected Dp105A with pG-CMV-mCherryp65 (n=8). Data from Dp105A taken from for comparison.

5.5 Intermolecular p105 Interactions

To test Dronpa as a FRET partner in other intermolecular system, different potential FRET partners were tested using other known interacting proteins. Figure 5-19 is a box plot of all combinations tested and the relative FRET efficiency for each combination tested. Results yielded several potential partners to test.

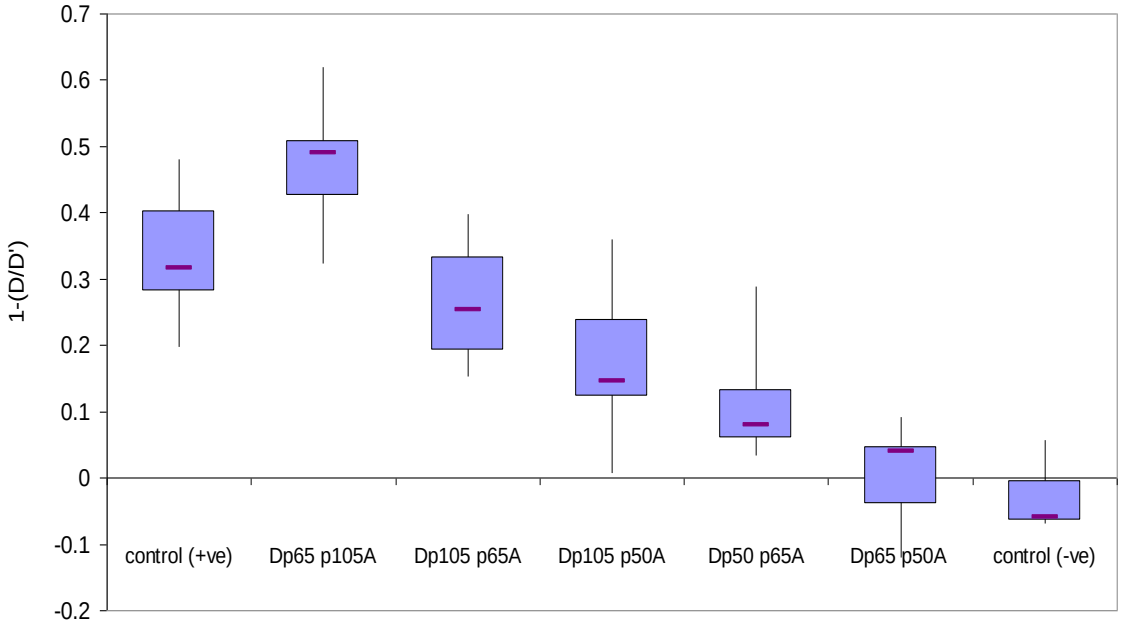

Figure 5-19 Array of intermolecular FRET interactions with p105.
FRET efficiencies between different NF-κB proteins co-expressed in SK-N-AS cells using change in AmCyan following Dronpa switching to indicate FRET efficiency.

Although FRET cannot be used to rule out interactions, or effectively quantify differences between different partners (as linker length might possibly affect conformation, molecular distances and fluorophore dipole alignment) interestingly. FRET efficiency between Dronpa-p65 and p105-AmCyan was the strongest interaction tested. Indeed, there was a significantly stronger FRET signal between Dronpa-p65 and p105-AmCyan than the positive control construct ($p=<0.05$ $Ch^2=15.73$) indicating a closely interacting complex. Furthermore FRET was not observable between directly translated pG-CMV-p50-AmCyan and pG-Dronpa-p65, with no statistically significant difference between the negative control ($p=0.087$ $Ch^2=3.83$) This indicates that the IκBγ domain is important for in interaction of p65 with p105, possibly more so than dimerisation with the RHD of the N terminal region of p105.

Significantly higher FRET efficiency was also seen between full length products from pG-CMV-Dronpa-p105 and pG-CMV-p65-AmCyan as opposed to mature products from pG-CMV-Dronpa-p50 and pG-CMV-p65-AmCyan. Interpretation of this data needs to be cautious however as linker composition was significantly different and may have affected molecular distance of fluorophores (see below).

Dronpa-p105 (2aa sequence)

Linker

ggtacc

Dronpa-p50 (24aa sequence)

Linker

ctcgagatcaacaagtttgtacaaaaaagcaggctggcgccggaaccaattcagtcg

actggatcc**ggtacc**

It should also be noted that Dronpa-p50 would have been produced from Dronpa-p105 in cells due to constitutive processing of the protein. Investigations to determine if interaction of p65 with the C-terminal region of p105 enhances formation of p65/p50 dimers could be answered through modification of linker sequences to match one another. Further analysis through FCS could help elucidate any differenced of fractions of molecular complexes between p65/p105 and p65/p50 .

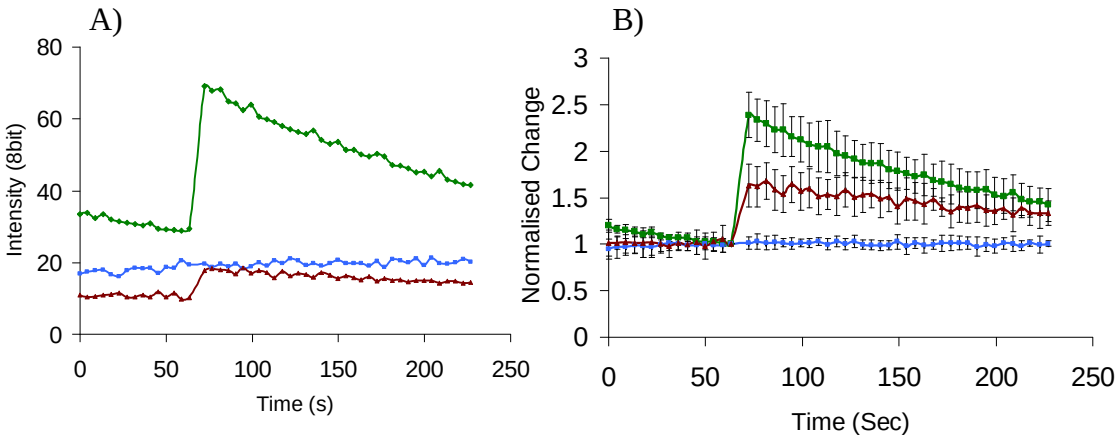

Figure 5-20 FRET in Cells expressing pG-CMV-Dronpa-p65 pG-CMV-p50-AmCyan.

A) is representative cell showing no quenching in AmCyan following photoswitching but a visible increase in F_C. B) represents normalised population of 10 cells expressing the construct. Indicates I_{DA} is not completely representative of sensitised emission due to no corresponding quenching of AmCyan following switching

Figure 5-20 indicates I_{DA} is not completely representative of sensitised emission due to detectable change in I_{DA} channel which does not correspond with the behaviour of AmCyan following switching. This calls into question data pertaining to sensitised emission. The most likely reason for this increase is probably due to unsubtracted spillover. Sensitised emission should be internally consistent to changes in FRET efficiency on a cell to cell basis and is the most effective way of displaying total FRET within a cell in relation to acceptor and donor fluorescence. Comparisons using sensitised emission become limited at low levels due to potential spillover reporting spurious FRET. For this reason, emphasis on quantifying FRET interactions was placed on changes in donor. An effective solution would be to increase stringency of spillover subtraction resulting in the binning of data from sensitised emission. While this would result in a loss of resolution, and make comparison between different microscopes much more variable, it would remove instances of spurious FRET detection.

5.5.1 p65/p50

As the archetypical heterodimer, p65-p50 is known to bind to discrete NF-κB transcription sites based on the combination of binding consensus sequences of both partners. NF-κB1 has been shown to bind p65 in both an ‘‘NF-κB’’-like and ‘‘IκB’’-like manner, utilizing their RHD and ANK domains, respectively (Figure 5-19)(Savinova, Hoffmann *et al.* 2009). Using this technology it was intended to observe realtime protein dynamics of this pair.

Cells were transiently co-transfected with pG-CMV-Dronpa-p105 and pG-CMV-p65-AmCyan. Cells where then imaged using optimised imaging conditions. Following the first time point, cells were treated with 10ng/ml TNFα. Cells were then monitored for overall changes in fluorescence.

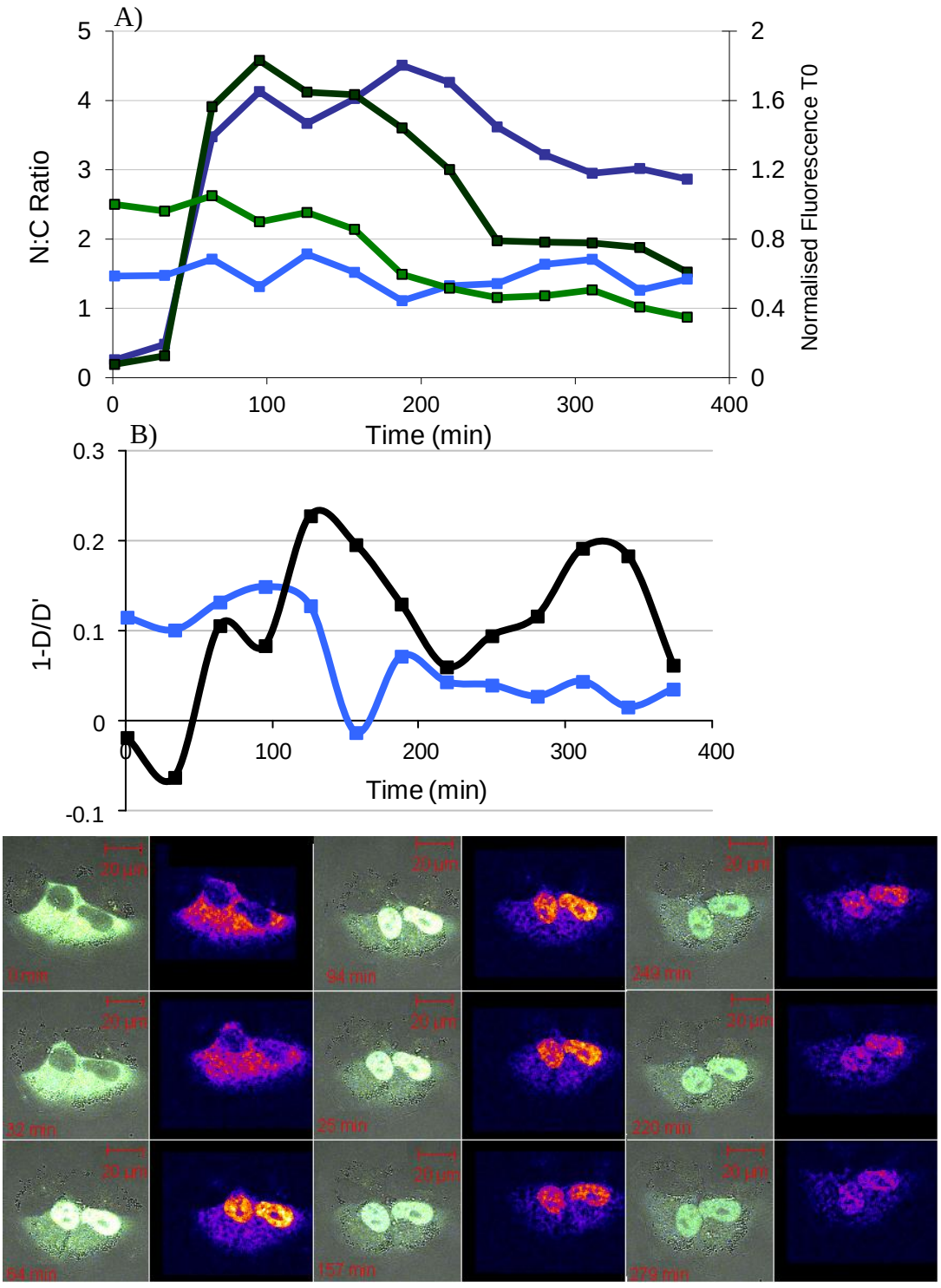

Figure 5-21 Changes in intermolecular FRET between pG-CMV-p65-AmCyan and pG-CMV-Dronpa-p105 in a single cell treated with TNFα.

pG-CMV-Dronpa-p105 and pG-CMV-p65-AmCyan transiently co-transfected into SK-N-AS cells. A) Fluorescence profile of the cell. Dark Green represents Nuclear:Cytoplasmic (N:C) ratio change over time of Dronpa, dark blue similarly shows N:C ratio change in AmCyan, green represents decreasing fluorescence of Dronpa of the whole cell over time. Light blue represents whole cell AmCyan. (Fluorescence was normalised to maximum Dronpa intensity) B) Blue cytoplasmic FRET, Black Nuclear FRET

Compared to the double tagged p105 construct the example cell showed a much shorter nuclear translocation period of p50 with p65 followed by a plateau in nuclear:cytoplasmic movement. The representative cell was observed for changes in donor quenching efficiency following stimulation as well as the localisation of peaks in sensitised emission using pixel by pixel analysis.

As expected, no measurable nuclear FRET was present in cells pre-stimulus. This helped reinforce that measuring FRET in the nuclear and cytoplasmic compartments were separable using the current image settings. Following nuclear translocation of p65 and processed p105 (p50), FRET response increased in the nuclear compartment. Both as measurement of sensitised emission and in quenching efficiency of donor fluorescence. Interestingly, donor quenching efficiency appeared to change over time in both nuclear and cytoplasm compartments, even once nuclear movement of p65/p50 had reached a plateau. Chen *et al.* has shown that the crystal structure that the subunits p65/p50 adopt is altered in a DNA-sequence-dependent manner (Chen, Huang *et al.* 1998). Changes in FRET efficiency may relate to DNA binding of dimers to consensus sites.

5.5.2 Interaction of p105/p65 using FCS

The FRET signal between p65 and the C-terminal region of p105 was shown to be strong whereas FRET from the n-terminal region of p50 was shown to be comparatively less efficient (Figure 5-19). Using FCS, the cross-correlation between p65 and n-/c- terminal p105 was measured using the constructs pG-CMV-p65-DsRedXP and either pG-CMV-p105-EGFP, or pG-CMV-EGFP-p105. A stronger cross-correlation was seen between pG-CMV-p65DsRedXP and pG-CMV-p105-EGFP, implying stronger association between p65 and the IκBγ terminal of p105. This result implies that p65 forms dimers with full length p105 preferentially over processed p50.

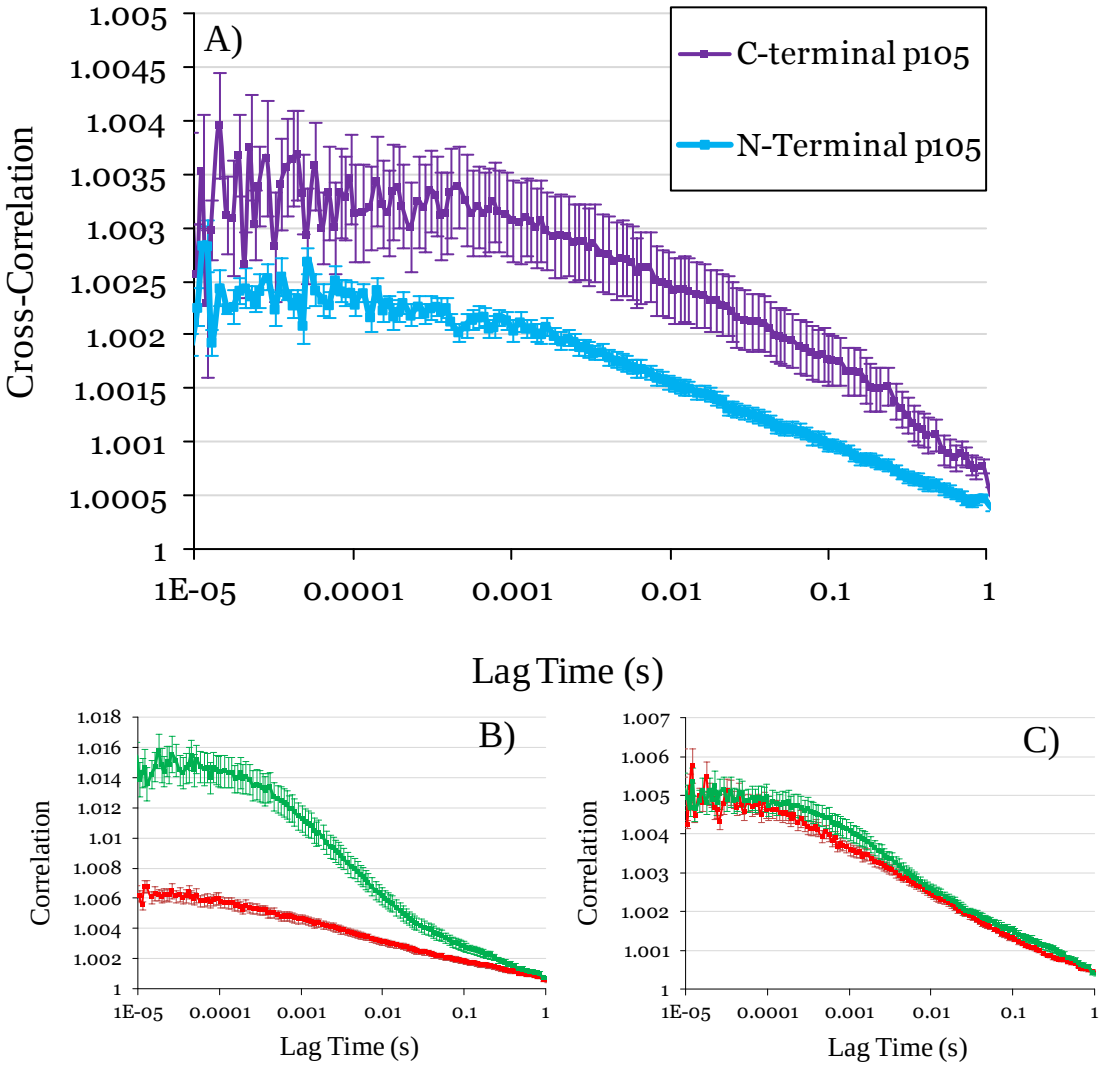

Figure 5-22 Cross-correlation and autocorrelation curves for p65 and N and C terminally tagged p105.

A) Cross-correlation of pG-CMV-p65DsRedxp and pG-CMV-EGFP-p105 (blue) and pG-CMV-p65-DsRedxp pG-CMV-p105-EGFP (purple) B) Autocorrelation curves for pG-CMV-DsRedxp-p65 (red) and pG-CMV-p105-EGFP (green) C) Autocorrelation curves for pG-CMV-DsRedxp-p65 (red) and pG-CMV-EGFP-p105 (green)

5.6 Discussion

The work described in this chapter has shown that Dronpa can be succesfully used as a reversably switchable element in a FRET pair, and can be applied to a biological system to make assertions on protein behaviour. Furthermore, Dronpa can be switched repeatedly to show changes both in conformation and interactions of proteins over time.

While the primary application of Dronpa as a photoswitchable element in a FRET pair was to observe changes in energy exchange between fluorophores over a series of images, an argument can be made for its use over traditional acceptor photobleaching in circumstances where only a single measure of FRET efficiency is required in live cells. One of the criticisms of acceptor photobleaching in live cell imaging is the blurring effect caused by comparing two images which may be temporaly seperated by comparitivly long periods of time due to time intensive bleaching steps. These problems may be circumnavigated using the fast switching behaviour of Dronpa under 405nm excitation. Photodamage to cells is also minimised by using Dronpa.

5.6.1 The Dynamics of NF-κB1

The use of FRET to probe the activity of p105 in single cells has given interesting insight into this protein. Traditionally p105 is often seen as an inert cytoplasmic component which inhibits nuclear localisation of NF-κB Rel family members and generates functional p50 via proteolytic cleavage (Mercurio, DiDonato *et al.* 1993; Salmeron, Janzen *et al.* 2001; Lang, Janzen *et al.* 2003; Savinova, Hoffmann *et al.* 2009). Here we show both through FRET and FCCS that some intact p105 is resident in the nucleus of cells. Furthermore, FRET efficiency between p105 N and C terminal regions appears to be consistantly stronger in the nucleus compared to the cytoplasm (Figure 5-10) implying conformational changes within p105 dependent on spatial localisation. This could be a result of which proteins p105 is associated with. The presence of p65 appears to modulate the intramolecular FRET efficiency of p105, as co-expression with p65 leads to p105 adopting FRET efficiency of no statistically significant difference from intermolecular FRET interactions (Figure 5-

18). Furthermore, no detectable FRET was seen in the nucleus between pG-CMV-p65-AmCyan and pG-CMV-Dronpa-p105 pre-TNFα stimulus again indicating that dimerisation partners play a role in the overall conformation of p105 and result in different FRET efficiencies. A simple experiment to confirm dimerisation partners of p105 in nuclear compartment would be to conduct a co-immunoprecipitation on nuclear extracted proteins, and assess complex size of full length p105 using an IκBγ specific antibody to pull down potential complexes.

Over time p105 also shows interesting characteristics. In resting cells, p105 shows a variable FRET response to Dronpa switching implying that p105 conformation is in a state of fluctuation within cells. By stimulation cells with TNFα, FRET behaviour seems to generally synchronise showing an increase and subsequent decrease in FRET efficiency over time (Figure 5-10). It was thought that this change in FRET efficiency might be caused via phosphorylation of p105 by IKK, which is shown to alter p105 conformation (MacKichan, Logeat *et al.* 1996). A way of testing the effect of phosphorylation and subsequent changes in conformation of p105 could be to generate phospho-mutants of p105 at serine 927 and 932, which have been shown to be essential for the processing of p105 (Lang, Janzen *et al.* 2003). Inhibiting phosphorylation directly could tell us if observed changes in efficiency were due to processing of p105 or are an artefact of cells stimulated with TNFα.

The generation of stable cell lines expressing Dronpa-p105-AmCyan under its own promoter should yield interesting results. Due to decreases in the levels of fluorescence following stimulation, FRET response becomes increasingly susceptible to detector noise reporting false positives, and is further limited by protein half-life. If p105 production was driven by its own promoter, FRET imaging may yield interesting dynamics in p105 changes which were potentially seen in cells actively expressing p105 Figure 5-14.

Chapter 6: General Discussion

6.1 Summary of main discoveries in thesis

The primary aim of this project was to pioneer the use of photoswitchable fluorescent proteins in FRET and demonstrate their value for generating quantifiable data pertaining to the interaction of proteins. Dronpa was chosen due to the robust and repeatable nature of its switching ability, as characterised in the literature (Habuchi, Ando *et al.* 2005; Andresen, Stiel *et al.* 2007).

The optical characteristics of fluorescent proteins can often be taken at face value in the field of routine microscopy. For the purpose of this project however, fluorescent fusions required rigorous testing to ensure that the FRET responses were not artefacts of aberrant fluorophore behaviour. Unforeseen characteristics of widely used fluorophores were discovered. When using the optimised illumination strategy for switching Dronpa with 405nm illumination both mTFP and DsRedExpress showed consistent changes in their spectral properties that would confound interpretation of FRET data. Fluorophores AmCyan and mStrawberry were singled out as the most suitable candidates to use with Dronpa, due to their resistance to photobleaching and their consistent behaviour in the switching assay. This gave the option of using Dronpa as either a donor or an acceptor for FRET. Much of the following work presented in this thesis used Dronpa as an acceptor so that confounding spillover would not cause problems when measuring FRET. Additionally using Dronpa as an acceptor required far less data manipulation so should be relatively more quantitative.

The next step in the development of this technology was to generate positive control constructs that would allow the characterisation of FRET using Dronpa switching. In characterising the behaviour and interaction of FRET using photoswitching fluorophores, FRET interactions were as expected. The FRET response was linear in proportion to Dronpa fluorescence levels, at least when the fluorophores were in a 1:1 ratio. This meant that the FRET data obtained through the use of photoswitchable Dronpa could be analysed by standard FRET methodology which had already been established in the literature.

Finally, the application of this technology to a working biological system showed the applicability of this technology to solve biological questions about the dynamics of protein interactions over time. The NF-κB family member p105 was selected due to its potential intermolecular and intramolecular interactions. Using various fusions of p105 and other REL family members, including single and double tagged variants, p105 showed both strong inter- and intra-molecular interactions. Furthermore, TNFα stimulation resulted in measurable changes in FRET over time.

6.2 Relationship of real-time FRET assay to protein interaction assays

A key aim of systems biology is to develop quantitative assays for important cellular processes. The development of fluorescence and luminescence probes have made a major contribution to microscopy and, in particular, fluorescent proteins have had a particularly important impact (Chalfie, Tu *et al.* 1994; Badr and Tannous 2011). The assay developed during this project provides one approach for the real-time measurement of protein interactions in living cells. The aim of this section of the discussion is to review the available alternative methods so as to discuss the advantages and disadvantages of the new method in this context.

6.2.1 Biochemical Assays

The majority of approaches to measure protein interactions that are currently used in molecular cell biology and biochemistry involve the bulk analysis of protein extracts. The main methods are pull-down assays where one protein is recognised by a specific antibody and used in a co-immunoprecipitation assay to pull down interacting proteins. Specific interacting proteins can then be recognised by Western blotting (Phizicky and Fields 1995) (Anderson 1998) or mass spectroscopy. This approach uses a heterogeneous population of cells to observe general protein expression and protein interactions in cell extracts. As a result, data on protein expression and interactions is an average of the cell population, rather than measurement of single cells. At the same time there is no inherent temporal resolution unless the procedure is carried out at multiple time points. One key advantage however is that pull-down assays can be performed with endogenous

proteins, without any requirement for exogenous expression of the proteins. This means that it can be used to study interactions in the unperturbed cell system. Depending on the process being studied, cell synchronisation may allow this approach to provide improved information on dynamic changes in protein expression, but there is little potential for true single cell studies (Banfalvi 2011).

Other approaches allow for the extensive screening of protein libraries for interacting proteins of interest. These approaches included genetic and proteomic screens. The most common genetic screen has been the two-hybrid assay where proteins are genetically tagged so that their interaction creates a functional transcription factor that can activate a target reporter gene, which may be either easily detected or selectable. This assay has most often been conducted in yeast and can allow whole libraries of expressed proteins to be screened for potential interactions (Fields and Song 1989; Van Criekinge and Beyaert 1999). The yeast two-hybrid assay has some disadvantages, including false positives and false negatives, which require careful controls to account for spurious results. In addition, the assay is conducted in the nucleus, and does not incorporate the spatial or temporal context of when or where proteins are normally localised in cells. Positive interactions need to be confirmed by other methods such as biochemical assays, such as co-IP.

In contrast to the two hybrid assay (and related assays), proteomic interaction assays can be conducted in a more biological context. The most favoured approach has been Tandem affinity purification or TAP-tag approach. TAP-tag uses a fusion protein baring the TAP-tag which will facilitate whole proteome pull-down associated with the target fusion protein. Following this, mass spectrometry is used to identify interacting proteins. TAP-tag is not suitable for the observation of transient protein interactions (Rigaut, Shevchenko *et al.* 1999; Puig, Caspary *et al.* 2001). Both the yeast two hybrid assay and proteomic screens are useful for identifying interacting protein networks but lack the ability to quantify protein interactions in single cells, or provide dynamic information on protein localisation and protein half-life.

6.2.2 Biophysical Assays

In the context of single cell assays for protein interactions FRET has become the most common approach. Classically, spectrally-detected FRET is performed in fixed cells at a single time-point through the use of irreversible acceptor photobleaching, and lacks the capacity for real-time measurement (Weber 1978; Karpova, Baumann *et al.* 2003; Gu, Di *et al.* 2004). More recently, spectrally detected FRET has been suggested for live cell assays for the measurement of protein interactions. This has been achieved through the use of sensitised image detection (F_C), which allows the direct collection of light pertaining to FRET from acceptor fluorophores (Youvan, Silva *et al.* 1997; Gordon, Berry *et al.* 1998; Zal and Gascoigne 2004). This technique requires the careful subtraction of spillover, and as a result is liable to spurious reporting of FRET, and is fundamentally concentration dependent. There are many examples of FRET sensors that measure cell signalling such as cameleon biosensors for Ca^{2+} detection and cAMP sensors. These sensors have both interacting fluorophores on the same protein which circumvents the need to consider the concentration dependence of spectrally-derived FRET measurements. Generally the species to be assayed changes the conformation of the FRET pair to give a measurable signal (Miyawaki, Llopis *et al.* 1997). The main limitation with these sensors is generally a poor dynamic range.

The combination of FRET and Fluorescence Lifetime Imaging (FLIM) has the capability for concentration and spillover independent measurement of protein interactions over time (Wouters and Bastiaens 2006). There are two main approaches to FLIM, time domain and frequency domain measurements. The former involves providing a fast emission pulse and then measuring the decay of the resulting fluorescence with a fast detector. The latter uses a frequency modulated emission source with a time-gated detector for analysis of fluorescence lifetime peak following excitation (Alvarez, Alegra et al. 1991{Chang, 2007 #291; Clegg, Holub et al. 2003; Chang, Sud et al. 2007; Padilla-Parra, Auduge et al. 2009). The main advantage of FLIM-FRET is that measurements are independent of fluorophore concentration, giving a better opportunity to measure FRET efficiency as a function of molecular distance, and are not prone to artefacts caused by unequal expression. A key issue related to the use of FLIM approaches to measure FRET is due to the relatively long

time needed for the acquisition of quantitative life-time measurement over a time series. This has often been limiting for real-time experiments. There are few examples of long time-course FRET assays with or without the use of FLIM. The assays described in this thesis remain relatively unproven biologically, but offers the potential for accurate real-time and non-invasive quantification of protein interactions in single cells.

6.2.3 Protein-Fragment Complementation Assays

Protein-fragment complementation assays (PCA) make use of reversible characteristics of split fluorescent and luminescent reporters (Michnick, Ear *et al.* 2007). These reporters are synthesised as two separate chains of amino acids as fusions to biologically functional proteins. When split sequences are re-associated through the close proximity facilitated by protein interaction, they regain their fluorescent or luminescent properties. Biomolecular fluorescence complementation specifically makes use of split fluorescent proteins. When these proteins re-associate, the fluorescent properties of the fluorophore are restored (Ozawa, Natori *et al.* 2007). A significant issue with the use of these split fluorophores is that once they re-associate, they remain associated, preventing any further measurement of the dynamics of interaction. An advantage of this method is that, due to the completed fluorophore representing a single band of emission, the method is free from complication from spillover and associated false positives. Furthermore, other fusion constructs may be co-expressed alongside the protein-fragment complementation assay (Zhang, Ma *et al.* 2004; Ozawa, Natori *et al.* 2007).

Luciferase-based luminescence imaging is typically used as a reporter of gene transcription through the expression of luciferase in the presence of luciferin, and the oxidative decarboxylation of luciferin and the generation of light (de Wet, Wood *et al.* 1987) When the enzyme luciferase is used as the reporter in PCA, luciferase can report on protein interactions through the association of complementary fragments of the luciferase protein fused to other functional proteins (Ozawa, Kaihara *et al.* 2001; Hida, Awais *et al.* 2009). There is a particular advantage for quantification, because the luminescence can be detected over a negligible biological luminescence background. This can be detected by luminescence imaging in living cells in the

presence of luciferin, but requires long exposure using a low light level cameras and a completely light-free environment. A possible advantage to split-luciferase imaging lies in the observation that some dynamics of protein interactions can be observed (M. Awais and T. Ozawa, personal communication). However, it is unclear whether the luminescence decay observed following dissociation of a protein complex is due to the two parts of the luciferase coming apart, or perhaps more likely due to the burn-out of the active luciferase in the presence of luciferin (White, Wood *et al.* 1996) and subsequent reexpression. The half-life of the normal luciferase enzyme in mammalian cells in the presence of luciferin has been measured as being approximately 40 minutes (Harper, Finkenstädt *et al.* 2011). While luminescence imaging using protein complementation may provide insight into the temporal dynamics of protein interaction, due to the nature of the technique, little spatial resolution can be detected, beyond detection on a whole cell level.

6.2.4 Fluorescence Fluctuation Assays

Fluorescence Correlation Spectroscopy (FCS) is a highly quantitative process whereby the fluctuations of fluorescence intensity caused by low numbers of diffusing labelled particles is measured in a diffraction limited confocal volume of light. This allows the analysis of their concentration and mobility (Bacia, Kim *et al.* 2006; Kim, Heinze *et al.* 2007; Spiller, Wood *et al.* 2010). Fluctuations are recorded over time and statistically analyzed by autocorrelation analysis. By using two spectrally distinct fluorophores simultaneously, Fluorescence Cross-Correlation Spectroscopy (FCCS) provides information on molecular binding as well as dynamic co-localisation through the cross-correlation amplitude of both fluorophore's fluctuations over time (Bacia, Kim *et al.* 2006). In contrast to FRET, FCCS does not depend on the very close proximity of the interacting fluorescent labels. FCCS is however limited by requiring single point illumination within cells. This means that long term measurement of protein dynamics via FCCS cannot easily be automated, limiting the available number of data points within an experiment. Furthermore, as a result of illumination within such as small confocal volume, FCCS becomes very easily susceptible to fluorophore bleaching over the course of experiments, which can lead to the generation of false positives and negatives, and will more often than not mean measurements must be taken from different cells at different time points.

FCCS is often seen as a competitive assay to FRET. They are however more complementary in nature. While FCCS allows the measurement of protein association in a concentration-independent manner, FRET allows the measurement of molecular distances, and the more robust monitoring of single cells over time. Furthermore FCCS can be used to estimate direct molecular number. The potential for combining this technique with FRET could mean that a more quantitative FRET efficiency values could be estimated intermolecularly, by using not only molecular counting, but component diffusion times to estimate the degree of binding. This could allow for example, discrimination of whether changes in FRET efficiency between p65 and p50 within the nucleus are due to changes in molecular distance, or changes in binding partners within the nucleus itself.

Raster image correlation spectroscopy (RICS) is another technique comparable to FCS that measures molecular diffusion, concentration, and interaction (Brown, Dalal *et al.* 2008; Digman, Wiseman *et al.* 2009). RICS is an improvement on the image correlation spectroscopy (ICS) (Costantino, Comeau *et al.* 2005) technique, that extends the spatially-resolved diffusion times measured in ICS to include fast-diffusion dynamics (Digman, Brown *et al.* 2005; Digman, Sengupta *et al.* 2005). Whereas FCS proceeds through observing the movement of molecules through the confocal volume fixed at one position, the RICS approach involves measuring the change in pixel to pixel intensity present in raster-scanned confocal laser microscopy images. Note that as each pixel intensity is recorded at a different time, temporal information is included in each image. The major advantage of the ICS/RICS approaches is that they are able to map interactions in the spatial domain. While it could be argued that no other method has the capability to measure overall molecular flow in living cells (Hinde, Cardarelli *et al.* 2010), the use of pixel by pixel analysis of FRET maps does have this potential.

6.2.5 Discussion of Techniques in Context

FRET occupies a discrete niche with regard to most molecular and biophysical techniques. While molecular techniques are direct measures of interaction due to physical binding of proteins, they offer less information on protein behaviour and physiological interaction partners, which could be separated by time and localisation.

FRET on the other hand is the inferred interaction of proteins due to the proximity of fluorophore interaction. Compared to most biophysical assays, FRET gives a clear advantage for measurement of intermolecular interaction, which other techniques will struggle to measure accurately (perhaps with the exception of Protein-fragment complementation assays). However, due the potential for false positives in FRET, it would be naive to ignore other complementary techniques. As previously discussed, the combination of techniques such as FCCS or RICS could help circumnavigate issues of protein concentration for measuring protein interactions, and help determine if changes in intermolecular FRET efficiencies are due to changing binding rates between protein partners or changes in molecular distance, inferring conformational changes.

With regard to the specific comparison between FLIM-FRET and spectrally determined FRET, both have advantages and disadvantages. Primarily, FLIM currently provides a more quantitive approach to using FRET to estimate complex formation due to concentration independence (Wouters and Bastiaens 1999). FLIM however requires large quantities of light to be input into the system, risking the photobleaching of fluorophores and inducing phototoxicity in live cell experiments. Furthermore, the specialised equipment is not only expensive, but requires specialised expertise to deconvolve fluorescence lifetime data (specifically in the case of frequency domain FLIM, which requires Fourier transforms to deconvolve multi peak multi-fluorophore data sets (Soloviev, Tahir *et al.* 2007).

The comprehensive use of different methodologies for measuring protein interaction is key to informing interacting protein partners in a wider physiological context. FRET is one tool in the identification of protein dynamics, and is best combined with other techniques.

6.3 Remaining issues in live cell FRET

Overall, the use of Dronpa as a photoswitchable element in a FRET pair has proved to be successful. The behaviour of Dronpa been shown to be consistent as a FRET partner (either as an acceptor or donor) by use of positive control constructs. It has

also shown the ability to consistently discriminate between different biological fusions using changes in donor fluorescence following Dronpa switching. These properties are giving valuable information concerning how proteins interact. Finally, the assay applied across a time series provided insight into changes in the conformation and dynamics of proteins over time.

Dronpa was still susceptible to problems experienced using spectral FRET. The most prevalent issue, which was highlighted by the photoswitching characteristics of Dronpa, was the contribution of spillover to sensitised emission. Multiple spillover calibration settings were used to attempt to control for possible differences in experimental conditions, but this did not seem to be completely satisfactory. A solution to this would be to increase the stringency of the spillover reduction to force negative controls to display no detectable sensitised emission. This has the danger that associations may be under-reported and any quantitative measure of FRET efficiency would be underestimated. This is of vital consideration when using Dronpa as a donor, as measurements of FRET efficiency are entirely dependent on sensitised emission. This highlights the importance of the assay; to modulate fluorescence to observe corresponding changes in fluorescence ensures spurious FRET reporting is avoided more effectively.

Concentration dependence and donor/acceptor occupancy also remain a problem for spectral imaging. This effect could be mitigated somewhat through the selection of cells with greater number of Dronpa molecules to AmCyan. This was unavoidable when observing FRET in p105 due to the predisposed molecular ratio of p50:p105 (1:1). By ensuring Dronpa was in excess of AmCyan, the relative change in AmCyan from switching remained more consistent to self normalisation. An excess of unbound AmCyan would have artificially reduced the reported value for quenching efficiency.

6.3.1 Improvements to the Assay

While the switching assay was successful and revealed interesting biological insights into the behaviour of p105 and interacting Rel proteins, changes could be made to improve the potential time resolution and reduce noise in the data. During the course

of the project, new Dronpa variants were generated by Ando *et.al.(Ando, Flors et al. 2007)*. These variants are reported to exhibit faster and more complete switching of fluorescence, which would improve time resolution between switching events and could well allow more uniform modulation of different fusion proteins.

While mStrawberry proved to be a good acceptor for Dronpa, showing little to no variation over the predefined switching protocol, AmCyan proved to be somewhat inconsistent as a donor. Furthermore, due to less efficient excitation of AmCyan by 458 excitation line, brightness of the fluorophore was less than optimal, resulting in detector gain being set past its optimal signal to noise boundary. Other cyan fluorophores may provide more consistent behaviour and brighter fluorescence resulting in less detector noise, which would improve accurate detection of changes at lower fluorescence concentrations.

Finally, minor software modifications could allow for the development of a better photoswitching assay. Specifically, the need for Dronpa activation via the bleaching function adds unnecessary time. If the imaging protocol could be modified to incorporate 405nm excitation for a limited number of frames, Dronpa switching could be switched with no delay in the imaging protocol. Furthermore, a mean value could potentially be used to quantify FRET response helping to further reduce detector noise effects on spurious FRET reporting (specifically at lower fluorescence intensities).

6.4 Biological insights into p105

The use of FRET to probe the activity of p105 in single cells has given interesting insight into this protein. p105 is often seen as an inert cytoplasmic component which inhibits nuclear localisation of NF-κB Rel family members and generates functional p50 via proteolytic cleavage (Mercurio, DiDonato *et al.* 1993; Salmeron, Janzen *et al.* 2001; Lang, Janzen *et al.* 2003; Savinova, Hoffmann *et al.* 2009). It was observed here that intact p105 is present in the nucleus of resting cells. Furthermore, the presence of p65 appears to modulate the intramolecular FRET efficiency of p105, as co-expression with p65 leads to p105 adopting FRET efficiency of no statistically significant difference from intermolecular FRET interactions [chap 5]. Furthermore,

no detectable FRET was seen in the nucleus between pG-CMV-p65-AmCyan and pG-CMV-Dronpa-p105 pre-TNFα which could explain consistently higher FRET efficiency in intramolecular p105 FRET.

Over time, p105 also shows interesting characteristics. In resting cells, p105 shows a variable FRET response to Dronpa switching implying that p105 conformation is in a state of fluctuation within cells. By stimulating cells with TNFα, FRET behaviour seems to generally synchronise showing an increase and subsequent decrease in FRET efficiency over time (chapter 5) It was thought that this change in FRET efficiency was caused by phosphorylation of p105 via IKK, which is thought to alter p105 conformation (MacKichan, Logeat *et al.* 1996). FRET efficiency was shown to differ in cells still expressing p105. However, an increased FRET efficiency to TNFα stimulation presumably caused by the influx of unphosphorylated p105. It could be argued that this is a far more physiological response to TNFα due to stimulation resulting in the synthesis of p105 shown in [chapter 1]. If p105 were under constitutive expression, FRET imaging may yield interesting dynamics in p105 changes which were seen in cells actively expressing p105. Overall, the characterisation of p105 as an inert repressor of activity needs to be challenged due to its presence in the nuclear compartment of cells pre TNFα stimulus.

6.5 Potential future work: 3 way FRET, and applications in model species eg *Drosophila*.

There are many potential avenues for uses of this technology for biological applications. The continuation of this technology to look at the intramolecular and intermolecular dynamics of p105 should include the generation of stable cell lines expressing the fusion proteins from their own promoters. As endogenous blotting of p105 indicated, p105 levels remain relatively constant following stimulation of cells by TNFα. This would allow the interpretation of p105 dynamics without the added complication of changing expression levels. Further work should also include the study of protein modification to p105 (Phospho-mutants of serine 927 and 932), which are significant serine phosphorylation sites for the processing of p105 (Lang, Janzen *et al.* 2003). These would serve as a useful control to ascertain the importance of phosphorylation and processing to potential conformational changes inferred from changes in FRET efficiency following TNFα stimulation. Use of proteosomal

inhibitors would also work to elucidate whether changes in FRET efficiency are due to phosphorylation or processing of p105. Mutant proteins that lack the GRR might also provide some insight.

The potential to observe nuclear conformational change in p65-p50 dimers also presents an interesting opportunity. The changing FRET efficiency in p65-p50 represents two possibilities: Either changing dimerisation of partners; or conformational change of p65-p50 caused by dynamic binding of the dimeric transcription factor to DNA. Following characterisation of the temporal dynamics of this interaction, use of RICS and FCS could then be used to observe any potential changes in cross-correlation between the two partners over time.

Preliminary work has shown that this assay has real potential to be used in a model species such as *Drosophila melenogaster*. Constructs were made to monitor changes in actin cytoskeletal dynamics in *Drosophila* embryonic cell line (S2R+) cells by using two independent actin fusion proteins with Dronpa and AmCyan. The positive control construct p-Actin-Dronpa-7aa-AmCyan (the fusion construct under the constitutive actin promoter) was also used and tested in S2R+ cells, showing a strong FRET response, proving the possible application of this technology to other systems. Using the drug treatment latrunculin as a negative control to inhibit formation of Filamentous Actin, changes in FRET efficiency were to be used to monitor the relative changes in actin dynamics. Work was then set to move into stable mutant S2R+ cells with phosphorylated mutant variants of proteins thought to be key in the regulation of the cell cytoskeleton and important for movement and migration of cells. The technique was then to be implemented in mulicellular systems to visualise the formation of actin rich protrusions, key in the invasion and migration of cells through tissue.

Finally, the potential for the monitoring of 3 way FRET interactions is a natural progression for this technology. Through the use of mStrawberry and AmCyan as acceptor and donor to Dronpa respectively, changes in interaction dynamics could potentially be seen through changes in FRET efficiency over time. For example, preliminary data indicate E2F1 and IkBα competitively bind to p65 which results in a change co-localisation of p65 and the associated protein (personal communication

Ankers) It would be interesting to express all three proteins in a single cell with the appropriate fluorophores.

6.6 Future of live cell imaging and systems biology

The kinds of data produced by this assay are ideal for the discrimination of protein behaviour over time. However data is inherently complex in nature and requires a broad systems biology approach to decipher trends in protein behaviour. A key aim in systems biology is to make quantitative measurements of the components of a system to give insight and understanding into the underlying mechanisms that control the system. This means it is necessary to measure all processes; from ligand binding to eventual cell fate. This includes processes like second messenger signalling, protein interactions, protein modifications, protein translocation and protein and RNA stability/degradation, as well as target gene transcription, translation and expressed protein dynamics (Spiller, Wood *et al.* 2010). It is important to link these processes to robust differential cell fate decisions including apoptosis, cell division or cell differentiation. Live cell imaging over varying timescales can play a key role in this systems biology research because it reports on dynamic processes in single cells(Bakstad, Adamson *et al.* 2012). A major problem is that the experimental toolbox for these processes is limited. Many of the current measurements that underlie our biological understanding come from bulk biochemical measurements, which can be poorly quantitative and give the mean behaviour for populations that may have inherently stochastic attributes.

The ability to non-invasively measure specific protein interactions in live cells is an important task for the development of a more quantitative understanding of how cells transmit and decode signals. The present study provides a new tool with potential to add to such measurements. A related deficiency is the lack of generic assays for protein modifications in single live cells. It might be envisaged that expressed antibody affinity tags that bind to modified proteins could be expressed in cells and might in the future allow protein interaction assays to detect and quantify protein modifications. Thus, the live cell FRET technology could have a wider potential application in cell biology and cell signalling.

Systems biology requires quantitative measurements for the fitting and constraint of mathematical models that can be used to provide predictions/hypotheses and a better quantitative understanding of the functional mechanisms of complex dynamic signalling systems. Over the past few years it has emerged that a series of key signalling systems can exhibit unexpected dynamic behaviour including oscillations. These processes include signalling through calcium (Dolmetsch, Lewis *et al.* 1997), cAMP, ERK2, STAT3 (Yoshiura, Ohtsuka *et al.* 2007), Wnt/FGF/Notch (Pourquie 2003), p53 (Lahav, Rosenfeld *et al.* 2004) as well as NF-κB (Nelson, Ihekwaba *et al.* 2004). In addition, other key cellular processes such as the cell cycle and circadian clock are described as oscillators and there are well described oscillations in metabolism (Ghosh and Chance 1964). For many years scientists have only seen these processes in averaged cells at a limited series of timepoints. The ability to track NF-κB dynamics demonstrated the existence of oscillations into and out of the nucleus and it was later suggested that the timing of these oscillations could change the pattern of gene expression.

There is therefore a continuing need for an improved toolbox for the quantification of cellular processes in single living cells over time. The combination with mathematical modelling offers huge potential for developing a better understanding of biological dynamics, gene function and cell function in the context of a living organism. By combining these disciplines, data can synergistically feedback into model development facilitating the development of more scientifically pertinent questions and relevant biological tools.

Chapter 7: References

Abbe, E. (1873). "Beiträge zur Theorie des Mikroskops und der mikroskopischen Wahrnehmung." Archiv für Mikroskopische Anatomie **9**(1): 413-418.

Alvarez, F., A. Alegra, et al. (1991). "Relationship between the time-domain Kohlrausch-Williams-Watts and frequency-domain Havriliak-Negami relaxation functions." Physical Review B **44**(14): 7306-7312.

Anderson, N. G. (1998). Co-Immunoprecipitation

Protein Targeting Protocols. R. A. Clegg, Humana Press. **88:** 35-45.

Ando, R., C. Flors, et al. (2007). "Highlighted generation of fluorescence signals using simultaneous two-color irradiation on Dronpa mutants." Biophys J **92**(12): L97-99.

Ando, R., H. Mizuno, et al. (2004). "Regulated Fast Nucleocytoplasmic Shuttling Observed by Reversible Protein Highlighting." Science **306**(5700): 1370-1373.

Andresen, M., A. C. Stiel, et al. (2007). "Structural basis for reversible photoswitching in Dronpa." Proc Natl Acad Sci U S A **104**(32): 13005-13009.

Bacia, K., S. A. Kim, et al. (2006). "Fluorescence cross-correlation spectroscopy in living cells." Nat Methods **3**(2): 83-89.

Bacia, K. and P. Schwille (2007). "Practical guidelines for dual-color fluorescence cross-correlation spectroscopy." Nat Protoc **2**(11): 2842-2856.

Badr, C. E. and B. A. Tannous (2011). "Bioluminescence imaging: progress and applications." Trends in Biotechnology **29**(12): 624-633.

Bakstad, D., A. Adamson, et al. (2012). "Quantitative measurement of single cell dynamics." Curr Opin Biotechnol **23**(1): 103-109.

Bancos, I., N. Natt, et al. (2012). "Evidence-based endocrinology: illustrating its principles in the management of patients with pituitary incidentalomas." Best Pract Res Clin Endocrinol Metab **26**(1): 9-19.

Banfalvi, G. (2011). Overview of Cell Synchronization

Cell Cycle Synchronization. G. Banfalvi, Humana Press. **761:** 1-23.

Baudendistel, N., G. Müller, et al. (2005). "Two-Hybrid Fluorescence Cross-Correlation Spectroscopy Detects Protein–Protein Interactions In Vivo." ChemPhysChem **6**(5): 984-990.

Berney, C. and G. Danuser (2003). "FRET or no FRET: a quantitative comparison." Biophys J **84**(6): 3992-4010.

Bourgeois, D. and V. Adam (2012). "Reversible photoswitching in fluorescent proteins: A mechanistic view." Iubmb Life **64**(6): 482-491.

Bours, V., G. Franzoso, et al. (1993). "The oncoprotein Bcl-3 directly transactivates through κB motifs via association with DNA-binding p50B homodimers." Cell **72**(5): 729-739.

Bowie, J. U., R. Luthy, et al. (1991). "A method to identify protein sequences that fold into a known three-dimensional structure." Science **253**(5016): 164-170.

Brown, C. M., R. B. Dalal, et al. (2008). "Raster image correlation spectroscopy (RICS) for measuring fast protein dynamics and concentrations with a commercial laser scanning confocal microscope." J Microsc **229**(Pt 1): 78-91.

Chalfie, M., Y. Tu, et al. (1994). "Green fluorescent protein as a marker for gene expression." Science **263**(5148): 802-805.

Chang, C. W., D. Sud, et al. (2007). Fluorescence Lifetime Imaging Microscopy. Methods in Cell Biology. S. Greenfield and E. W. David, Academic Press. **Volume 81:** 495-524.

Chen, F. E., D. B. Huang, et al. (1998). "Crystal structure of p50/p65 heterodimer of transcription factor NF-kappaB bound to DNA." Nature **391**(6665): 410-413.

Chen, H., H. L. Puhl, 3rd, et al. (2006). "Measurement of FRET efficiency and ratio of donor to acceptor concentration in living cells." Biophys J **91**(5): L39-41.

Chen, Y., L. N. Wei, et al. (2003). "Probing protein oligomerization in living cells with fluorescence fluctuation spectroscopy." Proc Natl Acad Sci U S A **100**(26): 15492-15497.

Chudakov, D. M., V. V. Belousov, et al. (2003). "Kindling fluorescent proteins for precise in vivo photolabeling." Nat Biotech **21**(2): 191-194.

Chudakov, D. M., V. V. Verkhusha, et al. (2004). "Photoswitchable cyan fluorescent protein for protein tracking." Nat Biotechnol **22**(11): 1435-1439.

Clegg, R. M., O. Holub, et al. (2003). [22] Fluorescence lifetime-resolved imaging: Measuring lifetimes in an image. Methods in Enzymology. I. P. Gerard Marriott, Academic Press. **Volume 360:** 509-542.

Coons, A. H., H. J. Creech, et al. (1941). "Immunological Properties of an Antibody Containing a Fluorescent Group." Proceedings of the Society for Experimental Biology and Medicine. Society for Experimental Biology and Medicine (New York, N.Y.) **47**(2): 200-202.

Costantino, S., J. W. Comeau, et al. (2005). "Accuracy and dynamic range of spatial image correlation and cross-correlation spectroscopy." Biophys J **89**(2): 1251-1260.

Dale, R. E., J. Eisinger, et al. (1979). "The orientational freedom of molecular probes. The orientation factor in intramolecular energy transfer." Biophys J **26**(2): 161-193.

de Wet, J. R., K. V. Wood, et al. (1987). "Firefly luciferase gene: structure and expression in mammalian cells." Molecular and Cellular Biology **7**(2): 725-737.

Dickson, K. M., A. L. Bhakar, et al. (2004). "TRAF6-dependent NF-kB transcriptional activity during mouse development." Dev Dyn **231**(1): 122-127.

Digman, M. A., C. M. Brown, et al. (2005). "Measuring fast dynamics in solutions and cells with a laser scanning microscope." Biophys J **89**(2): 1317-1327.

Digman, M. A., P. Sengupta, et al. (2005). "Fluctuation correlation spectroscopy with a laser-scanning microscope: exploiting the hidden time structure." Biophys J **88**(5): L33-36.

Digman, M. A., P. W. Wiseman, et al. (2009). "Detecting protein complexes in living cells from laser scanning confocal image sequences by the cross correlation raster image spectroscopy method." Biophysical Journal **96**(2): 707-716.

Dobrzanski, P., R. P. Ryseck, et al. (1993). "Both N- and C-terminal domains of RelB are required for full transactivation: role of the N-terminal leucine zipper-like motif." Mol Cell Biol **13**(3): 1572-1582.

Dolmetsch, R. E., R. S. Lewis, et al. (1997). "Differential activation of transcription factors induced by Ca2+ response amplitude and duration." Nature **386**(6627): 855-858.

Domanov, Y. A. and G. P. Gorbenko (2002). "Analysis of resonance energy transfer in model membranes: role of orientational effects." Biophysical Chemistry **99**(2): 143-154.

Dross, N., C. Spriet, et al. (2009). "Mapping eGFP oligomer mobility in living cell nuclei." PLoS One **4**(4): e5041.

Egger, M. D. and M. Petran (1967). "New reflected-light microscope for viewing unstained brain and ganglion cells." Science **157**(3786): 305-307.

Fara, P. (2009). "A microscopic reality tale." Nature **459**(7247): 642-644.

Felgner, P. L., T. R. Gadek, et al. (1987). "Lipofection: a highly efficient, lipid-mediated DNA-transfection procedure." Proceedings of the National Academy of Sciences **84**(21): 7413-7417.

Fields, S. and O.-k. Song (1989). "A novel genetic system to detect protein–protein interactions." Nature **340**(6230): 245-246.

Förster, T. (1948). "Zwischenmolekulare Energiewanderung und Fluoreszenz." Annalen der Physik **437**(1-2): 55-75.

Friedman, S. J., C. L. Dewar, et al. (1986). "Cytolocalization artifacts with immunofluorescent probes." Biochemistry and Cell Biology **64**(12): 1326-1332.

Ganchi, P. A., S. C. Sun, et al. (1993). "A novel NF-kappa B complex containing p65 homodimers: implications for transcriptional control at the level of subunit dimerization." Mol Cell Biol **13**(12): 7826-7835.

Ganesan, S., S. M. Ameer-Beg, et al. (2006). "A dark yellow fluorescent protein (YFP)-based Resonance Energy-Accepting Chromoprotein (REACh) for Forster resonance energy transfer with GFP." Proc Natl Acad Sci U S A **103**(11): 4089-4094.

Gavin, A. C., M. Bosche, et al. (2002). "Functional organization of the yeast proteome by systematic analysis of protein complexes." Nature **415**(6868): 141-147.

Ghosh, A. and B. Chance (1964). "Oscillations of glycolytic intermediates in yeast cells." Biochemical and Biophysical Research Communications **16**(2): 174-181.

Gordon, G. W., G. Berry, et al. (1998). "Quantitative Fluorescence Resonance Energy Transfer Measurements Using Fluorescence Microscopy." Biophys J **74**(5): 2702-2713.

Gross, L. A., G. S. Baird, et al. (2000). "The structure of the chromophore within DsRed, a red fluorescent protein from coral." Proc Natl Acad Sci U S A **97**(22): 11990-11995.

Gu, Y., W. L. Di, et al. (2004). "Quantitative fluorescence resonance energy transfer (FRET) measurement with acceptor photobleaching and spectral unmixing." Journal of Microscopy **215**(2): 162-173.

Gurskaya, N. G., V. V. Verkhusha, et al. (2006). "Engineering of a monomeric green-to-red photoactivatable fluorescent protein induced by blue light." Nat Biotech **24**(4): 461-465.

Habuchi, S., R. Ando, et al. (2005). "Reversible single-molecule photoswitching in the GFP-like fluorescent protein Dronpa." Proceedings of the National Academy of Sciences of the United States of America **102**(27): 9511-9516.

Harper, C. V., B. Finkenstädt, et al. (2011). "Dynamic Analysis of Stochastic Transcription Cycles." PLoS Biol **9**(4): e1000607.

Haruta, H., A. Kato, et al. (2001). "Isolation of a Novel Interleukin-1-inducible Nuclear Protein Bearing Ankyrin-repeat Motifs." Journal of Biological Chemistry **276**(16): 12485-12488.

Hassell, J. and A. R. Hand (1974). "Tissue fixation with diimidoesters as an a;ternative to aldehydes I. Comparison of crosslinking and ultrastructure obtained with dimethylsiberimidate and glutaraldehyde." Journal of Histochemistry & Cytochemistry **22**(4): 223-239.

Haugland, R. P. (2001). Antibody Conjugates for Cell Biology. Current Protocols in Cell Biology, John Wiley & Sons, Inc.

Hayden, M. S. and S. Ghosh (2004). "Signaling to NF-kappaB." Genes Dev **18**(18): 2195-2224.

Hayden, M. S. and S. Ghosh (2004). "Signaling to NF-kB." Genes & Development **18**: 2195-2224.

Hayden, M. S. and S. Ghosh (2012). "NF-kappaB, the first quarter-century: remarkable progress and outstanding questions." Genes Dev **26**(3): 203-234.

Hayden, M. S., A. P. West, et al. (2006). "NF-kappaB and the immune response." Oncogene **25**(51): 6758-6780.

Heessen, S., M. G. Masucci, et al. (2005). "The UBA2 domain functions as an intrinsic stabilization signal that protects Rad23 from proteasomal degradation." Molecular Cell **18**(2): 225-235.

Heim, R., A. B. Cubitt, et al. (1995). "Improved green fluorescence." Nature **373**(6516): 663-664.

Heimstädt, O. (1911). "Das Fluoreszenzmikroskop
" z. wiss. mikrosk. **28**: 330-337.

Heissmeyer, V., D. Krappmann, et al. (1999). "NF-kappaB p105 is a target of IkappaB kinases and controls signal induction of Bcl-3-p50 complexes." EMBO J **18**(17): 4766-4778.

Henderson, J. N. and S. J. Remington (2006). "The kindling fluorescent protein: a transient photoswitchable marker." Physiology (Bethesda) **21**: 162-170.

Hida, N., M. Awais, et al. (2009). "High-sensitivity real-time imaging of dual protein-protein interactions in living subjects using multicolor luciferases." PLoS One **4**(6): e5868.

Hinde, E., F. Cardarelli, et al. (2010). "In vivo pair correlation analysis of EGFP intranuclear diffusion reveals DNA-dependent molecular flow." Proc Natl Acad Sci U S A **107**(38): 16560-16565.

Hoffmann, A., A. Levchenko, et al. (2002). "The IkappaB-NF-kappaB signaling module: temporal control and selective gene activation." Science **298**(5596): 1241-1245.

Huang, Y., F. Liu, et al. (2005). "NF-kappaB precursor, p105, and NF-kappaB inhibitor, IkappaBgamma, are both elevated in Alzheimer disease brain." Neurosci Lett **373**(2): 115-118.

Inoue, J., L. D. Kerr, et al. (1992). "I kappa B gamma, a 70 kd protein identical to the C-terminal half of p110 NF-kappa B: a new member of the I kappa B family." Cell **68**(6): 1109-1120.

Inouye, S. and F. I. Tsuji (1994). "Aequorea green fluorescent protein: Expression of the gene and fluorescence characteristics of the recombinant protein." FEBS Lett **341**(2–3): 277-280.

Johnson, L. N. and D. Barford (1993). "The effects of phosphorylation on the structure and function of proteins." Annu Rev Biophys Biomol Struct **22**: 199-232.

Karin, M., Y. Cao, et al. (2002). "NF-kappaB in cancer: from innocent bystander to major culprit." Nat Rev Cancer **2**(4): 301-310.

Karpova, T. S., C. T. Baumann, et al. (2003). "Fluorescence resonance energy transfer from cyan to yellow fluorescent protein detected by acceptor photobleaching using confocal microscopy and a single laser." J Microsc **209**(Pt 1): 56-70.

Kim, S. A., K. G. Heinze, et al. (2007). "Fluorescence correlation spectroscopy in living cells." Nat Methods **4**(11): 963-973.

Kornberg, R. D. (1999). "Eukaryotic transcriptional control." Trends Cell Biol **9**(12): M46-49.

Kvam, E. and R. M. Tyrrell (1997). "Induction of oxidative DNA base damage in human skin cells by UV and near visible radiation." Carcinogenesis **18**(12): 2379-2384.

Lahav, G., N. Rosenfeld, et al. (2004). "Dynamics of the p53-Mdm2 feedback loop in individual cells." Nat Genet **36**(2): 147-150.

Lan, L., S. Nakajima, et al. (2005). "Accumulation of Werner protein at DNA double-strand breaks in human cells." J Cell Sci **118**(Pt 18): 4153-4162.

Lang, V., J. Janzen, et al. (2003). "βTrCP-Mediated Proteolysis of NF-κB1 p105 Requires Phosphorylation of p105 Serines 927 and 932." Molecular and Cellular Biology **23**(1): 402-413.

Lin, L., G. N. DeMartino, et al. (1998). "Cotranslational biogenesis of NF-kappaB p50 by the 26S proteasome." Cell **92**(6): 819-828.

Lin, L. G., S. (1996). "A glycine-rich region in NF-kappaB p105 functions as a processing signal for the generation of the p50 subunit " Molecular and Cellular Biology **16**(5): 2248-2254.

Liu, S. F. and A. B. Malik (2006). "NF-κB activation as a pathological mechanism of septic shock and inflammation." American Journal of Physiology - Lung Cellular and Molecular Physiology **290**(4): L622-L645.

Lukyanov, K. A., D. M. Chudakov, et al. (2005). "Innovation: Photoactivatable fluorescent proteins." Nat Rev Mol Cell Biol **6**(11): 885-891.

Lyulcheva, E., E. Taylor, et al. (2008). "Drosophila pico and its mammalian ortholog lamellipodin activate serum response factor and promote cell proliferation." Dev Cell **15**(5): 680-690.

MacKichan, M. L., F. Logeat, et al. (1996). "Phosphorylation of p105 PEST Sequences via a Redox-insensitive Pathway Up-regulates Processing to p50 NF-B." Journal of Biological Chemistry **271**(11): 6084-6091.

Makarov, S. (2001). "NF-kappaB in rheumatoid arthritis: a pivotal regulator of inflammation, hyperplasia, and tissue destruction." Arthritis Res **3**(4): 200 - 206.

Maréchal, X. M., Y. Asano, et al. (2012). "Design, development, and operation of a fiber-based Cherenkov beam loss monitor at the SPring-8 Angstrom Compact Free Electron Laser." Nuclear Instruments and Methods in Physics Research Section A: Accelerators, Spectrometers, Detectors and Associated Equipment **673**(0): 32-45.

McRae, S. R., C. L. Brown, et al. (2005). "Rapid purification of EGFP, EYFP, and ECFP with high yield and purity." Protein Expression and Purification **41**(1): 121-127.

Mercurio, F., J. A. DiDonato, et al. (1993). "p105 and p98 precursor proteins play an active role in NF-kappa B-mediated signal transduction." Genes & Development **7**(4): 705-718.

Michnick, S. W., P. H. Ear, et al. (2007). "Universal strategies in research and drug discovery based on protein-fragment complementation assays." Nat Rev Drug Discov **6**(7): 569-582.

Mikkelsen, L., S. Sarrocco, et al. (2003). "Expression of the red fluorescent protein DsRed-Express in filamentous ascomycete fungi." FEMS Microbiology Letters **223**(1): 135-139.

Miyawaki, A., J. Llopis, et al. (1997). "Fluorescent indicators for Ca2+based on green fluorescent proteins and calmodulin." Nature **388**(6645): 882-887.

Moorthy, A. K. and G. Ghosh (2003). "p105.Ikappa Bgamma and prototypical Ikappa Bs use a similar mechanism to bind but a different mechanism to regulate the subcellular localization of NF-kappa B." J Biol Chem **278**(1): 556-566.

Moorthy, A. K., O. V. Savinova, et al. (2006). "The 20S proteasome processes NF-kappaB1 p105 into p50 in a translation-independent manner." EMBO J **25**(9): 1945-1956.

Nelson, D. E., A. E. Ihekwaba, et al. (2004). "Oscillations in NF-kappaB signaling control the dynamics of gene expression." Science **306**(5696): 704-708.

Nelson, G., L. Paraoan, et al. (2002). "Multi-parameter analysis of the kinetics of NF-kappaB signalling and transcription in single living cells." J Cell Sci **115**(Pt 6): 1137-1148.

Nooren, I. M. and J. M. Thornton (2003). "Structural characterisation and functional significance of transient protein-protein interactions." J Mol Biol **325**(5): 991-1018.

Orian, A., A. L. Schwartz, et al. (1999). "Structural motifs involved in ubiquitin-mediated processing of the NF-kappaB precursor p105: roles of the glycine-rich region and a downstream ubiquitination domain." Mol Cell Biol **19**(5): 3664-3673.

Ozawa, T., A. Kaihara, et al. (2001). "Split Luciferase as an Optical Probe for Detecting Protein−Protein Interactions in Mammalian Cells Based on Protein Splicing." Analytical Chemistry **73**(11): 2516-2521.

Ozawa, T., Y. Natori, et al. (2007). "Imaging dynamics of endogenous mitochondrial RNA in single living cells." Nat Meth **4**(5): 413-419.

Padilla-Parra, S., N. Auduge, et al. (2009). "Quantitative comparison of different fluorescent protein couples for fast FRET-FLIM acquisition." Biophys J **97**(8): 2368-2376.

Pahl, H. L. (1999). "Activators and target genes of Rel/NF-kappaB transcription factors." Oncogene **18**(49): 6853-6866.

Palombella, V. J., O. J. Rando, et al. (1994). "The ubiquitin-proteasome pathway is required for processing the NF-kappa B1 precursor protein and the activation of NF-kappa B." Cell **78**(5): 773-785.

Paszek, P., T. Lipniacki, et al. (2005). "Stochastic effects of multiple regulators on expression profiles in eukaryotes." J Theor Biol **233**(3): 423-433.

Paszek, P., S. Ryan, et al. (2010). "Population robustness arising from cellular heterogeneity." Proc Natl Acad Sci U S A **107**(25): 11644-11649.

Patterson, G., R. N. Day, et al. (2001). "Fluorescent protein spectra." J Cell Sci **114**(Pt 5): 837-838.

Patterson, G. H. and J. Lippincott-Schwartz (2002). "A Photoactivatable GFP for Selective Photolabeling of Proteins and Cells." Science **297**(5588): 1873-1877.

Pawley, J. B. (2006). Handbook of biological confocal microscopy. New York, NY, Springer.

Phizicky, E. M. and S. Fields (1995). "Protein-protein interactions: methods for detection and analysis." Microbiol Rev **59**(1): 94-123.

Pietraszewska-Bogiel, A. and T. W. Gadella (2011). "FRET microscopy: from principle to routine technology in cell biology." J Microsc **241**(2): 111-118.

Pourquie, O. (2003). "The Segmentation Clock: Converting Embryonic Time into Spatial Pattern." Science **301**(5631): 328-330.

Prasher, D. C., V. K. Eckenrode, et al. (1992). "Primary structure of the Aequorea victoria green-fluorescent protein." Gene **111**(2): 229-233.

Puig, O., F. Caspary, et al. (2001). "The Tandem Affinity Purification (TAP) Method: A General Procedure of Protein Complex Purification." Methods **24**(3): 218-229.

Rigaut, G., A. Shevchenko, et al. (1999). "A generic protein purification method for protein complex characterization and proteome exploration." Nat Biotech **17**(10): 1030-1032.

Rutter, G. A., M. R. White, et al. (1995). "Involvement of MAP kinase in insulin signalling revealed by non-invasive imaging of luciferase gene expression in single living cells." Curr Biol **5**(8): 890-899.

Ryseck, R. P., P. Bull, et al. (1992). "RelB, a new Rel family transcription activator that can interact with p50-NF-kappa B." Mol Cell Biol **12**(2): 674-684.

Salim, K., T. Fenton, et al. (2002). "Oligomerization of G-protein-coupled receptors shown by selective co-immunoprecipitation." Journal of Biological Chemistry **277**(18): 15482-15485.

Salmeron, A., J. Janzen, et al. (2001). "Direct phosphorylation of NF-kappaB1 p105 by the IkappaB kinase complex on serine 927 is essential for signal-induced p105 proteolysis." J Biol Chem **276**(25): 22215-22222.

Savinova, O. V., A. Hoffmann, et al. (2009). "The Nfkb1 and Nfkb2 proteins p105 and p100 function as the core of high-molecular-weight heterogeneous complexes." Mol Cell **34**(5): 591-602.

Schauvliege, R., J. Vanrobaeys, et al. (2002). "Caspase-11 gene expression in response to lipopolysaccharide and interferon-gamma requires nuclear factor-kappa B and signal transducer and activator of transcription (STAT) 1." J Biol Chem **277**(44): 41624-41630.

See, V., N. K. Rajala, et al. (2004). "Calcium-dependent regulation of the cell cycle via a novel MAPK--NF-kappaB pathway in Swiss 3T3 cells." J Cell Biol **166**(5): 661-672.

Sen, R. and D. Baltimore (1986). "Multiple nuclear factors interact with the immunoglobulin enhancer sequences." Cell **46**(5): 705-716.

Shakhov, A. N., D. V. Kuprash, et al. (1990). "Structural analysis of the rabbit TNF locus, containing the genes encoding TNF-beta (lymphotoxin) and TNF-alpha (tumor necrosis factor)." Gene **95**(2): 215-221.

Shaner, N. C., R. E. Campbell, et al. (2004). "Improved monomeric red, orange and yellow fluorescent proteins derived from Discosoma sp. red fluorescent protein." Nat Biotechnol **22**(12): 1567-1572.

Shaner, N. C., G. H. Patterson, et al. (2007). "Advances in fluorescent protein technology." J Cell Sci **120**(Pt 24): 4247-4260.

Shaner, N. C., P. A. Steinbach, et al. (2005). "A guide to choosing fluorescent proteins." Nat Methods **2**(12): 905-909.

Shaner, N. C., P. A. Steinbach, et al. (2005). "A guide to choosing fluorescent proteins." Nat Meth **2**(12): 905-909.

Shen, H., G. Nelson, et al. (2006). "Automated tracking of gene expression in individual cells and cell compartments." Journal of The Royal Society Interface **3**(11): 787-794.

Sheppard, C. J. and T. Wilson (1981). "The theory of the direct-view confocal microscope." J Microsc **124**(Pt 2): 107-117.

Shimomura, O., F. H. Johnson, et al. (1962). "Extraction, Purification and Properties of Aequorin, a Bioluminescent Protein from the Luminous Hydromedusan, Aequorea." Journal of Cellular and Comparative Physiology **59**(3): 223-239.

Silverman, N., R. Zhou, et al. (2000). "A Drosophila IkappaB kinase complex required for Relish cleavage and antibacterial immunity." Genes Dev **14**(19): 2461-2471.

Solan, N. J., H. Miyoshi, et al. (2002). "RelB cellular regulation and transcriptional activity are regulated by p100." J Biol Chem **277**(2): 1405-1418.

Soloviev, V. Y., K. B. Tahir, et al. (2007). "Fluorescence lifetime imaging by using time-gated data acquisition." Appl. Opt. **46**(30): 7384-7391.

Spector, D. L. and R. D. Goldman (2006). "Constructing and Expressing GFP Fusion Proteins." CSH Protoc **2006**(7).

Spiller, D. G., C. D. Wood, et al. (2010). "Measurement of single-cell dynamics." Nature **465**(7299): 736-745.

St Johnston, D. (2002). "The art and design of genetic screens: Drosophila melanogaster." Nat Rev Genet **3**(3): 176-188.

Stark, D. A. and P. M. Kulesa (2007). "An in vivo comparison of photoactivatable fluorescent proteins in an avian embryo model." Dev Dyn **236**(6): 1583-1594.

Stirland, J. A., Z. C. Seymour, et al. (2003). "Real-time imaging of gene promoter activity using an adenoviral reporter construct demonstrates transcriptional dynamics in normal anterior pituitary cells." J Endocrinol **178**(1): 61-69.

Sun, S.-C. (2012). "The noncanonical NF-κB pathway." Immunological Reviews **246**(1): 125-140.

Tartaglia, L. A. and D. V. Goeddel (1992). "Two TNF receptors." Immunol Today **13**(5): 151-153.

Tsien, R. Y. (1998). "The green fluorescent protein." Annu Rev Biochem **67**: 509-544.

Turcatti, G., K. Nemeth, et al. (1996). "Probing the Structure and Function of the Tachykinin Neurokinin-2 Receptor through Biosynthetic Incorporation of Fluorescent Amino Acids at Specific Sites." Journal of Biological Chemistry **271**(33): 19991-19998.

Valeur, B. (2001). Molecular Fluorescence: Principles and Applications, Wiley-VCH.

Van Criekinge, W. and R. Beyaert (1999). "Yeast Two-Hybrid: State of the Art." Biol Proced Online **2**: 1-38.

van Meer, G., E. H. Stelzer, et al. (1987). "Sorting of sphingolipids in epithelial (Madin-Darby canine kidney) cells." J Cell Biol **105**(4): 1623-1635.

Verma, I. M., J. K. Stevenson, et al. (1995). "Rel/NF-kappa B/I kappa B family: intimate tales of association and dissociation." Genes Dev **9**(22): 2723-2735.

Waddell, W. J. and R. G. Bates (1969). "Intracellular pH." Physiol Rev **49**(2): 285-329.

Wakatsuki, T., B. Schwab, et al. (2001). "Effects of cytochalasin D and latrunculin B on mechanical properties of cells." Journal of Cell Science **114**(5): 1025-1036.

Wallrabe, H., Y. Chen, et al. (2006). "Issues in confocal microscopy for quantitative FRET analysis." Microsc Res Tech **69**(3): 196-206.

Wang, B. G., K. Konig, et al. (2010). "Two-photon microscopy of deep intravital tissues and its merits in clinical research." J Microsc **238**(1): 1-20.

Wang, H. G., U. R. Rapp, et al. (1996). "Bcl-2 targets the protein kinase Raf-1 to mitochondria." Cell **87**(4): 629-638.

Weber, J. (1978). "Investigation of energy transfer by means of photobleaching." Zeitschrift für Physik B Condensed Matter **31**(4): 417-421.

White, J. G., W. B. Amos, et al. (1987). "An evaluation of confocal versus conventional imaging of biological structures by fluorescence light microscopy." J Cell Biol **105**(1): 41-48.

White, M. R., C. D. Wood, et al. (1996). "Real-time imaging of transcription in living cells and tissues." Biochem Soc Trans **24**(3): 411S.

Wood, E. J. (1994). "Molecular probes: Handbook of fluorescent probes and research chemicals: By R P Haugland. pp 390. Interchim (Molecular Probes Inc, PO Box 22010 Eugene, OR 97402-0414, USA, or 15 rue des Champs, 92600 Asnieres, Paris). 1992–1994. $15." Biochemical Education **22**(2): 83-83.

Wouters, F. S. and P. I. Bastiaens (2006). "Imaging protein-protein interactions by Fluorescence Resonance Energy Transfer (FRET) microscopy." Curr Protoc Neurosci **Chapter 5**: Unit 5 22.

Wouters, F. S., P. I. Bastiaens, et al. (1998). "FRET microscopy demonstrates molecular association of non-specific lipid transfer protein (nsL-TP) with fatty acid oxidation enzymes in peroxisomes." EMBO J **17**(24): 7179-7189.

Wouters, F. S. and P. I. H. Bastiaens (1999). "Fluorescence lifetime imaging of receptor tyrosine kinase activity in cells." Current Biology **9**(19): 1127-S1121.

Wouters, F. S., P. J. Verveer, et al. (2001). "Imaging biochemistry inside cells." Trends Cell Biol **11**(5): 203-211.

Yinon, B.-N. and L. Steven (2006). Control of NF-?B Activity by Ubiquitination. Handbook of Transcription Factor NF-kappaB, CRC Press**:** 53-85.

Yoshiura, S., T. Ohtsuka, et al. (2007). "Ultradian oscillations of Stat, Smad, and Hes1 expression in response to serum." Proceedings of the National Academy of Sciences **104**(27): 11292-11297.

Youvan, D. C., C. M. Silva, et al. (1997). "Calibration of fluorescence resonance energy transfer in microscopy using genetically engineered GFP derivatives on nickel chelating beads." Biotechnology **3:**: 1–18.

Zal, T. and N. R. Gascoigne (2004). "Photobleaching-corrected FRET efficiency imaging of live cells." Biophys J **86**(6): 3923-3939.

Zhang, M., H. Chang, et al. (2012). "Rational design of true monomeric and bright photoactivatable fluorescent proteins." Nat Methods **9**(7): 727-729.

Zhang, S. F., C. Ma, et al. (2004). "Combinatorial marking of cells and organelles with reconstituted fluorescent proteins." Cell **119**(1): 137-+.

Zimmermann, T., J. Rietdorf, et al. (2002). "Spectral imaging and linear un-mixing enables improved FRET efficiency with a novel GFP2–YFP FRET pair." FEBS Lett **531**(2): 245-249.